# Effect of Non-Uniform Flow in Fracture Networks on Recovery from Naturally Fractured Reservoirs

Gong, Jiakun

**DOI**
10.4233/uuid:fffbf4b9-4921-47eb-95ef-49bec87e5b70

**Publication date**
2017

**Document Version**
Final published version

**Citation (APA)**
Gong, J. (2017). *Effect of Non-Uniform Flow in Fracture Networks on Recovery from Naturally Fractured Reservoirs*. [Dissertation (TU Delft), Delft University of Technology]. https://doi.org/10.4233/uuid:fffbf4b9-4921-47eb-95ef-49bec87e5b70

TU Delft

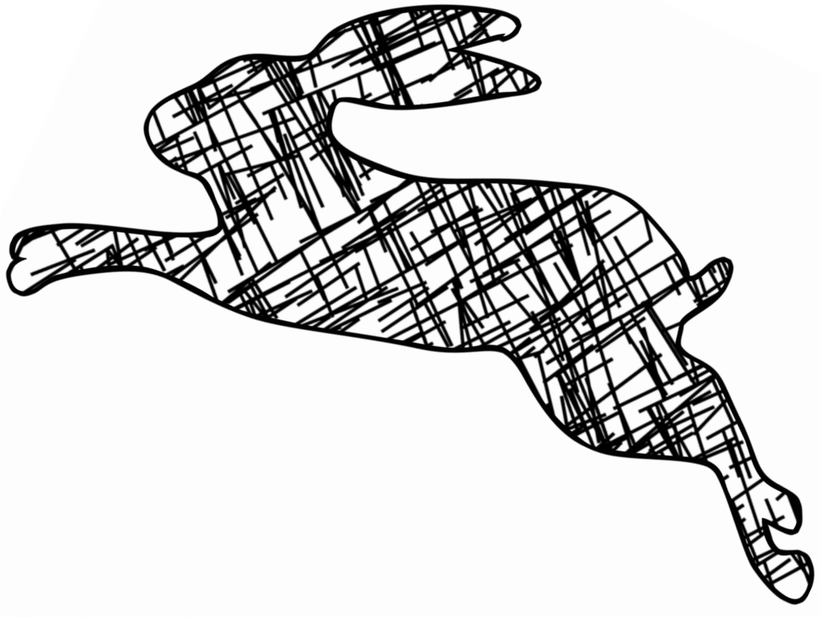

ISBN 978-94-6186-862-6

Effect of Non-Uniform Flow in Fractures on Recovery from Naturally Fractured Reservoirs Jiakun Gong

# Effect of Non-Uniform Flow in Fracture Networks on Recovery from Naturally Fractured Reservoirs

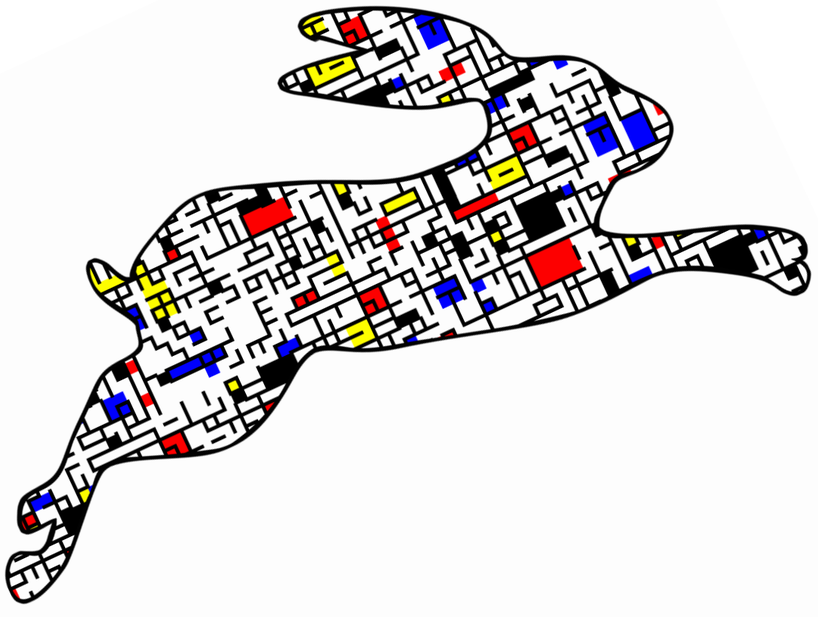

Jiakun Gong

## INVITATION

You are cordially invited to attend the public defense of my PhD thesis

**Effect of Non-Uniform Flow in Fracture Networks on Recovery from Naturally Fractured Reservoirs**

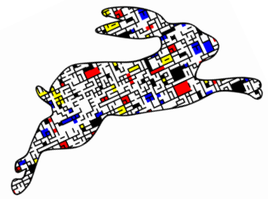

At 10 am on Tuesday
14th November, 2017

In the Senaatszaal of the Aula, Delft University of Technology, Mekelweg 5, Delft.

A brief presentation will be given at 9:30 am.

You are most welcome to attend the reception that will take place at i.d-Kafee at 18:00 pm.

**Jiakun Gong**

gongjiakun@gmail.com

# EFFECT OF NON-UNIFORM FLOW IN FRACTURE NETWORKS ON RECOVERY FROM NATURALLY FRACTURED RESERVOIRS

# EFFECT OF NON-UNIFORM FLOW IN FRACTURE NETWORKS ON RECOVERY FROM NATURALLY FRACTURED RESERVOIRS

**Proefschrift**

ter verkrijging van de grad van doctor
aan de Technishe Universiteit Delft,
op gezag van de Rector Magnificus Prof. ir. K.C.A.M. Luyben;
voorzitter van het College voor Promoties,
in het openbaar te verdedigen op
dinsdag 14 november 2017 om 10:00 uur

door

**Jiakun GONG**

Master of Science in Geotechnical Engineering,

Hohai University, Nanjing, China

geboren te Zhangjiakou, China.

This dissertation has been approved by

promotor: Prof. dr. W. R. Rossen

Composition of the doctoral committee:

| | |
|---|---|
| Rector Magnificus | Chairman |
| Prof. dr. W. R. Rossen | Delft University of Technology |

Independent members:

| | |
|---|---|
| Prof. dr. B. Noetinger | IFP Energies Nouvelles |
| Prof. dr. P. King | Imperial College |
| Dr. D. V. Voskov | Delft University of Technology |
| Dr. H. Hajibeygi | Delft University of Technology |
| Prof. dr. D. F. Bruhn | Delft University of Technology |
| Prof. dr. G. Bertotti | Delft University of Technology |
| Prof. dr. ir. J. D. Jansen | Delft University of Technology |

*Funded by:* China Scholarship Council (CSC), Saudi Aramco

*Keywords:* Fractured reservoir; oil recovery; dual-porosity; dual-permeability; percolation; non-uniform flow; fracture spacing; Peclet number



Cover designed by Xiaoyan Zhao

ISBN 978-94-6186-862-6

An electronic version of this dissertation is available at

http://repository.tudelft.nl/

*to my parents*

*to Yan*

# CONTENTS

# 1

# INTRODUCTION

## 1.1 Rationale

Naturally fractured reservoirs produce a significant portion of oil and gas globally (Saidi 1987). These reservoirs are recognized as “fractured” primarily if the fractures form an interconnected network (Fig. 1.1), allowing flow over long distances exclusively through the fractures, without the need to pass through the rock matrix between the fractures. What makes naturally fractured reservoirs special is the high conductivity of the fracture network combined with much slower flow within the matrix, where oil resides. Fractured reservoirs containing a well-connected fracture network are the focus of this study. However, the rate of oil recovery from these reservoirs has been rather low. Therefore more-accurate reservoir simulation is required for efficient exploitation of naturally fractured reservoirs.

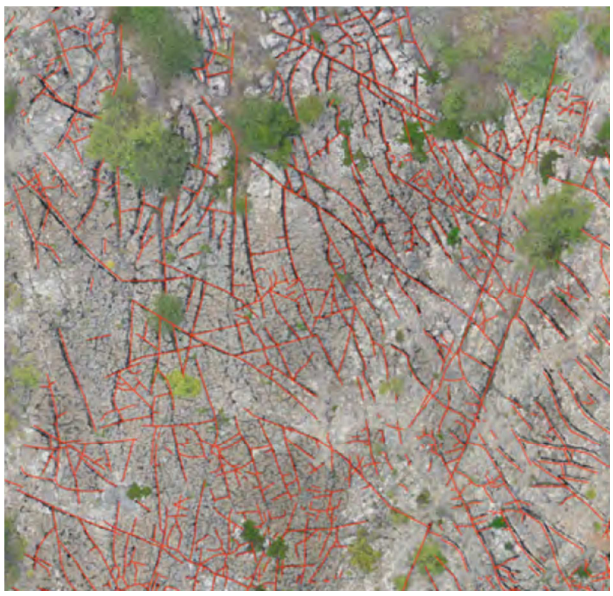

***Figure 1.1*** *Example of a fracture network outcrop (Bisdom 2016) .*

Geological information is required to generate reliable models for fractured-reservoir simulation. Reservoir simulation is one of the most practical methods for studying flow problems. The discrete fracture model (DFM) is one approach for simulating flow in fractured reservoirs. DFM accounts explicitly for the effect of individual fractures on fluid flow (Geiger et al. 2004; Karimi-Fard et al. 2004; Karimi-Fard, Firoozabadi 2003; Kim, Deo 2000; Li, Lee 2008; Li et al. 2009; Matthäi et al. 2007). Previously, the usage of DFM was restricted by the limited information from the subsurface, and the computational effort required to take into account every single fracture. However, nowadays, computing capabilities have increased dramatically, which enables DFM simulation in some cases. Nevertheless, DFM is still computationally too expensive for field-scale reservoir simulation. Also, even if detailed geological information is given, it is difficult to predict the flow pattern through the fracture networks; some simplification is needed.

Field-scale simulation of a reservoir with a well-connected fracture network is often done with dual-porosity/dual-permeability methods (DP/DK) (Moinfar et al. 2011). In the DP/DK concept, the fracture and the matrix systems are treated as separate domains; the interconnected fractures serve as fluid paths between the injection and production wells, while the matrix provides fluid storage for nearby fractures (Fig. 1.2). Limited fluid flow between the matrix blocks is allowed in dual-permeability models (Gilman, Kazemi 1988; Hill, Thomas 1985). The flow between the fracture and the matrix domains is represented by an exchange function which is characterized by a shape factor (Barenblatt et al. 1960; Kazemi et al. 1976; Warren, Root 1963). Although the dual-porosity/dual-permeability models are much-simplified characterizations of naturally fractured reservoirs, for reservoirs with many fractures and a very high degree of interconnection, they are still more feasible than the DFM methods.

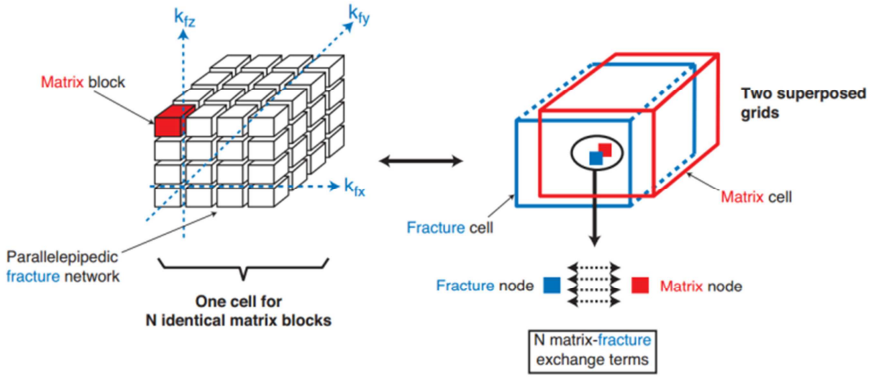


***Figure 1.2*** *Dual-porosity representation of a fractured formation (Lemonnier, Bourbiaux 2010). The dual-porosity/dual-permeability concept can be applied to matrix columns, i.e. without horizontal fractures.*

With the DP/DK approach, average properties are assigned to each grid block, such as porosity, permeability, matrix-fracture interaction parameters (typical fracture spacing or shape factor), etc. (Dershowitz et al. 2000). Therefore, the discrete fracture network considered to generate the DP/DK model parameters is crucial. However, if the fracture network shows non-uniform flow, the characteristic fracture spacing or the shape factor can be ambiguous.

Naturally fractured reservoirs, like all reservoirs, are exploited in two stages: primary recovery and secondary recovery. The oil-recovery mechanisms are different in these two processes. During primary production, fluid is produced mainly by fluid expansion. The pressure drops rapidly in fractures connected to the production well because of their high permeability while, in contrast, the matrix remains at high pressure. This in turn creates a pressure difference between the fracture and the adjacent matrix block and leads to flow of oil from the matrix to the fracture. In this scenario, as long as the fractures are much more conductive than the matrix, one might expect that all the connected fractures are conductive enough to bring oil from the matrix to the production wells. In secondary recovery (or an enhanced oil recovery (EOR) process), the injected water or EOR agent from an injection well reaches the matrix through the fractures, while the oil residing in the matrix flows into the adjacent fractures and then to a production well. Since the fractures have much higher permeability than the matrix, the injected water or EOR agent invades the fractures much faster than the matrix. The injected agent rapidly flows through the fracture network and surrounds a matrix block. If the matrix block has water-wet characteristics, water imbibes into the matrix block because of capillary pressure. Oil residing in the matrix block in turn flows into adjacent fractures by co-current imbibition or counter-current imbibition (Ramirez et al. 2009). Oil recovery, of course, requires that fractures carry injected agent to the adjacent matrix. The size of matrix blocks formed by the fractures plays a significant role in fluid exchange between the matrix and the fractures. If fractures do not carry a significant portion of injected water or EOR agent, it is questionable whether they should be included in defining the size of matrix blocks.

Shape factor is the heart of dual-porosity/dual-permeability flow modeling. It characterizes the geometry and boundary conditions of the matrix blocks. Different recovery mechanisms in primary and secondary production suggest that the relevant fracture spacing or the shape factor for the dual-porosity/dual-permeability simulation should depend on the process involved. Specifically, it should be different for primary and for secondary or tertiary recovery.

## 1.2 Thesis Outline

This work is aimed at providing further insights into the implications of non-uniform flow in the fracture networks to the dual-porosity/dual-permeability simulation of the fractured reservoirs, and the roles that fractures play in different recovery processes.

This dissertation contains work from several articles which are either already published or are currently under review for publication in peer-reviewed journals. It proceeds as follows.

This introduction serves as **chapter 1**.

**Chapter 2** examines the non-uniform flow in well-connected fracture networks. For simplicity in this initial study, we examine flow in a two-dimensional fractured reservoir, in which the matrix is assumed to be impermeable; fluid can only flow through the connected fracture networks (Fig. 1.3). Two fracture sets that are nearly orthogonal to each other are assumed, with almost equal numbers of fractures in the two sets. The fracture length follows a power-law distribution, and the fracture aperture is described by either a power-law distribution or a log-normal distribution; these are broadly recognized as acceptable representations of the fracture length (de Dreuzy et al. 2001a, b; Nicol et al. 1996; Odling 1997) and the aperture distribution (Barton et al. 1989; Belfield, Sovich 1994; Cacas et al. 1990a; Cacas et al. 1990b; Dverstorp, Andersson 1989; Long, Billaux 1987; Snow 1970; Tsang et al. 1996; Wong et al. 1989) for real fractured formations, respectively. However, we take no explicit account of the effect of geo-mechanical stresses on the fracture length and aperture distributions. Horizontal fractures are not considered in this study.

The results show that even in a well-connected fracture network, far above the percolation threshold, flow may be so unequally distributed that most of the network can be excluded without significantly reducing the effective permeability of the fracture network. Even a well-connected fracture network can behave like a much-sparser network when the aperture distribution is broad enough. We determine how broad the aperture distribution must be to behave in this way. The work presented in chapter 2 is published in *Petroleum Science* (Gong, Rossen 2017).

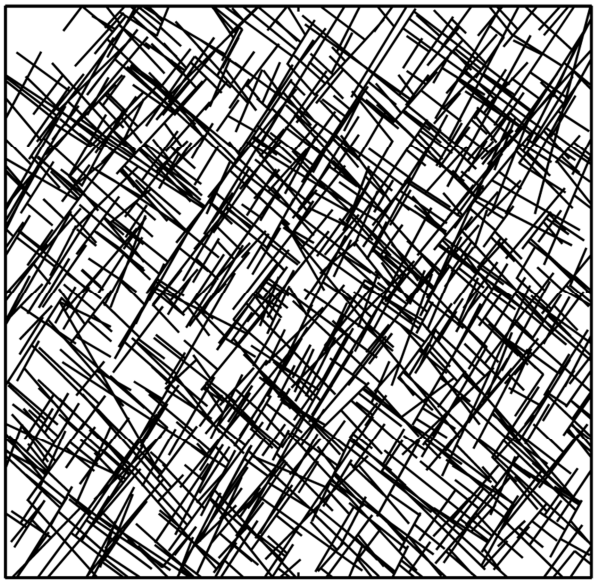

***Figure 1.3*** *Example of a well-connected fracture network studied in this work.*

**Chapter 3** discusses the implications of non-uniform flow in a fracture network for the shape factor for the dual-porosity/dual-permeability simulation. This is a follow-up study to chapter 2; the models used here are the same as the ones adopted in chapter 2. We focus on the influence on the characteristic

matrix-block size caused by eliminating unimportant fractures which carry little flow. We also check the influence of aperture distribution (exponent $\alpha$ in a power-law distribution and standard deviation $\sigma$ in a log-normal distribution) on the characteristic sizes of matrix blocks formed by the dominant sub-network formed by the fractures that carry most of the injected fluid. The characteristic matrix-block radius and length are adopted to represent the characteristic matrix-block size for the matrix blocks of varying shapes and sizes. The equivalent matrix-block size is employed to represent the average value of the resulting distribution of the matrix block sizes. This work is published in *Fuel* (Gong, Rossen 2016).

The results presented in chapters 2 and 3 suggest that the characteristic fracture spacing for the dual-porosity/dual-permeability simulation of waterflood or EOR in a naturally fractured reservoir should account not for all fractures but only the relatively small number of fractures carrying almost all the injected water or EOR agent. In contrast, in primary production, even a relatively small fracture represents an effective path for oil to flow to a production well. This distinction suggests that the "shape factor" in the dual-porosity/dual-permeability reservoir simulation and the repeating unit in homogenization should depend on the process involved. Specifically, it should be different for primary and secondary or tertiary recovery.

**Chapter 4** tests this hypothesis in a simple representation of a fractured region, which can be seen as a grid block in a dual-porosity/dual-permeability model with a non-uniform distribution of fracture-flow conductivities in primary production or a waterflood process. In Particular, we represent a region bounded by primary fractures and penetrated by secondary fractures (also by tertiary fractures in some cases). The primary fractures represent the dominant sub-network which carries most of the injected agent in chapters 2 and 3, and the secondary and, in some cases, tertiary fractures represent the remaining fractures.

We compare oil production, flow patterns in the matrix, and the pattern of oil recovery with and without the "secondary" fractures that carry only a small portion of the injected fluid.

The results show that the role of the secondary fractures depends on a dimensionless ratio of the characteristic times for the matrix and the fracture flow (Peclet number), and the ratio of the flow carried by different fractures. In primary production, for a large Peclet number, treating all fractures equally is a better approximation than excluding the secondary fractures; the shape factor should reflect both the primary and the secondary fractures. For a sufficiently small Peclet number, it is more accurate to exclude the secondary fractures. For waterflood or EOR, in most of the cases examined, the appropriate shape factor or the repeating-unit size should reflect both the primary and the secondary fractures. If the secondary fractures are much narrower than the primary fractures, then it is more accurate to exclude them. Yet-narrower "tertiary fractures" are not always helpful for oil production, even if they are more permeable than the matrix. They can behave as capillary barriers to imbibition, reducing oil recovery.

We present a new definition of Peclet number for primary and secondary production in fractured reservoirs that provides a more accurate predictor of the dominant recovery mechanisms in fractured reservoirs than the previously published definition.

The work presented in this chapter has been submitted to *Fuel*.

Finally, the main conclusions of this work are drawn in **chapter 5**, along with recommendations for further research on fractured reservoirs.

Note from the author: This text includes published papers in reviewed journals and scientific conferences. Consequently, the reader may find similar texts and sentences in some parts of the thesis.

# 2

# MODELING FLOW IN NATURALLY FRACTURED RESERVOIRS: EFFECT OF FRACTURE APERTURE DISTRIBUTION ON DOMINANT SUB-NETWORK FOR FLOW

The content described in this chapter is also published in : Gong, J. and Rossen, W.R. Modeling flow in naturally fractured reservoirs: effect of fracture aperture distribution on dominant sub-network for flow. Pet Sci. 2017;14(1):138-54. doi:10.1007/s12182-016-0132-3.

## 2.1 Introduction

A large number of oil and gas reservoirs across the world are naturally fractured, from which significant oil and gas are produced (Saidi 1987). Efficient exploitation of these reservoirs requires accurate reservoir simulation. Naturally fractured reservoirs, like all reservoirs, are exploited in two stages: primary recovery and secondary recovery (sometimes followed by tertiary recovery, i.e. enhanced oil recovery (EOR)), with different recovery mechanisms. During primary production, the reservoir is produced by fluid expansion. In secondary production and EOR, since the fractures are much more permeable than the matrix, the injected water or EOR agent flows rapidly through the fracture network and surrounds the matrix blocks. Oil recovery then depends on efficient delivery of water or EOR agent to the matrix through the fracture network. Dual-porosity/dual-permeability models are still the most widely used methods for field-scale fractured-reservoir simulation, as they address the dual-porosity nature of fractured reservoirs and are computationally cheaper, although they are much-simplified characterizations of naturally fractured reservoirs. To generate a dual-porosity/dual-permeability model, it is necessary to define average properties for each grid cell, such as porosity, permeability, matrix-fracture interaction parameters (typical fracture spacing, matrix-block size or shape factor), etc. (Dershowitz et al. 2000). Therefore, the fracture network used to generate the dual-porosity model parameters is crucial. Homogenization and other modelling approaches likewise require one to designate a typical fracture spacing (Salimi 2010). The hierarchical fracture model (Lee et al. 2001) also requires that one define effective properties of the matrix blocks and fractures which are too small to be represented explicitly.

This chapter is the first part of a three-part study showing that the appropriate characterization of a fractured reservoir differs with the recovery process. In this chapter, we show that even in a well-connected fracture network, far above the percolation threshold, flow may be so unequally distributed that most of the network can be excluded without significantly reducing the effective permeability of the fracture network. The implications of this finding for characterization of naturally fractured reservoirs are the subject of parts two and three. Briefly, in primary production, any fracture much more permeable than the matrix provides a path for escape of fluids, while in waterflood or EOR, the fractures that carry most injected water or EOR agent play a dominant role. In this chapter we restrict our attention to flow of injected fluids, as a first step toward modeling recovery processes that depend on contact of injected fluids with matrix.

Field studies and laboratory experiments show flow channeling in individual fractures and highly preferential flow paths in fracture networks (Neretnieks 1993; Neretnieks et al. 1982; Tsang, Neretnieks 1998). Cacas et al (1990a; 1990b) proposed that a broad distribution of fracture conductivities is the main cause of the high degree of flow channeling. In order to understand these phenomena, many theoretical studies have been done. The separate influences of fracture-network connectivity distributions (Balberg et al. 1991; Berkowitz 1995; Berkowitz, Balberg 1993; Berkowitz, Scher 1997, 1998; de Dreuzy et al. 2001a; Hestir, Long 1990; Robinson 1983, 1984) and fracture-conductivity distributions (Charlaix et al. 1987; Nordqvist et al. 1996; Tsang, Tsang 1987; Tsang et al. 1988) on flow channeling have been considered, and also the interplay of these two key factors (de Dreuzy et al. 2001b; de Dreuzy et al. 2002; Margolin et al. 1998). Berkowitz (2002) further pointed out that even a well-connected fracture network can exhibit sparse preferential flow paths if the distribution of fracture conductivities is sufficiently broad. Katz and Thompson (1987) proposed a similar finding for pore networks. Although the “unimportant” fractures carry little flow, they still can be important to the connectivity and the preferential flow paths. It is not clear whether one can eliminate those “unimportant” fractures without significantly affecting the flow properties of the fracture network. Also, how broad the distribution of fracture conductivities must be to obtain this result is still an open question.

We propose that, for the dual porosity/dual permeability simulation of a waterflooding process or EOR or in homogenization, for the purpose of modeling the fluid exchange between fractures and matrix blocks, only the sub-network which carries by far most of the injected water is of primary importance in

characterizing the reservoir. It is important to understand the factors that influence the sub-network. Since the effect of fracture connectivity on flow properties of fracture networks is well discussed, we focus here on the influence of fracture aperture (i.e. fracture conductivity) distribution.

As the first step in our research, in this work, we systematically study the influence of the fracture aperture distribution on the dominant sub-network for flow. In this work, we define "the dominant sub-network" as the sub-network obtained by eliminating a portion of fractures while retaining 90% of the original-network equivalent permeability. In other words, we are interested in how broad the aperture distribution must be that a well-connected fracture network can exhibit a sparse dominant sub-network with nearly the same permeability. The properties of the dominant sub-network are also examined. If the fracture network is poorly connected, i.e. near the percolation threshold, it is well established that only a small portion of the fractures connects the injection well and the production well. Here we focus on well-connected fracture networks. Since information on fracture apertures, especially in the subsurface, is limited, we test power-law distributions (from narrow to broad), log-normal distributions (from narrow to broad), and one case in which the aperture is proportional to the fracture length.

This report is organized as follows: In Section 2, we introduce the numerical model and the research process of this study. In Section 3 we analyze the dominant sub-network. In Section 4, the possibility of identifying the dominant sub-network without doing flow simulations is discussed. Our conclusions are summarized in the last section.

## 2.2 Numerical Model & Research Process

### 2.2.1 Numerical Model

For simplicity in this initial study, we examine flow in a quasi-two-dimensional fractured reservoir. We use the commercial fractured-reservoir simulator FracMan™ (Dershowitz et al. 2011) to generate fracture networks. A 3D fracture network is generated in a 10 m × 10 m × 0.01 m region. The shape of each fracture is a rectangle. Each fracture is perpendicular to the plane along the flow direction and penetrates the top and bottom boundaries of the region. The Enhanced Baecher Model (Dershowitz, Einstein 1988) is employed to allocate the location of fractures. Two fracture sets which are nearly orthogonal to each other are assumed, with almost equal numbers of fractures in the two sets.

Because of the uncertainties in data and the influence of cut-offs in measurements, in previous studies fracture-trace lengths have been described by exponential, log-normal and power-law distributions (Bour, Davy 1997; Rouleau, Gale 1985; Segall, Pollard 1983). Currently, a power-law distribution is assumed by many researchers to be the correct model for fracture length(de Dreuzy et al. 2001a, b; Nicol et al. 1996; Odling 1997), with exponent $\alpha$ ranging from 1.5 to 3.5. As proposed by de Dreuzy, if $\alpha$ is less than 2, flow is mostly channeled into longer fractures. On the other hand, if $\alpha$ is larger than 3, fracture networks are essentially made up of short fractures. For $\alpha$ in the range 2-3, both long and short fractures contribute to the flow. We set $\alpha$ = 2 which is a reasonable value in the real world. For this value of $\alpha$, both short and long fractures make contribution to the flow through the fracture network. In this study, fracture length follows a power-law distribution ($p(x)$):

$$p(x) = \frac{\alpha-1}{x_{min}}\left(\frac{x_{min}}{x}\right)^{\alpha} \tag{2.1}$$

Where $p(x)$ is the probability density function for a fracture of length $x$, $\alpha$ is the power law exponent (i.e., 2), $x$ is the fracture length and $x_{min}$ the lower bound on $x$, which we take to be 0.2 m. We truncate the length distribution on the upper end at 6 m; thus there are no extremely short or long fractures. In particular, the opposite sides of our region of interest cannot be connected by a single fracture. Since even the smallest fracture is much taller than the thickness of the region of interest (0.01 m), and there is no change of the model on Z direction, the 3D model is in essence a 2D fracture network.

For fracture apertures, we adopt two kinds of distribution which have been proposed in previous studies: power-law and log-normal. In each kind of distribution, a range of parameter values are examined. The aperture is randomly assigned to each fracture. In the case where the aperture is proportional to the fracture length, the fracture aperture follows the same power-law distribution as fracture length. The details of the aperture distribution are introduced below.

To focus on the influence of fracture aperture distributions on the dominant sub-network, except for the aperture distribution, all the other parameters remain the same for all the cases tested in this study, including fracture length, orientation, etc.

### 2.2.2 Flow Simulation Model

We assume that a fracture can be approximated as the slit between a pair of smooth, parallel plates; thus the aperture of each fracture is uniform. The dependence of fracture permeability ($k$) on aperture ($d$) is defined as: $k = d^2/12$, where $k$ is defined based on the cross-sectional area of the fracture. Steady-state flow through a 10 m ×10 m × 0.01 m fractured rock mass is considered. In this chapter, we assume that fracture permeability is much greater than matrix permeability, which is common in fractured reservoirs (van Golf-Racht 1982; Nick et al. 2011). The flow regimes of highly fractured rock mass can be characterized by the fracture-matrix permeability ratio. If the ratio is greater than $10^5$ - $10^6$, fractures carry nearly all the flow (Matthai, Belayneh 2004; Matthai, Nick 2009). Since we are interested in the non-uniform flow in well-connected fracture networks, for simplicity we assume that the matrix is impermeable; fluid flow takes place only in the fracture network. For computing flow in discrete fracture networks, as in most numerical simulation methods, Darcy's Law for steady-state incompressible flow is employed, and mass is conserved at each intersection of fractures. In our models, we induce fluid flow from the left side to the right side by applying a constant difference in hydraulic head across the domain while all the other boundaries are impermeable. The equivalent permeability of the fracture network $K$ (in $m^2$) is defined by

$$K = \frac{Q/L \cdot W}{\Delta h/L} \cdot \frac{\mu}{\rho g} \tag{2.2}$$

Where $Q$ is the volumetric flow rate ($m^3/s$), $L$ the length of square region (m), and $W$ the thickness of the region (m), $\mu$ the fluid viscosity (Pa·s), $\rho$ the fluid density ($kg/m^3$), $g$ the acceleration due to gravity ($m/s^2$) and $\Delta h$ the difference in hydraulic head between inflow and outflow boundaries; in petroleum engineering, this is equal to $\Delta p/\rho g$, where $\Delta p$ is the pressure difference (Pa). Mafic™, a companion program of FracMan™, is employed to simulate flow in the fracture networks.

### 2.2.3 Methodology

As mentioned above, we believe that when the aperture distribution is broad enough, there is a dominant sub-network which approximates the permeability of the entire fracture network. Our main interest lies in examining the influence of the aperture distribution (the exponent $\alpha$ in a power-law distribution and the standard deviation $\sigma$ in a log-normal distribution) on the dominant sub-network. Countless criteria can be used to decide which portion of fractures to remove, such as fracture length, aperture, [length × aperture], velocity, etc. Here we choose a criterion based on the flow-simulation results. Mafic™ subdivides the fractures into finite elements for the flow calculations. The flow velocity at the center of each finite element and the product of flow velocity and aperture ($Q_{nodal}$) can be obtained. Based on this value, we compute the average value ($Q$) of all the elements in each fracture. $Q$ is then used as the criterion to eliminate fractures: fractures are eliminated in order, starting from the one with the smallest value of $Q$ to the one with the largest value of $Q$. After each step, we calculate the

equivalent network permeability of the truncated network. It should be noted that the elimination of fractures is based on the flow in the original fracture network, not the truncated network.

We also describe the properties of the "backbone", i.e. the set of fracture segments that conduct flow, specifically its aperture distribution. The backbone is determined by removing fractures which do not belong to the spanning cluster, as well as dead-ends. In other words, the backbone is formed by the fracture segments with non-zero *Q*. The dead ends are often parts of a fracture rather than the entire fracture. In order to describe the properties of the conducting backbone, we reduce the fracture network to its backbone at the start, and at each step after eliminating fractures.

Because the generation of the fracture network is a random process, an infinite number of fracture networks could be generated with the same parameter values for the density, orientation, fracture length and the aperture distribution. In this study, for each set of parameter values, we generate one hundred realizations.

### 2.2.4 Percolation Theory

Percolation theory is a powerful mathematical tool to analyze transport in complex systems (Aharony, Stauffer 2003; Sahimi 2011). It has been widely used to describe the connectivity and the conductivity of fracture networks.

Our research focuses on well-connected fracture networks, so we employ percolation theory here to analyze the connectivity of the initial fracture network, to illustrate how far above percolation threshold, and how well-connected, the initial fracture network is.

The simplest percolation models are site percolation and bond percolation, in which sites or bonds on an infinite lattice are occupied and open to flow with a probability *p*. To analyze a fracture network, continuum percolation is more applicable, in which fractures can be placed anywhere and can be of variable length. To analyze the connectivity of a fracture network using percolation theory, one must choose a parameter equivalent to the occupancy probability used in site or bond percolation. Different choices have been considered in previous studies. The first is the average number of intersections per fracture (Robinson 1983). A second is the number of factures in the system (Balberg et al. 1991; Berkowitz 1995). A third is the dimensionless density, defined as $p = Nl^2/L^2$, where *N* is the number of fractures, *l* is the (uniform) fracture length and *L* is the system size (Bour, Davy 1997). A fourth choice is the probability that a point is within the effective area of a fracture (Masihi et al. 2005; Masihi et al. 2008). As the fracture networks used in this study are generated using the Enhanced Baecher Model, in which the fracture centers are located using a Poisson process, we choose the fourth option described above as the percolation parameter *p* :

$$p = 1 - \exp\left(\frac{-N\langle a_{ex}\rangle}{4L^2}\right) \tag{2.3}$$

where *N* is the number of fractures in the system and $\langle a_{ex}\rangle$ is the average excluded area. Excluded area is defined as the area around a fracture in which the center of other fractures cannot lie in order to ensure the fractures do not intersect (Balberg et al. 1984). For fracture networks comprising two orthogonal fracture sets of uniform fracture length *l*, the average excluded area is defined as (Belayneh et al. 2006).

$$\langle a_{ex}\rangle = l^2/2 \tag{2.4}$$

Masihi *et al.* (2008) proposed that if a fracture network has a distribution of fracture lengths, its connectivity is identical to that of a system with fixed fracture length equal to the so-called effective length $l_{eff}$, which is the root-mean-square fracture length:

$$l_{eff}{}^2 = \langle l^2 \rangle \tag{2.5}$$

The percolation threshold $p_c$ is the value at which a cluster of fractures connects the opposite sides of the region. The threshold value is affected by the position, the orientation, and the length distribution of fractures, the system size, etc. Masihi *et al.* (2008) studied the percolation threshold of fracture networks with different fracture-length distributions and different system sizes. For fracture networks generated in a 10 m × 10 m region with random orientation, when the length follows a power-law distribution with exponent $\alpha$ = 2, they proposed that the percolation threshold is around 0.66. In our case, the system size and the power-law exponent are consistent with their work, but the fractures are not randomly orientated, but in two perpendicular sets. As suggested by Masihi *et al*. (2005; 2008), the percolation threshold for a fracture network with two perpendicular fracture sets is lower than that for a model with randomly oriented fractures. Also, the truncation of the fracture-length distribution impacts the threshold value. Since the percolation threshold value is not our focus, here we consider 0.5 to 0.7 as a reasonable estimate of the percolation threshold. For the cases we study here, the value of the percolation parameter $p$ of initial fracture networks is around 0.9. Considering the definition of $p$ in Eq. (2.4), a value $p$ = 1 corresponds to infinite fracture density (zero probability of not intersecting another fracture). Thus our fracture network is far above the percolation threshold and is well-connected.

## 2.3 Identifying the Dominant Sub-Network Based on Flow Simulation Results

### 2.3.1 Models without Correlation between Fracture Aperture and Length

**Power-Law Aperture Distribution.** Some field observations and experimental studies show that a power-law distribution can describe the fracture-aperture distribution, although the available data is limited, especially from subsurface populations (Barton et al. 1989; Wong et al. 1989; Barton, Zoback 1992; Belfield, Sovich 1994; Marrett 1996). The power-law probability density function for aperture $d$ is:

$$p(d) = d^{-\alpha} \tag{2.6}$$

If the power-law aperture distribution is described by Eq. (2.6), the studies cited above find that the value of the exponent $\alpha$ in nature is 1, 1.1, 1.8, 2.2, or 2.8. In this study, the power-law aperture distribution with a lower bound follows the form of Eq. (2.1), in which $\alpha$ should be larger than 1. To include the entire range of feasible cases (from narrow to broad aperture distribution), here we examine $\alpha$ in the range from 1.001 to 6. In each case, the fracture aperture is limited to the interval between 0.01 mm and 10 mm. Because of this truncation, as the exponent $\alpha$ increases from 1 to 6, the fracture apertures concentrate in a narrow range near the lower limit (Fig. 2.1). For $\alpha$ = 1.001, the apertures occupy the entire range from 0.01 mm to 10 mm: the difference between the smallest and the largest aperture is nearly three orders of magnitude. For $\alpha$ = 4 to 6, most apertures lie between 0.01 mm and 0.03 mm. The absolute magnitude of aperture is not important in the dimensionless results to follow, but a narrow range of apertures does affect the results.

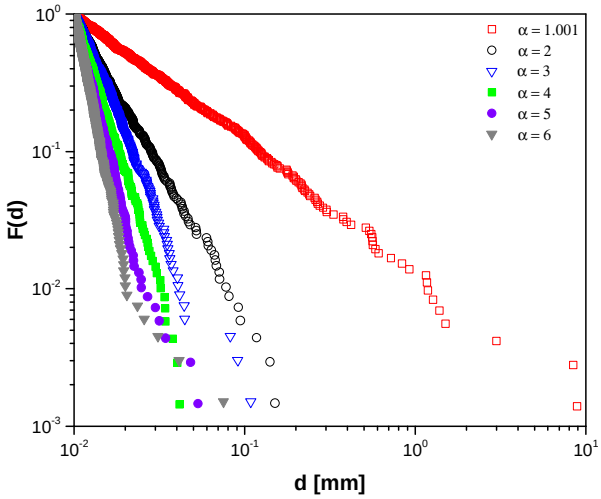


***Figure 2.1*** *The fraction of fractures* F *with aperture (*d*) larger than the given value, for power-law distributions with different values of the exponent α.*

In this chapter, we mainly show the results for $\alpha$ with values 1.001, 2, and 6. The results for $\alpha$ with additional values examined in this study can be found elsewhere (Gong, Rossen 2015).

After running flow simulations on the percolation cluster of the original fracture network, we determine the value of $Q$ for each fracture. The fractures with the smallest $Q$ are eliminated first, then the larger ones. After a given number (10) of fractures are eliminated, we calculate the permeability of the remaining network and the cumulative length of the conducting backbone, $l_b$, in that network. We then eliminate 10 more fractures and repeat until the network becomes disconnected. The normalized equivalent permeability of the truncated fracture network is shown in Fig. 2.2 for all 100 realizations for $\alpha$ with values 1.001, 2, and 6. The scatter in Fig. 2.2 reflects differences among the realizations. The red curve in each case shows the average trend through the 100 realizations. Figure 2.3 compares this average trend for the different values of $\alpha$ ($\alpha$ = 1.001 to 6). The results show that for all of the cases, a portion of fractures can be eliminated without significantly affecting the overall network permeability. Especially when the power-law aperture distribution exponent $\alpha$ = 1.001, the cumulative length of the conducting backbone of the truncated fracture network which retains 90% of the original-network equivalent permeability is roughly 30% of the total fracture length of the original fracture network. That is, there is a sparse sub-network which carries almost all the flow and can be a good approximation of the original fracture network. We call this sub-network retaining 90% of the original equivalent permeability the dominant sub-network. As exponent $\alpha$ increases from 1.001 to 6, the dominant sub-network becomes denser, and the length of the pathway becomes longer. For $\alpha$ = 2, about 50% of fracture length can be removed while remaining 90% of the original permeability. In the case of $\alpha$ = 6, the cumulative length of the conducting backbone of the dominant sub-network is around 60% of the total length of the original fracture network. It is worth noting that the largest ratio of $l_b/l_o$ for all the cases is around 0.8, reflecting the length of dangling and dead-ends in the original fracture network, which represents about 20% of its total length.

If we compare cases with aperture distributions from narrow to broad, we find that when the aperture distribution is broad ($\alpha \leq 2$), most of fractures can be eliminated without significantly affecting the equivalent permeability: the fracture network behaves as a sparser sub-network. As the aperture distribution becomes narrower ($\alpha$ increase from 1.001 to 6), to retain a certain percent of the original fracture network permeability, more fractures are needed (Fig. 2.3).

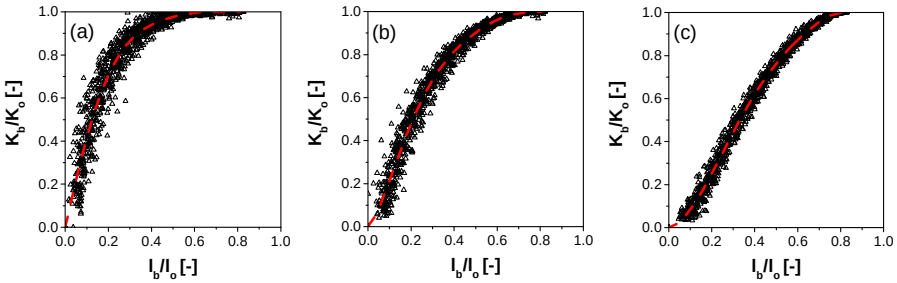


***Figure 2.2*** *Sub-network equivalent permeability ($K_b$) normalized by the equivalent permeability of the original fracture network ($K_o$), plotted against the length of the backbone of the truncated fracture network ($l_b$) normalized by the total length of the original fracture network ($l_o$): power law aperture distributions with (a) α = 1.001, (b) α = 2, (c) α = 6. Results of 100 realizations shown for each value of α. Red curve is the average trend curve.*

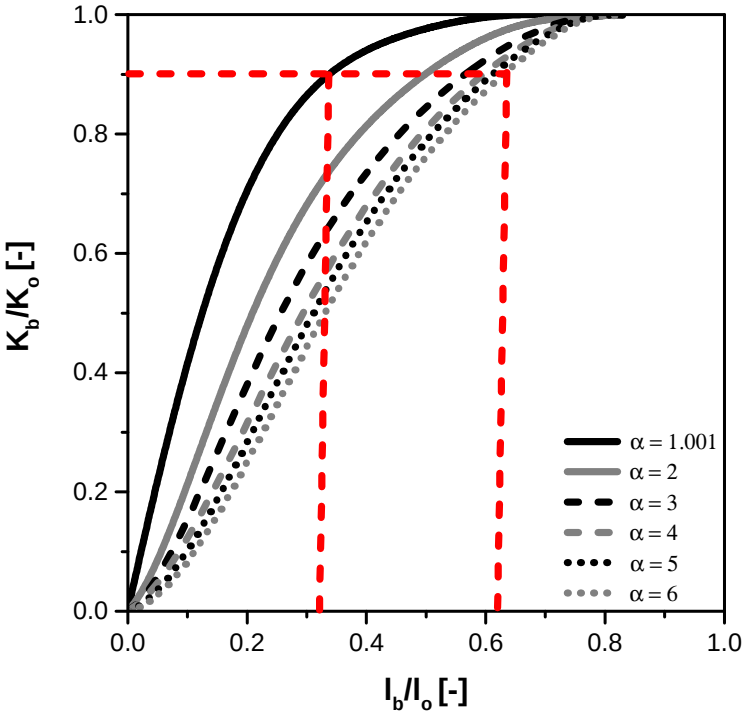


***Figure 2.3*** *Average curves from Fig.2.2, including additional values of* α.

In the network, some subsets of fractures do not participate in fluid flow; these are known as dead-end or dangling fractures. To identify the flow structure in fracture networks, the backbone of the original fracture network and its sub-network are determined by removing fractures which do not belong to the spanning cluster, as well as dead-ends (Fig. 2.4). As presented in Fig. 2.4, the structure of the sub-network that retains 90% of the original equivalent network permeability depends on $\alpha$. For $\alpha$ = 1.001 (Fig. 2.4b), the backbone is much sparser than that for larger values of $\alpha$, because many more fractures can be removed without reducing the permeability greatly.

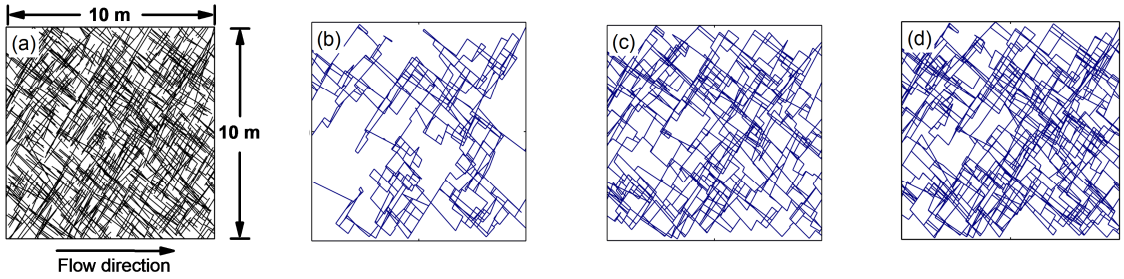


***Figure 2.4*** *(a) One realization of the fracture network examined in this study. The size of the fractured region is 10 m × 10 m × 0.01 m. The left and right boundaries are each at fixed hydraulic head; the difference in hydraulic head is 1 m. Water flows from left to right; the top and bottom edges are no-flow boundaries. (b) Dominant sub-network for one realization with a power-law aperture distribution with* α *= 1.001. (c) Dominant sub-network for one realization with a power-law aperture distribution with* α *= 2. (d) Dominant sub-network for one realization with a power-law aperture distribution with* α *= 6.*

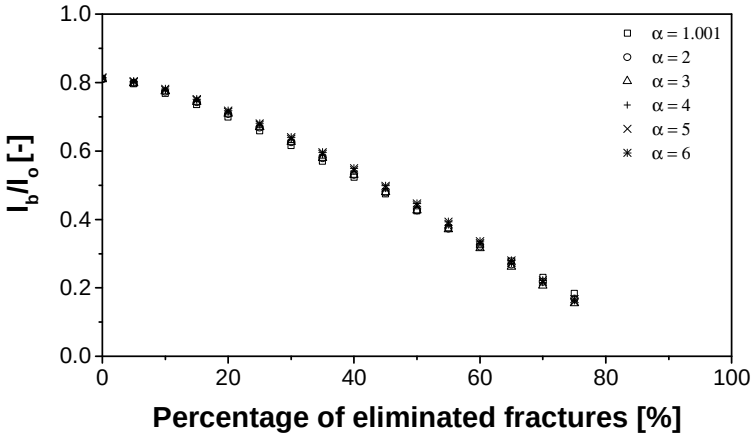


***Figure 2.5*** *Length of the backbone of the truncated fracture network ($l_b$) normalized by the total length of the original fracture network ($l_o$) plotted against percentage of eliminated fractures, for power-law aperture distributions with exponent* α *= 1.001 to 6. Average trend curve for 100 realizations shown for each value of* α*.*

For this initial study, for simplicity, we chose to study a 10 m × 10 m region with no flow boundaries on top and bottom in Fig. 2.4. As a result, the region near those boundaries shows fewer fractures in the dominant sub-network. However, Fig. 2.4 suggests that the size of the region affected by the boundaries is limited, and that the main conclusion of our work, that most flow passes through relatively few fractures, and the rest fractures can be eliminated without significantly affecting the network permeability is not dependent on finite-size limitations.

The importance of fractures to fluid flow is not simply related to fracture length or fracture aperture. Figure 2.5 shows that when fractures are deleted according to flow-simulation results, the cumulative length of the conducting backbone of truncated fracture networks decreases almost linearly. This shows, for instance, that it is not exclusively short fractures that are eliminated first. The trend is nearly the same for different values of $\alpha$. The length $l_b$ here is not the cumulative length of all fractures with some segment in the backbone, but the cumulative length of all the fracture segments in the backbone. Thus for the original network, the reduction in length by about 20% arises mostly because of eliminating segments, not whole fractures. The plots in Fig. 2.5 end at the point where some sub-networks in the 100 realizations are disconnected entirely.

To understand why the dominant sub-network is sparser when the aperture distribution is broader, we examine one randomly selected realization for each value of $\alpha$ in detail. The only difference among the specific realizations used for different value of $\alpha$ is the aperture distribution. First, we examine the distribution of the values of $Q$ for each fracture in the original fracture network. As presented in Fig. 2.6, when $\alpha$ = 1.001, the fracture network shows strongly preferential flow paths: a small portion of the

fractures carry much more flow than the others. Specifically, the range in *Q* for most fractures in the backbone extends over at least 5 orders of magnitude for $\alpha$ = 1.001 (from 4 through 8 in Fig. 2.6a). For $\alpha$ = 6, the value of *Q* for most fractures lie within a range of about 2 orders of magnitude (from 5 to 7 in Fig. 2.6c). Thus, when the aperture distribution is broad, the equivalent permeability is not strongly affected as the "unimportant" fractures that are eliminated. As the aperture distribution becomes narrower, flow does not concentrate in a small portion of fractures: most fractures play a roughly similar role in the flow, which means fewer fractures can be removed without significantly reducing the equivalent network permeability.

The relationship between the aperture and *Q* for each fracture is shown in Fig. 2.7. The importance of individual fractures to the overall flow properties of fracture networks cannot be simply related to the aperture of each fracture. There are some fractures with small aperture that carry more flow than fractures with larger aperture. This is true for all the cases with aperture distribution, from narrow to broad.

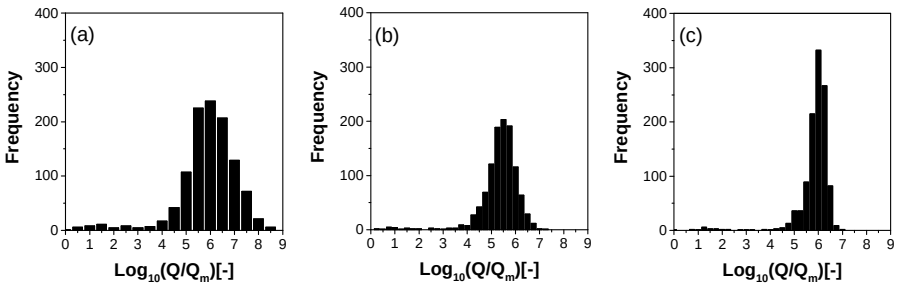


***Figure 2.6*** *Histogram of Q for each fracture normalized by the minimum value of Q for all fractures in the backbone ($Q_m$) in log-10 space: power-law aperture distributions with (a) α = 1.001, (b) α = 2, (c) α = 6. Results of one realization shown for each value of α.*

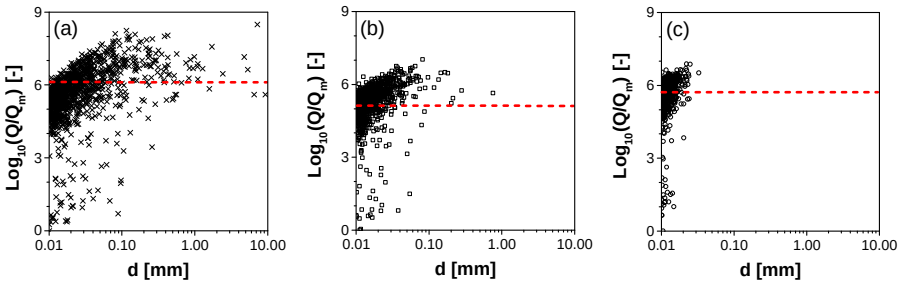


***Figure 2.7*** Q *for each fracture normalized by the minimum value of* Q *for all the fractures in log-10 space plotted against aperture d: power-law aperture distributions with (a)* α *= 1.001, (b)* α *= 2, (c)* α *= 6. Results of one realization shown for each value of* α*. The red dashed line indicates the value of* Q *below which the fractures are eliminated while retaining 90% of the original permeability.*

Similar to the lack of a simple relation between the aperture and *Q*, there is no clear relationship between the fracture length and the flow each fracture carries (Fig. 2.8). There are some relatively long fractures that carry very little flow, and some short fractures playing a more-important role than the longer fractures. Fracture networks with narrow and broad aperture distribution show similar lack of correlation between the fracture length and the flow each fracture carries in Fig. 2.8.

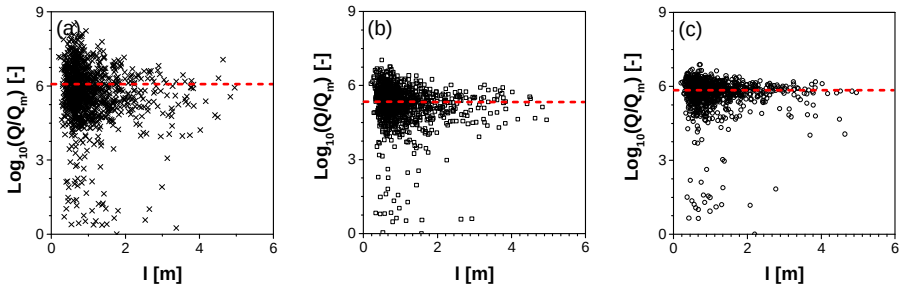


***Figure 2.8*** *Q of each fracture normalized by the minimum value of Q in log-10 space plotted against the fracture length l: power-law aperture distributions with (a) α = 1.001, (b) α = 2, (c) α = 6. Results of one realization shown for each value of α. The red dashed line indicates the value of Q below which the fractures are eliminated while retaining 90% of the original permeability.*

In principle, each individual fracture could play a different role in the original fracture network and the dominant sub-network. Most of the fractures carry nearly the same flow in the original fracture network and the dominant sub-network, however, as shown in Fig. 2.9. This holds for the aperture distribution ranging from narrow to broad. In the dominant sub-network, some fractures carry more flow, and some carry less, compared to the original fracture network. There is no fluid flow through some fractures in the dominant sub-network at all. When some fractures that carry little flow are eliminated from the fracture network, their removal disconnects some other fractures from the backbone. This could happen, for instance, if several fractures carrying little flow feed into one fracture that carries the sum of all their flows. Then the removal of the fractures carrying little flow can lead to the disconnection of a fracture that carries more flow from the backbone. But, in fact, there are relatively few fractures disconnected from the backbone in the dominant sub-network.

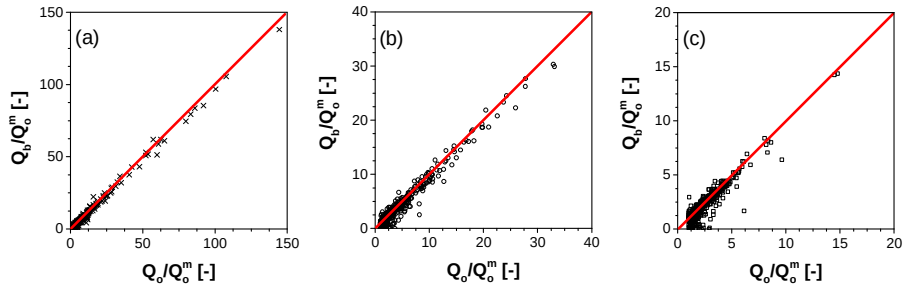


***Figure 2.9*** *Comparison of Q for fractures in the original fracture network ($Q_o$) and in the dominant sub-network ($Q_b$): power-law aperture distributions with (a) α = 1.001, (b) α = 2, (c) α = 6. Both of $Q_o$ and $Q_b$ are normalized by the minimum value of Q in the original fracture network ($Q_o^m$). Results of one realization shown for each value of α.*

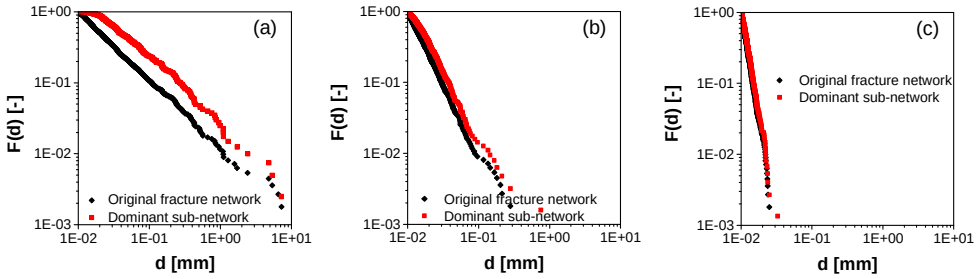


***Figure 2.10*** *Comparison of the aperture distribution of the original fracture network and the dominant sub-network: power-law aperture distributions with (a) α = 1.001, (b) α = 2, (c) α = 6. F(d) is the fraction of fractures with aperture (d) larger than the given value. Results of one realization shown for each value of α.*

Figure 2.10 compares the aperture distribution of the dominant sub-network to that of the original fracture network. The plots are similar to each other, which indicates again that the fractures with small aperture are not systematically removed.

We may summarize our arguments of the cases with power-law aperture distributions as follows. For all of the cases with a power-law aperture distribution, at least a portion of fractures can be eliminated without significantly affecting the effective network permeability. The number of fractures can be removed is strongly affected by the value of $\alpha$, i.e. the breadth of the aperture distribution. The broader the aperture distribution is, the more fractures can be eliminated without significantly affecting the overall flow behavior. When the aperture distribution is broad enough ($\alpha \leq 2$), the original fracture network behaves as a sparse sub-network, and the total length of the fractures in the sub-network is much shorter than that of the original fracture network. The importance of each fracture to the flow behavior of the entire fracture network cannot be simply related to its aperture or length; some fractures with narrow aperture or short length play a more-important role than others with broader aperture or greater length.

**Log-Normal Aperture Distribution.** Some researchers proposed a log-normal distribution for apertures based on field studies and hydraulic tests (Snow 1970; Long, Billaux 1987; Dverstorp, Andersson 1989; Cacas et al. 1990a; Cacas et al. 1990b; Tsang et al. 1996). Fracture-network models with log-normal distributions of apertures have been widely used to simulate experiments and derive theoretical relationships (Charlaix et al. 1987; Feng et al. 1987; Long, Billaux 1987; Dverstorp, Andersson 1989; Cacas et al. 1990a; Cacas et al. 1990b; Tsang et al. 1996; Margolin et al. 1998; de Dreuzy et al. 2001b). The log-normal distribution is specified by the following probability density function:

$$p(d) = \frac{1}{d\log_{10}(\sigma)\sqrt{2\pi}} exp\left\{-\frac{1}{2}\left(\frac{\log_{10}(d)-\mu}{\sigma}\right)^2\right\} \quad (2.7)$$

where $\mu$ and $\sigma$ are the mean and the standard deviation in log-10 space. The truncated log-normal distribution has two additional parameters: a minimum and a maximum value of apertures, which are 0.01 mm and 10 mm, respectively, in this study. Field studies and hydraulic tests found values of $\sigma$ from 0.1 to 0.3, 0.23, and 0.47 (Snow 1970; Dverstorp, Andersson 1989; Tsang et al. 1996). To test the widest range of feasible values, we test values of $\sigma$ from 0.1 to 0.6, as illustrated in Fig. 2.11. As shown in Fig. 2.11, the upper and lower bounds have little effect on these distributions. The aperture distribution becomes broader as $\sigma$ increases from 0.1 to 0.6.

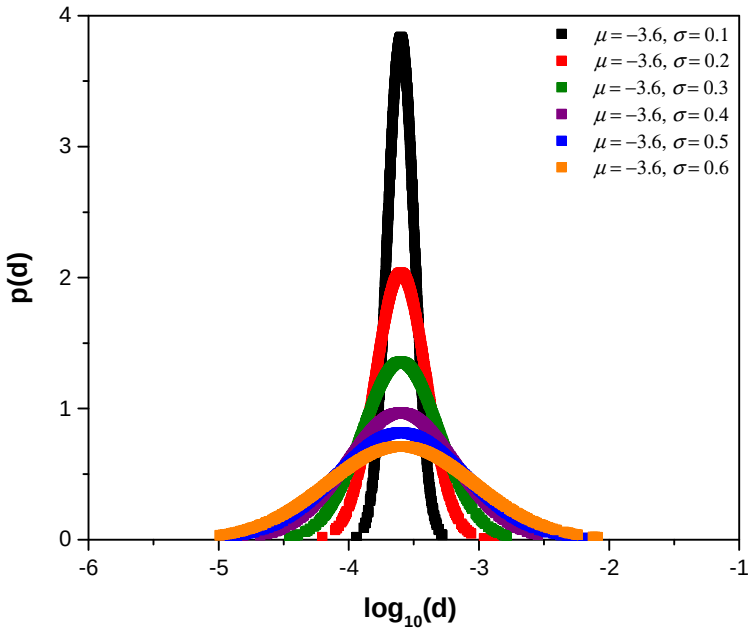


***Figure 2.11*** *Probability density function (*p(d)*) for fracture aperture for log-normal distributions with the same mean value but different standard deviations in log-10 space.*

In this chapter, we mainly show the results for $\sigma$ with values 0.1, 0.4, and 0.5. The results for $\sigma$ with additional values examined in this study can be found elsewhere (Gong, Rossen 2015).

Similar to our approach in dealing with the cases of power-law aperture distributions, first we run flow simulation for each realization, and then eliminate fractures based on the flow-simulation results, starting with the fracture with the smallest *Q*. For each sub-network, the equivalent permeability, the cumulative length of the conducting backbone, and the aperture distribution are calculated. The overall trend of the change of the equivalent permeability is obtained over the 100 realizations for each set of parameter values. Figure 2.12 presents the results for the cases with $\sigma$ = 0.1, 0.4, and 0.5, which are typical values observed in field studies. The broader the aperture distribution, the more fractures can be removed from the system while retaining a given fraction of the original network permeability (Fig. 2.13). For example, to retain 90% of the equivalent permeability of the original network, the cumulative length of the conducting backbone of the dominant sub-network is around 60% of total fracture length of the original fracture network when $\sigma$ = 0.1, while the ratio is roughly 35% and 30% when $\sigma$ = 0.4 and 0.5, respectively. Clearly, the dominant sub-network which retains 90% of the original equivalent permeability is strongly affected by the aperture distribution. When the standard deviation is larger than 0.4, the aperture distribution is broad enough that most fractures can be eliminated without significantly affecting the equivalent network permeability. The conducting backbone of the dominant sub-network is much sparser than that of the original fracture network (Fig. 2.14).

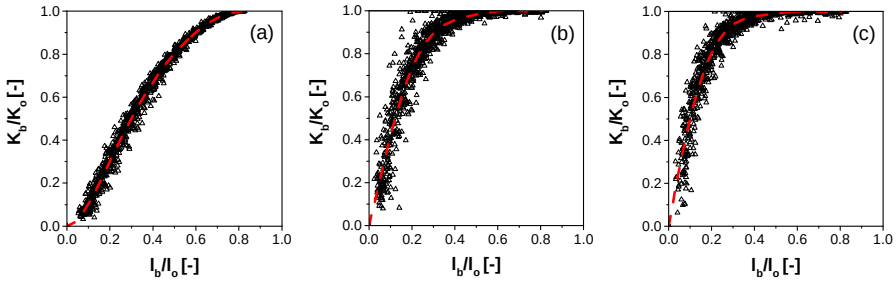


***Figure 2.12*** *Sub-network equivalent permeability ($K_b$) normalized by the equivalent permeability of the original fracture network ($K_o$), plotted against the length of the backbone of the truncated fracture network ($l_b$) normalized by the total length of the original fracture network ($l_o$): log-normal aperture distributions with (a) σ = 0.1, (b) σ = 0.4, (c) σ = 0.5. Results of 100 realizations shown for each value of σ. Red curve is the average trend curve.*

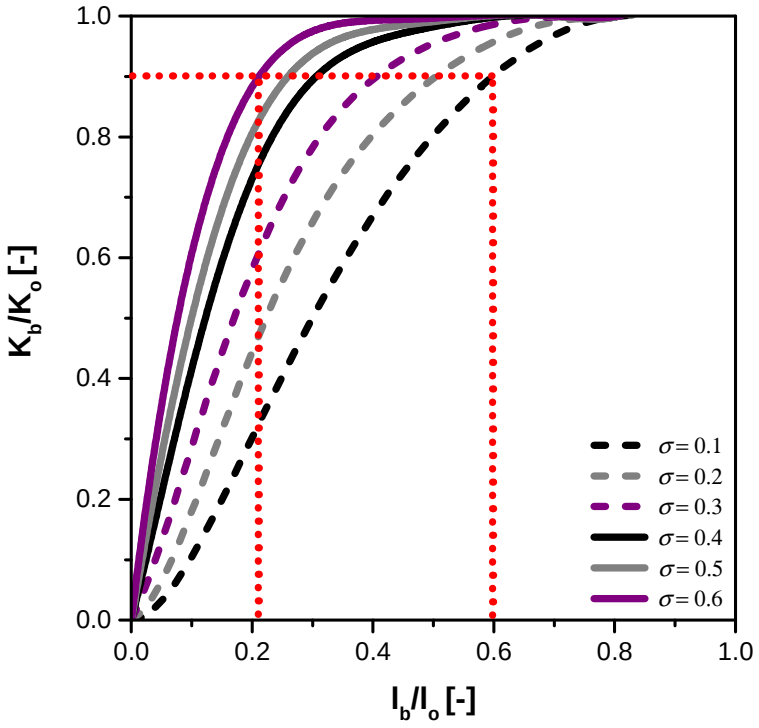


***Figure 2.13*** *Average curves from Fig. 2.12.*

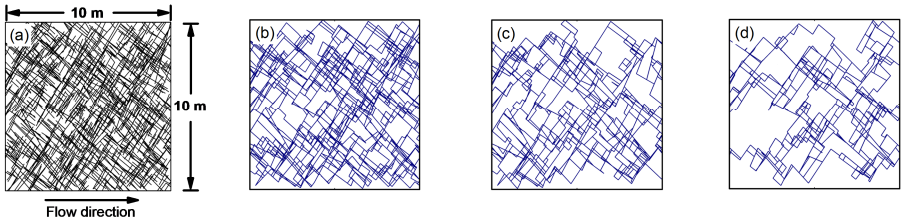


***Figure 2.14*** *(a) One realization of the fracture network examined in this study. (b) Dominant sub-network for one realization with a log-normal aperture distribution with σ = 0.1. (c) Dominant sub-network for one realization with a log-normal aperture distribution with σ = 0.4. (d) Dominant sub-network for one realization with a log-normal aperture distribution with σ = 0.5.*

As with the cases of power-law aperture distributions, in the cases of log-normal aperture distributions, the length of the backbone of sub-networks decreases nearly linearly with increasing portion of fractures being eliminated, based on the flow-simulation results. As in Fig. 2.3, the ratio shown in Fig. 2.15 starts at about 0.8 for zero fractures removed because not all fracture segments in the original network are in the backbone. The plots end at the point where some sub-networks are disconnected entirely.

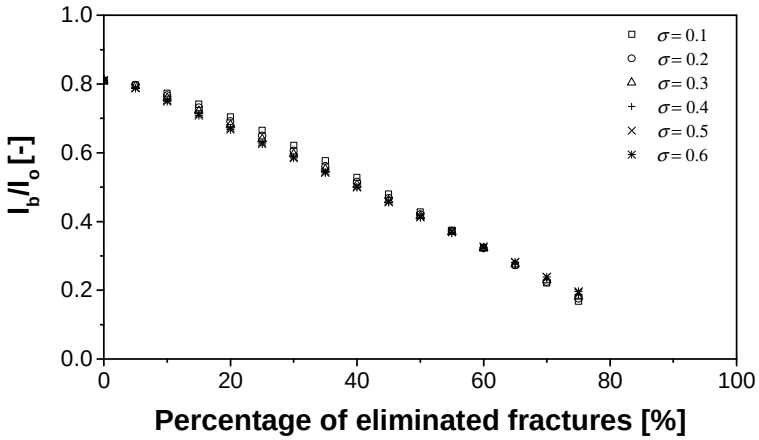


***Figure 2.15*** *Length of sub-network backbone ($l_b$) normalized by the total length of the original fracture network ($l_o$) plotted against the percentage of eliminated fractures, for the cases of log-normal aperture distributions with the same log-mean value but different log-standard deviations (σ) from 0.1 to 0.6. Average trend curve for 100 realizations shown for each value of σ.*

The distributions of *Q* for fractures in the original networks with log-normal aperture distributions are similar to those with power-law aperture distributions (cf. Fig. 2.6). When the aperture distribution is narrow ($\sigma$ = 0.1), the distribution of *Q* is also narrow: most of fractures carry a similar amount of flow. As a result, when a portion of fractures is eliminated, the equivalent network permeability is strongly affected. As the aperture distribution becomes broader, the distribution of *Q* is also broader, and there is a small portion of fractures which carry much more flow than the others. In other words, the fracture network shows stronger preferential flow paths when the aperture distribution becomes broader. Thus, removing a portion of fractures which carry little flow does not greatly reduce the equivalent network permeability, as the fractures that play a more important role are still in the system.

As presented in Fig. 2.16 and Fig. 2.17, the flow behavior of each fracture cannot be simply related to either aperture or length. However, compared to the cases with power-law aperture distributions, we find that for most of the fractures, the overall trend is that fractures with larger aperture tend to carry more flow than those with narrower aperture, which is different from the results for the cases with power-law aperture distributions (cf. Fig. 2.7). We believe a comparison between Figs. 2.1 and 2.11 provides the answer: there are many more small fractures (just above the cut-off for fracture aperture) in the power-law distribution than in the log-normal distribution. It may be that it is just as unlikely for a

narrow fracture to be important in a power-law distribution, but there are so many of them that some of them do play a role.

Similar to the cases of power-law aperture distributions, most fractures carry similar flow when they are in the dominant sub-network and in the original fracture network, which indicates that they behave similarly.

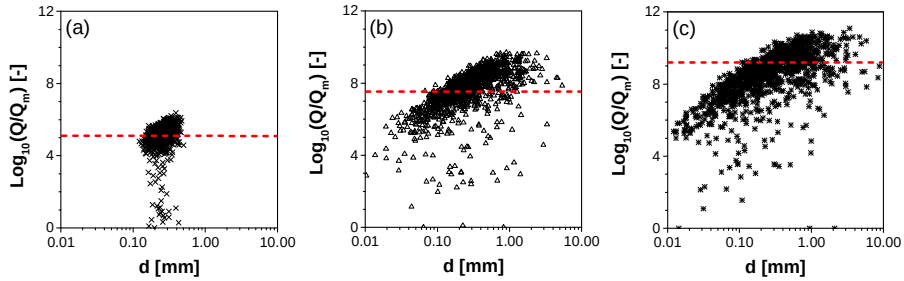


***Figure 2.16*** Q *for each fracture normalized by the minimum value of* Q *for all the fractures in log-10 space plotted against fracture aperture: log-normal aperture distributions with (a)* σ *= 0.1, (b)* σ *= 0.4, (c)* σ *= 0.5. Results of one realization shown for each value of* σ*. The red dashed line indicates the value of* Q *below which the fractures are eliminated in this case.*

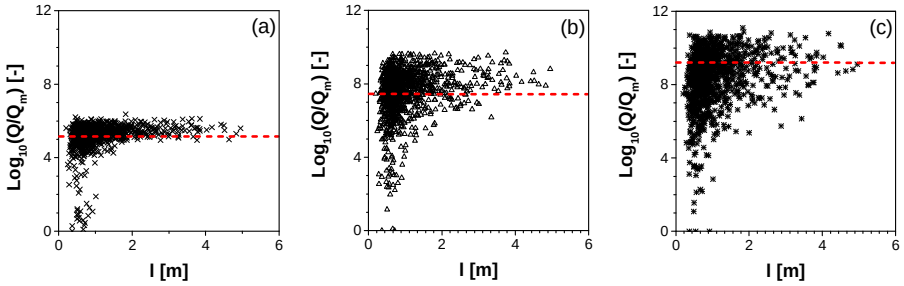


***Figure 2.17*** Q *for each fracture normalized by the minimum value of* Q *for all the fractures in log-10 space plotted against fracture length* l*: log-normal aperture distributions with (a)* σ *= 0.1, (b)* σ *= 0.4, (c)* σ *= 0.5. Results of one realization shown for each value of* σ*. The red dashed line indicates the value of* Q *below which the fractures are eliminated in this case.*

Figure 2.18 presents the aperture distribution of the original fracture network and that of the dominant sub-network for one realization for each value of $\sigma$. Compared to the original fracture network, the dominant sub-network lacks a portion of small fractures which means that fractures with small aperture are eliminated systematically. The aperture distributions are different from each other.

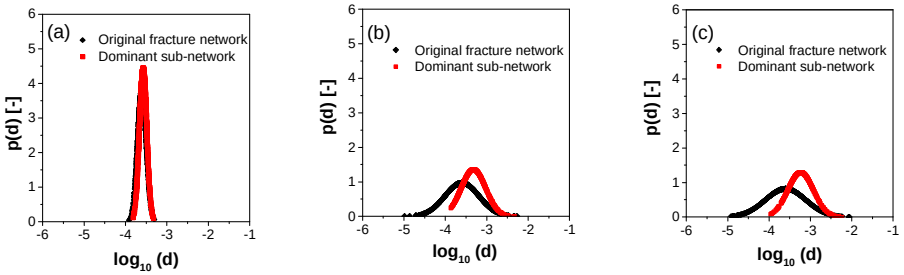


***Figure 2.18*** *Comparison of aperture distribution for the original fracture network and the dominant sub-network: log-normal aperture distributions with (a)* σ *= 0.1, (b)* σ *= 0.4, (c)* σ *= 0.5.* p(d) *is the probability density function. Results of one realization shown for each value of* σ*.*

In sum, for the log-normal aperture distributions, we conclude that when the aperture distribution is broad enough ($\sigma \geq 0.4$), most of fractures can be taken out without significantly affecting the equivalent network permeability. In contrast to the cases of power-law aperture distributions, the fractures with

larger aperture tend to play a more important role for the flow behavior of the fracture network, although the flow carried by each fracture cannot be simply related to the fracture aperture.

### 2.3.2 Aperture Proportional to Fracture Length

Field measurements and theoretical studies raise the possibility of a relationship between fracture aperture and fracture length (Stone 1984; Hatton et al. 1994; Vermilye, Scholz 1995; Johnston, McCaffrey 1996; Renshaw, Park 1997). Both nonlinear and linear relationships have been proposed in previous studies based on elastic theory and field data. Here we assume that the aperture of each fracture is uniform and proportional to fracture length:

$$d = Cl \tag{2.8}$$

where $d$ is aperture, $C$ is an empirical coefficient, and $l$ is fracture length. Vermilye and Scholz (1995) suggested the empirical coefficient lies between $1\times10^{-3}$ and $8\times10^{-3}$ Here for the Mafic$^{TM}$ flow calculations we use $2\times10^{-3}$. However, since we normalize the properties of the sub-network by those of the original fracture network, the value of $C$ is unimportant to what follows.

As mentioned above, all the cases we test in this study follow a power-law length distribution with exponent $\alpha = 2$, which is truncated between 0.2 m and 6 m. Since in this section aperture is proportional to fracture length, the apertures also follow a power-law distribution with exponent $\alpha = 2$, and lie in the range of 0.4 mm to 12 mm. For the case described above with $\alpha = 2$ and aperture independent of fracture length, the apertures lie mostly in the range of 0.01 mm to 0.1 mm. Whether or not aperture is dependent on fracture length, the difference between the smallest and the largest value is nearly one order of magnitude, although the absolute values are different. The absolute value does not matter to the normalized results presented below.

Figures 2.19 and 2.20 show the sub-network equivalent permeability after elimination of a portion of fractures, where the aperture is, respectively, proportional to and independent of the fracture length respectively. In the two types of cases, the overall flow behavior is roughly similar and the cumulative length of the conducting backbone of the dominant sub-networks are approximately 50% of the total fracture length separately.

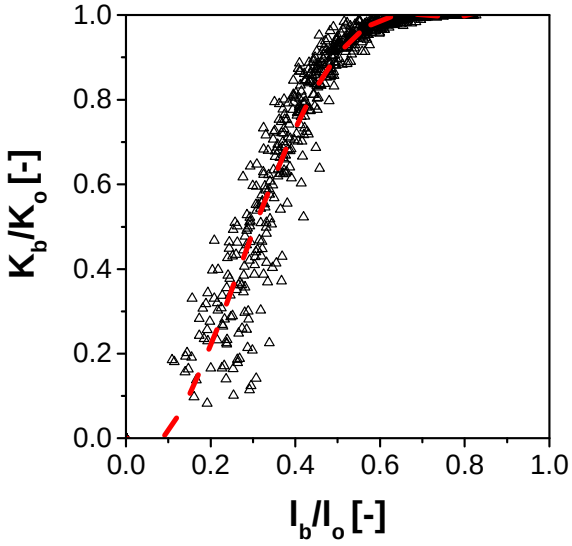


***Figure 2.19*** *Sub-network equivalent permeability ($K_b$) normalized by the equivalent permeability of the original fracture network ($K_o$), plotted against the length of the backbone of the truncated fracture network ($l_b$) normalized by the total length of the original fracture network ($l_o$): aperture is proportional to fracture length. Results of 100 realizations shown. Red curve is the average trend curve.*

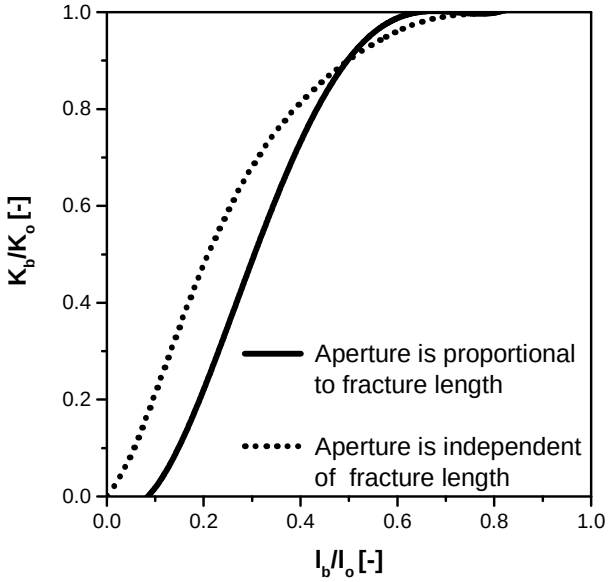


***Figure 2.20*** *Average curves from Fig. 2.2b and Fig. 2.19 .*

Figure 2.21 presents the distribution of *Q* among fractures for one realization where aperture is proportional to fracture length. The values of *Q* distribute more broadly when aperture is proportional to fracture length than when aperture is independent of fracture length (cf. Fig. 2.6b). In this realization, the original fracture network has 1120 fractures and the sub-network has 633 fractures when the aperture is independent of the length, but only 217 fractures when the aperture is proportional to the fracture length: similar cumulative length, but fewer fractures. This indicates that shorter fractures are eliminated preferentially.

Figure 2.22 shows the relationships between aperture and *Q*, which shows that, although there are some fractures with small aperture (shorter fractures) that carry a lot of flow, the overall trend is that fractures with larger aperture (and greater length) tend to carry more flow.

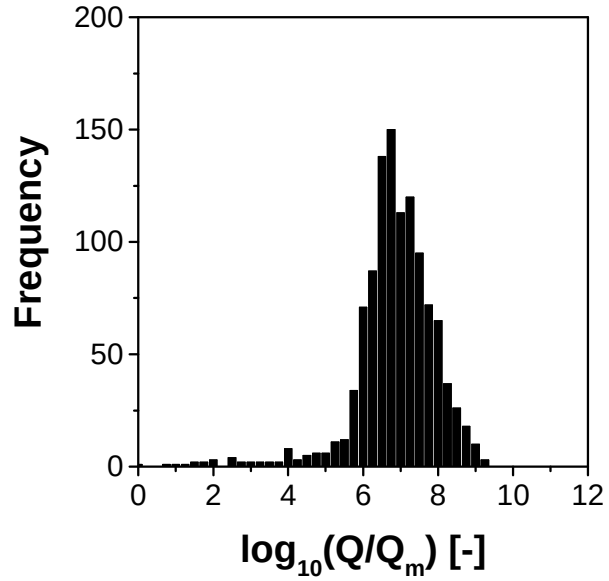


***Figure 2.21*** *Histogram of* Q *of each fracture normalized by the minimum value of* Q *of all the fractures in log-10 space: aperture is proportional to fracture length. Results of one realization shown.*

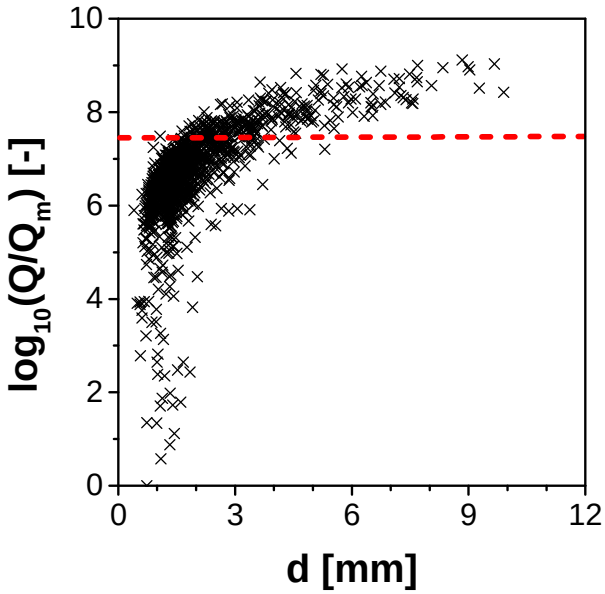


***Figure 2.22*** *Q of each fracture normalized by the minimum value of Q of all the fractures in log-10 space plotted against aperture: aperture is proportional to fracture length. Results of one realization shown. The red dashed line indicates the value of Q below which the fractures are eliminated in this case.*

Whether or not aperture is proportional to fracture length, the original fracture network behaves as a sparse network, and the cumulative length of the conducting backbone of the dominant sub-network is roughly half of the total length of the original fracture network. However, in contrast to the cases where the aperture is independent of the fracture length, the fractures with narrower aperture (shorter fractures) tend to be less important to flow in the network than those with larger aperture (longer fractures) when the aperture is proportional to the fracture length.

## 2.4 Possibility of Identifying Dominant Sub-Network without Doing Flow Simulation

In this section, we explore possible criteria to obtain a sparse dominant sub-network without doing flow simulations. The results in the previous section show clearly that the aperture distribution has a great influence on the dominant sub-network. Also, fracture length takes an important role in the flow behavior of fracture networks. Besides the aperture and the length, the other factor we consider here is the number of intersections each fracture has with other fractures. It is believed that this term reflects the importance of a fracture to the connectivity of the fracture network (Robinson 1983). We define criteria from these three individual factors and some of their combinations (Table 2.1). In the previous section, we discussed identifying the dominant sub-network based on flow simulation results. That is, we conduct a flow simulation on the original fracture network, and then eliminate the fractures starting with the smallest $Q$, in order of increasing $Q$. In this section, we explore the possibility of identifying the dominant sub-network without doing flow simulations first. The fractures are now eliminated according to some fracture property. For example, the fractures are eliminated based on aperture, starting with the smallest aperture, and then in order of increasing aperture.

We compare the effective permeability of the sub-network with a portion of fractures eliminated from the original fracture network using these criteria. Not all the cases examined above are tested here: for the cases with power-law aperture distributions, we examine $\alpha$ = 1.001, 2, and 6; for the cases of log-normal aperture distributions, we examine $\sigma$ = 0.1, 0.2, and 0.6; we also test the cases where the aperture is proportional to the fracture length.

**Table 2.1** Fracture-Elimination Criteria

| Criterion | Description |
|---|---|
| 1 | Aperture ($d$) |
| 2 | Length ($l$) |
| 3 | Number of intersections ($n$) |
| 4 | Flow simulation results ($q$) |
| 5 | Aperture × Length ($d \times l$) |
| 6 | Aperture$^2$ × Length ($d^2 \times l$) |
| 7 | Aperture$^3$ × Length ($d^3 \times l$) |
| 8 | Aperture × Length$^2$ ($d \times l^2$) |
| 9 | Aperture$^3$ / Length ($d^3 / l$) |
| 10 | Aperture × Number of intersections ($d \times n$) |
| 11 | Length × Number of intersections ($l \times n$) |
| 12 | Aperture × Length × Number of intersections ($d \times l \times n$) |

As presented in Figs. 2.23 and 2.24, aperture is a better criterion than the others (more fractures can be eliminated while retaining 90% of the original permeability). For the case in which the aperture is proportional to the fracture length, the results obtained according to the criteria of aperture and fracture length are the same; therefore, only four plots are shown in Fig. 2.25.

Nevertheless, eliminating fractures based on aperture is not nearly as efficient as eliminating fractures based on flow simulations.

We compare the effective permeability of the sub-network with a portion of fractures eliminated from the original fracture network using these criteria. Not all the cases examined above are tested here: for the cases with power-law aperture distributions, we examine $\alpha$ = 1.001, 2, and 6; for the cases of log-normal aperture distributions, we examine $\sigma$ = 0.1, 0.2, and 0.6; we also test the cases where the aperture is proportional to the fracture length.

As presented in Figs. 2.23 and 2.24, aperture is a better criterion than the others (more fractures can be eliminated while retaining 90% of the original permeability). For the case in which the aperture is proportional to the fracture length, the results obtained according to the criteria of aperture and fracture length are the same; therefore, only four plots are shown in Fig. 2.25. Nevertheless, eliminating fractures based on aperture is not nearly as efficient as eliminating fractures based on flow simulations.

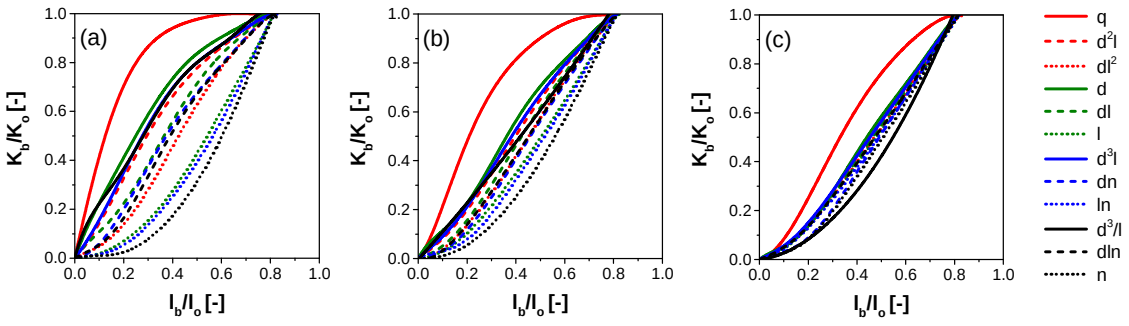


***Figure 2.23*** *Sub-network equivalent permeability ($K_b$) normalized by the equivalent permeability of the original fracture network ($K_o$), plotted against the length of the backbone of the truncated fracture network ($l_b$) normalized by the total length of the original fracture network ($l_o$) for power-law aperture distributions with (a) α = 1.001, (b) α = 2, (c) α = 6. Fractures are eliminated according to different criteria, as indicated.*

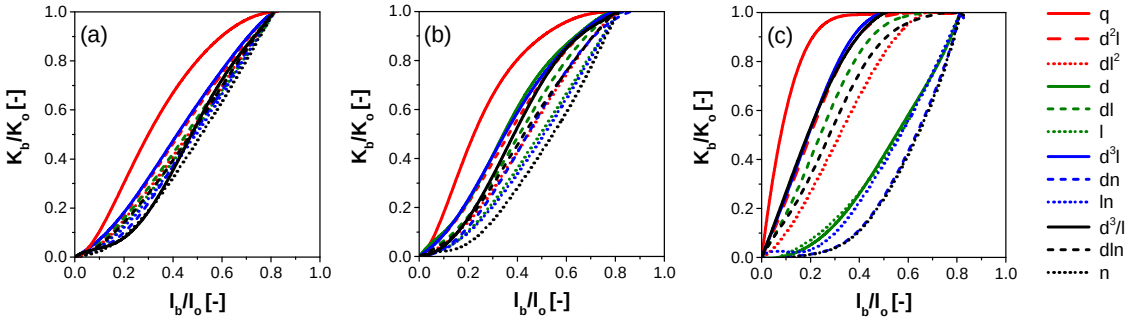


***Figure 2.24*** *Sub-network equivalent permeability ($K_b$) normalized by the equivalent permeability of the original fracture network ($K_o$), plotted against the length of the backbone of the truncated fracture network ($l_b$) normalized by the total length of the original fracture network ($l_o$) for log-normal aperture distributions with (a) σ = 0.1, (b) σ = 0.2, (c) σ = 0.6. Fractures are eliminated according to different criteria, as indicated.*

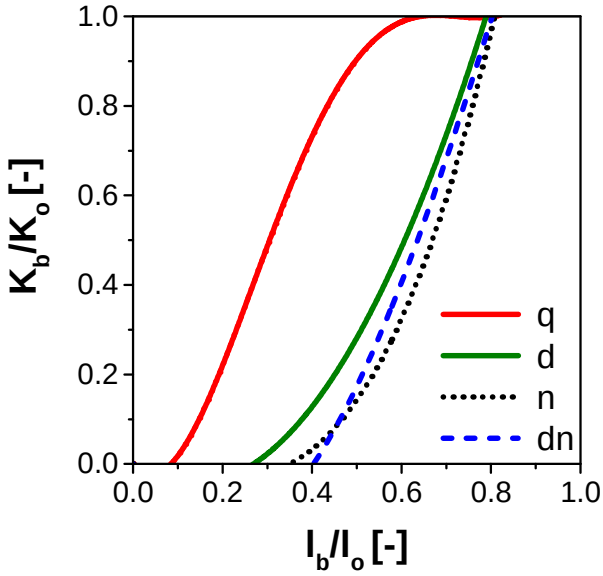


***Figure 2.25*** *Sub-network equivalent permeability ($K_b$) normalized by the equivalent permeability of the original fracture network ($K_o$), plotted against the length of the backbone of the truncated fracture network ($l_b$) normalized by the total length of the original fracture network ($l_o$), for the cases where the aperture is proportional to the fracture length. Fractures are eliminated according to different criteria, as indicated.*

## 2.5 Conclusions

This work focuses on the effect of fracture aperture distribution on the dominant sub-network that by itself retains 90% of the effective permeability of the original fracture network. A number of aperture distributions are tested: log-normal and power-law distributions (from narrow to broad), and one where the aperture is proportional to the fracture length. If the aperture distribution is broad enough ($\alpha \leq 2$ for power-law aperture distributions and $\sigma \geq 0.4$ for log-normal aperture distributions), most of the fractures can be eliminated without significantly reducing the effective permeability. As the exponent $\alpha$ of a power-law aperture distribution increases or the standard deviation $\sigma$ of a log-normal aperture distribution decreases, fewer and fewer fractures can be removed without significantly reducing the network equivalent permeability.

The importance of each fracture to the overall flow is not simply related to aperture or length. For the cases of both the log-normal and power-law aperture distributions, and that where the aperture is proportional to the fracture length, there are some fractures with relatively narrow aperture that play a

greater role in the overall flow than some others with larger aperture. It is also true that some fractures with relatively large aperture that carry much less flow than most of the fractures.

Flow simulations are more effective at identifying the largest sub-network that retains 90% of the original permeability than eliminating fractures based on length, aperture or number of intersections. Among those properties, eliminating fractures based on aperture is the most efficient choice considered here, but not as efficient as using flow calculations.

# 3

# SHAPE FACTOR FOR DUAL-PERMEABILITY FRACTURED RESERVOIR SIMULATION: EFFECT OF NON-UNIFORM FLOW IN 2D FRACTURE NETWORK

The content described in this chapter is also published in :: Gong, J, Rossen, W.R. Shape factor for dual-permeability fractured reservoir simulation: Effect of non-uniform flow in 2D fracture network. Fuel. 2016;184:81-8. doi:http://dx.doi.org/10.1016/j.fuel.2016.06.113.

## 3.1 Introduction

Naturally fractured reservoirs contain a significant amount of hydrocarbon reserves worldwide (Saidi 1987), However, the oil recovery from these reservoirs has been rather low. The low level of oil recovery indicates that more accurate reservoir characterisation and flow simulation is needed.

Reservoir simulation is one of the most practical methods of studying flow problems in porous media. For fractured reservoir simulation, the dual-porosity/dual-permeability concept and the discrete fracture model are two typical methods (Moinfar et al. 2011). In the dual-porosity/dual-permeability approach, the fracture and matrix systems are treated as separate domains, and interconnected fractures serve as fluid flow paths between injection and production wells, while the matrix acts only as fluid storage, and these two domains are connected with an exchange term (Barenblatt et al. 1960; Warren, Root 1963; Kazemi et al. 1976). In a dual-permeability model, fluid flow can also take place between matrix blocks, unlike from the dual-porosity model (Hill, Thomas 1985; Gilman, Kazemi 1988). In order to simulate the realistic fracture geometry and account explicitly for the effect of individual fractures on fluid flow, discrete fracture models have been developed (Kim, Deo 2000; Karimi-Fard, Firoozabadi 2003; Karimi-Fard et al. 2004; Geiger et al. 2004; Matthäi et al. 2007; Li, Lee 2008; Li et al. 2009). Compared to the dual-porosity/dual-permeability models, discrete fracture models represent a fracture network more explicitly and make the simulation more realistic. But discrete fracture models are typically difficult to solve numerically. For the naturally fractured reservoirs with many fractures and a very high degree of interconnection, DFN simulation simply isn't feasible. To generate a dual-porosity/dual-permeability model, it is necessary to define average properties for each grid cell, such as porosity, permeability, matrix-fracture interaction parameters (typical spacing or shape factor), etc (Dershowitz et al. 2000). It has been recognized that the fracture-matrix exchange coefficient or shape factor depends on matrix-block geometries. Many methods for evaluating the exchange coefficient or shape factor for blocks with various shapes have been proposed, such as the Laplace transform method (Barker 1985; Quintard, Whitaker 1993, 1996), asymptotic analysis (Lim, Aziz 1995; Zimmerman et al. 1993), random-walk method (Noetinger et al. 2016), equivalent –block-size methods (Kazemi et al. 1976; Warren, Root 1963), etc. Landereau et al. (2001) compares the most commonly used methods, and discusses the connection between them. In general, the fracture-matrix exchange coefficient is related to a characteristic length (equivalent block size) of the system. Therefore, the discrete fracture network considered to generate the dual-porosity model parameters is crucial. Using homogenization, one can treat matrix-fracture exchange more accurately than in dual porosity/dual permeability simulations (Salimi, Bruining 2010), but, again, one needs a characteristic matrix-block size.

As we presented in a previous study (Gong, Rossen 2014), even in a well-connected fracture network, there is a dominant sub-network which carries almost all the flow, but it is much more sparse than the original network (Fig. 3.1). The flow-path length of the dominant sub-network can be as little as roughly 30% of that of the corresponding original fracture network in the most extreme case. This suggests that in secondary production, the water injected flows mainly along a small portion of the fracture network. In contrast, in primary production even relatively small fractures can be an efficient path for oil to flow to a production well.

This chapter is organized as follows: we first introduce the numerical model and research process. Next, we analyse the sizes of the matrix blocks formed by the entire fracture network and the corresponding dominant sub-network. Finally, we point out the implications of this distinction for the dual-porosity/dual-permeability reservoir simulation.

## 3.2 Models

Since this is a follow-up study to our previous research (Gong, Rossen 2014), the models used here are the same as the ones adopted before (Fig. 3.1). Here we only introduce the models briefly, and more details can be found in the previous work. Fracture networks are generated in a 10 m × 10 m × 0.01 m region using the commercial fractured-reservoir simulator FracMan™ (Dershowitz et al. 2011). Two fracture sets which are nearly orthogonal to each other are assumed, with almost equal numbers of fractures in the two sets. Each fracture, with a rectangular shape, is located following the Enhanced Baecher Model and is perpendicular to the plane which follows the flow direction and penetrates the top and bottom boundaries of the region. Because of the uncertainties in data and the influence of cut-offs in measurements, fracture-trace lengths have been described by exponential, log-normal or power-law distributions in previous studies (Segall, Pollard 1983; Rouleau, Gale 1985; Bour, Davy 1997). Commonly, a power-law distribution is assumed by many researchers to be the correct model for fracture length (Nicol et al. 1996; Odling 1997; de Dreuzy et al. 2001a, b), with exponent $\alpha$ ranging from 1.5 to 3.5. In this study, the fracture length follows the power-law distribution ($f(x)$):

$$f(x) = \frac{\alpha-1}{x_{min}}\left(\frac{x_{min}}{x}\right)^{\alpha} \tag{3.1}$$

Where $\alpha$ is the power law exponent, $x$ is the fracture length and $x_{min}$ the lower bound on $x$, which we take to be 0.2 m. In order to make sure that there are no extremely short or long fractures, and in particular that opposite sides of our region of interest cannot be connected by a single fracture, we choose $\alpha$ = 2 and truncate the length distribution on the upper end at 6 m. Since even the smallest fracture length (0.2 m) is much larger than the thickness of the region of interest (0.01 m), the 3D model can be seen as a 2D fracture network.

For fracture apertures, two kinds of distribution which have been proposed in previous studies are adopted: power-law (Barton et al. 1989; Wong et al. 1989; Barton, Zoback 1992; Belfield, Sovich 1994; Marrett 1996; Ortega, Marrett 2000) and log-normal (Snow 1970; Tsang, Tsang 1987; Long, Billaux 1987; Dverstorp, Andersson 1989; Cacas et al. 1990a; Cacas et al. 1990b). In each kind of distribution, to include the entire range of feasible cases (from narrow to broad aperture distribution), different parameter values ($\alpha$ for a power-law aperture distribution and $\sigma$ for a log-normal aperture distribution) are examined. The aperture is randomly assigned to each fracture.

The power-law distribution can also be defined as:

$$f(x) = x^{-\alpha} \tag{3.2}$$

If the power-law aperture distribution is described by Eq. (3.2), the studies cited above found that the value of the exponent $\alpha$ in nature is 1, 1.1, 1.8, 2.2, or 2.8. In this study, the power-law aperture distribution is defined by Eq. (3.1) as well as the fracture length distribution, where $x$ stands for aperture instead of length. Different from Eq. (3.2), Eq. (3.1) includes a minimum cut-off value, and $\alpha$ should be larger than 1. To include the entire range of feasible cases (from narrow to broad aperture distribution), here we examine $\alpha$ in the range from 1.001 to 6. In each case, the fracture aperture is limited to the interval between 0.01 mm and 10 mm. The aperture range can vary greatly at different locations, it also depends on the resolution and the size of the region studied. According to the field data collected from the Ship Rock volcanic plug in NW New Mexico (Delaney, Pollard 1981) and Culpeper Quarry and Florence Lake (Vermilye, Scholz 1995), the aperture range [0.01mm, 10mm] adopted here is realistic, at least at some locations in natural.

The log-normal distribution is specified by the following probability density function:

$$f(x) = \frac{1}{x log_{10}(\sigma)\sqrt{2\pi}} exp\left\{-\frac{1}{2}\left(\frac{log_{10}(x)-\mu}{\sigma}\right)^2\right\} \tag{3.3}$$

where $\mu$ and $\sigma$ are the mean and the standard deviation in the log-10 space. The truncated log-normal distribution has two additional parameters: a minimum and a maximum value of aperture. Field studies and hydraulic tests found values of $\sigma$ from 0.1 to 0.3, 0.23, and 0.47 (Dverstorp, Andersson 1989; Tsang et al. 1996; Snow 1970). To test the widest range of feasible values, we test values of $\sigma$ from 0.1 to 0.6. More details can be found in our previous study (Gong, Rossen 2014). In order to focus on the influence of fracture aperture distributions on the dominant sub-network, except for the aperture distribution, all the other parameter distributions remain the same for all the cases tested in this study, including the fracture length, the orientation, etc.

We assume that a fracture can be approximated as the slit between a pair of smooth, parallel plates; thus the aperture of each fracture is uniform. Steady state flow through the fractured region is considered (Fig. 3.1a). In this chapter, we consider that matrix permeability « fracture permeability, which is common in fractured reservoirs (van Golf-Racht 1982; Nick et al. 2011). The flow regimes of fractured rock mass can be defined by the fracture-matrix permeability ratio, especially, while the ratio is greater than $10^5$ - $10^6$, fractures carry nearly all the flow (Matthai, Belayneh 2004; Matthai, Nick 2009). Since we are interested in the non-uniform flow in well-connected fracture networks, the matrix is further assumed to be impermeable, so that fluid flow can take place only in the fracture network, similar to the flow regime between fractures and permeable rock mass with the fracture-matrix permeability ratio is greater than $10^5$ - $10^6$. For computing flow in discrete fracture networks, as in most numerical simulation methods, Darcy's Law for steady-state incompressible flow is employed, and mass is conserved at each intersection of fractures. In our models, we induce fluid flow from the left side to the right side by applying a constant difference in hydraulic head across the domain, while all the other boundaries are impermeable. Mafic™, a companion program of FracMan™, is employed to simulate flow in the fracture networks.

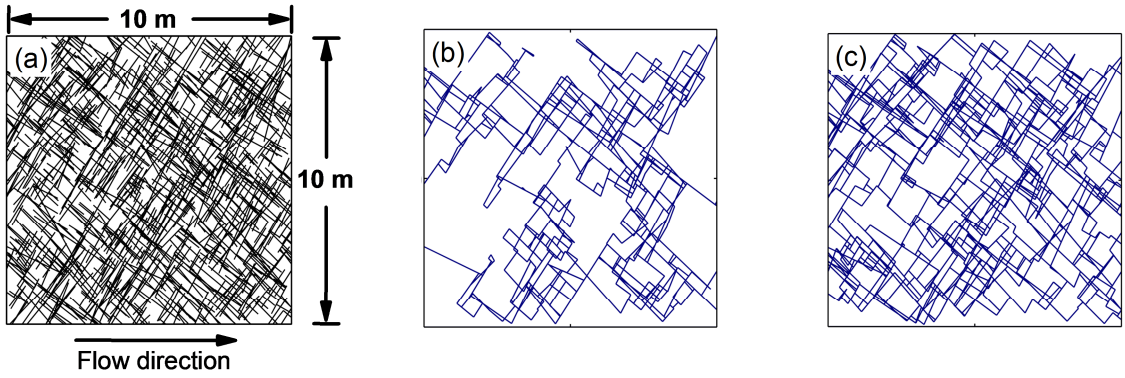


***Figure 3.1*** *(a )One realization of the fracture network examined in this study. The size of the fractured region is 10 m × 10 m × 0.01 m. The left and right boundaries are each at fixed hydraulic head; the difference in hydraulic head is 1m; water flows from left to right; the top and bottom edges are no-flow boundaries. (b) Dominant sub-network for one realization with a power-law aperture distribution (α = 1.001). (c) Dominant sub-network for one realization with a power-law aperture distribution (α = 2).*

## 3.3 Methodology

As presented in the previous study, even in a well-connected fracture network, when the aperture distribution is broad enough, there is a dominant sub-network which can be a good approximation of the actual fracture network. This dominant sub-network is also strongly affected by the aperture distribution. The "dominant sub-network" is defined as the sub-network obtained by eliminating a portion of fractures while retaining 90% of the original-network equivalent permeability. The threshold of 90% equivalent permeability is chosen to eliminate fractures that are the ones do not carry much water and being eliminated. There is no special meaning for this 90% threshold, it could vary to tighten, or loosen, the criterion for membership in the dominant network. this study, our main interest lies in

examining the change of the characteristic sizes of matrix blocks as more fractures are eliminated. We also check the influence of aperture distribution (exponent $\alpha$ in a power-law distribution and standard deviation $\sigma$ in a log-normal distribution) on the characteristic sizes of matrix blocks formed by the dominant sub-network. A Matlab program is employed to calculate the characteristic matrix block sizes. The equivalent matrix block size is employed to represent the average value of a series of matrix block sizes.

The approach used to decide which portion of fractures to remove is as follows. Mafic™ subdivides the fractures into finite elements for the flow calculations. The flow velocity at the centre of each finite element and the value of flow velocity × aperture (=$Q_{nodal}$) can be obtained. Based on this value, we compute the average value ($Q$) of all the elements in each fracture. $Q$ is then used as the criterion to eliminate fractures: fractures are eliminated in order, starting from the one with the smallest value of $Q$ to the one with the largest $Q$. That is to say, the fractures that conduct the least flow are eliminated first. After each step, we first calculate the equivalent network permeability of the truncated network.

Because the generation of the fracture network is a random process, an infinite number of fracture networks can be generated with the same parameter values for the density, the orientation, the fracture length and the aperture distribution. In this study, for each set of parameter values, we generate one hundred realizations.

## 3.4 Characteristic Matrix Block Sizes

The matrix blocks in fractured reservoirs can be of varying shapes and sizes. In order to quantitatively study the size and the recovery behavior of the matrix blocks, several parameters have been proposed (Cinco-Ley et al. 1985; Kazemi et al. 1992; Shouxiang et al. 1997; Rodriguez-N et al. 2001; Ranjbar et al. 2012). In this study, we adopt the characteristic radius and the characteristic length.

Zimmerman and Bodvarsson (Zimmerman, Bodvarsson 1995) argued that an irregularly-shaped matrix block can be modelled with reasonable accuracy as a spherical matrix block. The effective radius of the corresponding spherical block is defined as

$$r = \frac{3V}{S} \tag{3.4}$$

Where $V$ is the volume of the matrix block, and $S$ is the surface area. They also proposed that in the early-time regime (shortly after a change in the boundary condition imposed at the block surfaces), a series of spherical blocks with variable radii can be modelled using uniform blocks with an equivalent radius given by:

$$r_e = \left(\sum_{i=1}^{n} \frac{V_i}{V_t} r_i^{-1}\right)^{-1} \tag{3.5}$$

where $n$ is the number of matrix blocks, $i$ refers to one matrix block, $r_i$ is the effective radius of that matrix block, $V_i$ is the volume of that matrix block and $V_t$ is the total matrix volume. In this study, we adopt a similar idea to define the characteristic matrix-block radii of 2D fractured formations. The characteristic radius of each irregularly-shaped matrix block is defined as:

$$r_i = \frac{2S_{mi}}{L_{mi}} \tag{3.6}$$

where $i$ refers to one matrix block, $S_{mi}$ is the area of the matrix block, and $L_{mi}$ is the perimeter of the two-dimensional matrix block.

The equivalent matrix-block radius is then defined as:

$$r_e = \left(\sum_{i=1}^{n} \frac{S_i}{S_t} {r_i}^{-1}\right)^{-1} \tag{3.7}$$

where $n$ is the number of matrix blocks, $i$ refers to one matrix block, $S_i$ is the area of that matrix block and $S_t$ is the total matrix area.

The second parameter used in this study for representing the matrix-block size is the characteristic length, which was first proposed by Kazemi *et al.* (1992) and followed by other researchers (Shouxiang et al. 1997; Zhang et al. 1996; Mirzaei-Paiaman, Masihi 2013). Kazemi *et al*. (1992) proposed a shape factor ($F_s$) of a single matrix block for the imbibition process, which considered the effect of matrix-block shapes and boundary conditions:

$$F_{si} = \frac{1}{V_{mi}} \sum_{j=1}^{n} \frac{A_j}{d_j} \tag{3.8}$$

where $i$ refers to one matrix block, $V_{mi}$ is the volume of that matrix block, $j$ refers to one face of that matrix block which is open to imbibition, $A_j$ is the area of that face, $d_j$ is the distance from that face to the centre of the matrix block, and $n$ is the total number of faces of the matrix block open to imbibition. This shape factor is claimed to be valid for anisotropic matrix blocks with irregular shapes (Heinemann, Mittermeir 2012).

The characteristic length of an irregular matrix block $L_c$ is then defined as

$$L_{ci} = \frac{1}{\sqrt{F_{si}}} \tag{3.9}$$

In fractured reservoirs, the matrix block is the main storage of oil and it feeds the surrounding fractures; thus the bulk volume of the matrix is vital to the recovery rate. Therefore, we believe that a volume-weighted equivalent length is more reasonable than a number-based average value. An equivalent length for a series of matrix blocks is then represented as

$$L_e = \left(\sum_{i=1}^{n} \frac{V_i}{V_t} {L_{ci}}^{-1}\right)^{-1} \tag{3.10}$$

where $i$ refers to one matrix block, $V_i$ is the volume of that matrix block, $L_{ci}$ is the characteristic length of that matrix block, and $V_t$ is the total bulk volume of the matrix blocks.

In this study, the equivalent radius ($r_e$) and the equivalent length ($L_e$) defined above are used to represent the average size of the matrix blocks in a fractured region. Only fractures that belong to the spanning cluster are included in calculating the matrix block sizes; the dead-ends are systematically removed from the network. Also, the matrix blocks containing impermeable boundaries (i.e. along the top and bottom of the region of interest) are not considered. Only the matrix blocks formed by the fractures which have fluid flow through them and the permeable left and right boundaries are taken into account.

## 3.5 Results

In this section, we present the results for the cases with power-law aperture distributions (from narrow to broad) and log-normal aperture distributions (from narrow to broad).

### 3.5.1 Results for Cases with Power-Law Aperture Distribution

Figure 3.2 shows the normalized area-weighted harmonic-average of characteristic matrix radii ($r_e^b$). The scatter in Figs. 3.2a-3.2c reflects the difference among the 100 realizations, and the average trend curves are shown in Fig. 3.2d. As presented in Fig. 3.2, as more fractures are eliminated, the length of

the backbone of the truncated fracture network ($l_b$) decreases, while the equivalent radius of the matrix blocks ($r_e^b$) formed by the fracture network increases. The average trends are very close to each other for the cases with different values of power-law aperture distribution exponent $\alpha$, no matter whether the apertures distribute broadly or narrowly (Fig. 3.2d).

The normalized equivalent permeability of the truncated fracture network ($K_b$) is shown in Fig. 3.3 in which $K_b/K_o$ is the ratio between the equivalent permeability of the dominant sub-network ($K_b$) and the equivalent permeability of the original fracture network ($K_o$), while $l_b/l_o$ represents the ratio between the length of the backbone of the truncated fracture network ($l_b$) and the total length of the original fracture network ($l_o$). The results show that the dominant sub-network (the sub-network retaining 90% of the original equivalent network permeability after eliminating a portion of fractures) is strongly affected by the aperture distribution: for the broadest aperture distribution cases ($\alpha$ = 1.001), the flow-path length ($l_b$) is roughly 35% of the total length of the original fracture network ($l_o$), while for the narrowest aperture distribution ($\alpha$ = 6), the ratio of $l_b/l_o$ is approximately 0.6 (Fig. 3.3). Correspondingly, as presented in Fig. 3.2d, the equivalent matrix radius for the dominant sub-network is on average about twice that for the original fracture network when $\alpha$ = 1.001 (the red dashed line), while the ratio is approximately 1.5 for the cases with the narrowest aperture distribution with $\alpha$ = 6 (the red dotted line).
.

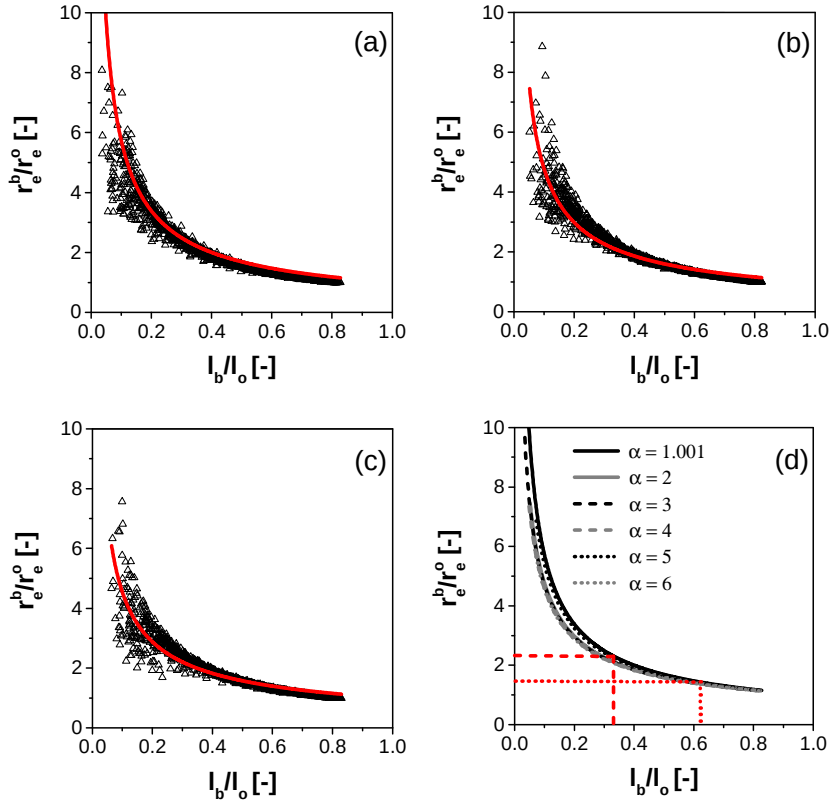


***Figure 3.2*** *Equivalent matrix radius of the dominant sub-network ($r_e^b$) normalized by the equivalent matrix radius of the original fracture network ($r_e^o$), plotted against the length of the backbone of the truncated fracture network ($l_b$) normalized by the total length of the original fracture network ($l_o$): power-law aperture distributions with (a) α = 1.001, (b) α = 2, (c) α = 6. Results of 100 realizations are shown for each value of α. The red curve is the average trend curve. (d) Average curves from (a-c), including additional values of α. Also shown are values of $l_b/l_o$ for the sub-network retaining 90% of the equivalent network permeability and resulting values of $r_e^b/r_e^o$ for α = 1.001 (red dashed line) and α = 6 (red dotted line), respectively.*

Figure 3.4 shows the characteristic radii ($r_c$) of all the matrix blocks formed by the entire fracture network and the dominant sub-network for one realization for each value of α (Fig. 3.4). The vertical axis ("CDF") shows for each case the portion of matrix with $r_c$ greater than the given value. In general, the characteristic radii of the matrix blocks formed by the dominant sub-network are larger than those

formed by the entire fracture network. The reason is that the dominant sub-network contains fewer number of the original fractures (Gong, Rossen 2014).

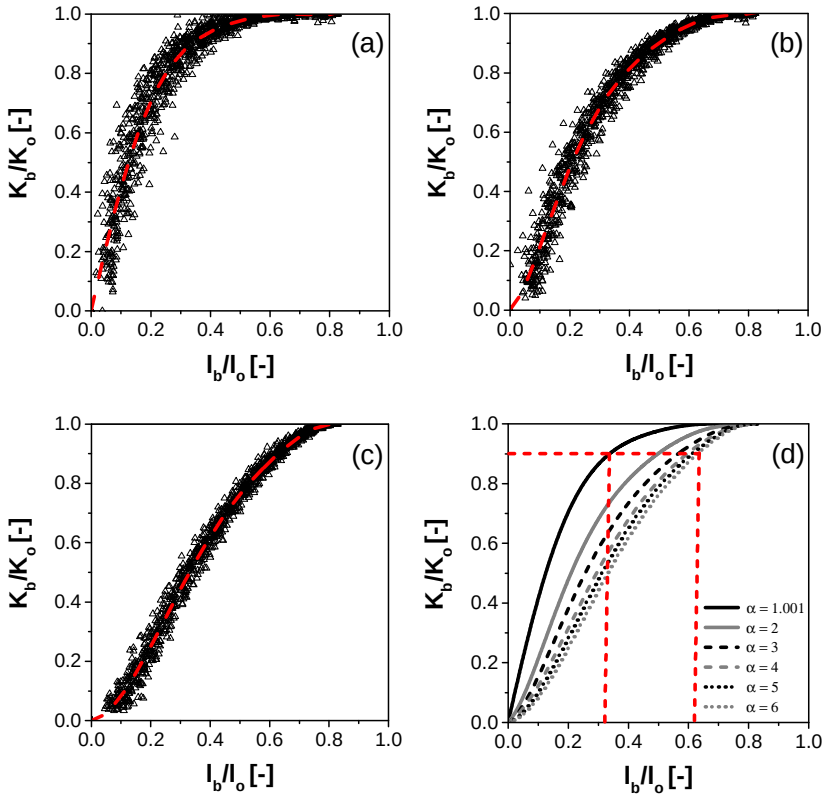


***Figure 3.3*** *Equivalent permeability of the dominant sub-network ($K_b$) normalized by the equivalent permeability of the original fracture network ($K_o$), plotted against the length of the backbone of the truncated fracture network ($l_b$) normalized by the total length of the original fracture network ($l_o$): power-law aperture distributions with (a) α = 1.001, (b) α = 2, (c) α = 6. Results of 100 realizations shown for each value of α. Red curve is the average trend curve. (d) average curves from (a-c), including additional values of α, also shown are values of $l_b/l_o$ retaining 90% of the equivalent network permeability for α = 1.001 and α = 6, respectively.*

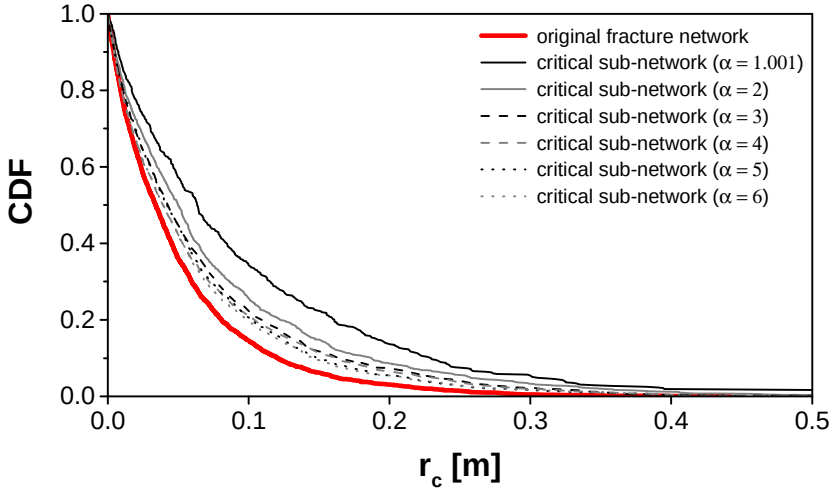


***Figure 3.4*** *Cumulative distribution function (CDF) for the characteristic radius of matrix blocks $r_c$ formed by the original fracture network (the bottom curve) and the dominant sub-network: power-law aperture distributions with α = 1.001 - 6. The results of one realization are shown for each value of α.*

The other parameter used in this chapter to represent the sizes of matrix of varying shapes is the characteristic length which is defined in Eq. 3.8 and Eq. 3.9. In Figure 3.5, we show the normalized equivalent matrix length ($L_e^b$) of the truncated fracture network, while in Figure 3.6, the characteristic

length ($L_c$) distribution of the matrix blocks formed by the original fracture network and the dominant sub-networks for one realization is presented. Similar results are obtained: for the cases with the broadest power-law aperture distribution, the equivalent length for the dominant sub-network is around twice that on average for the original fracture network. The ratio becomes smaller as the aperture distribution is narrower, and decreases to 1.5 for $\alpha = 6$.

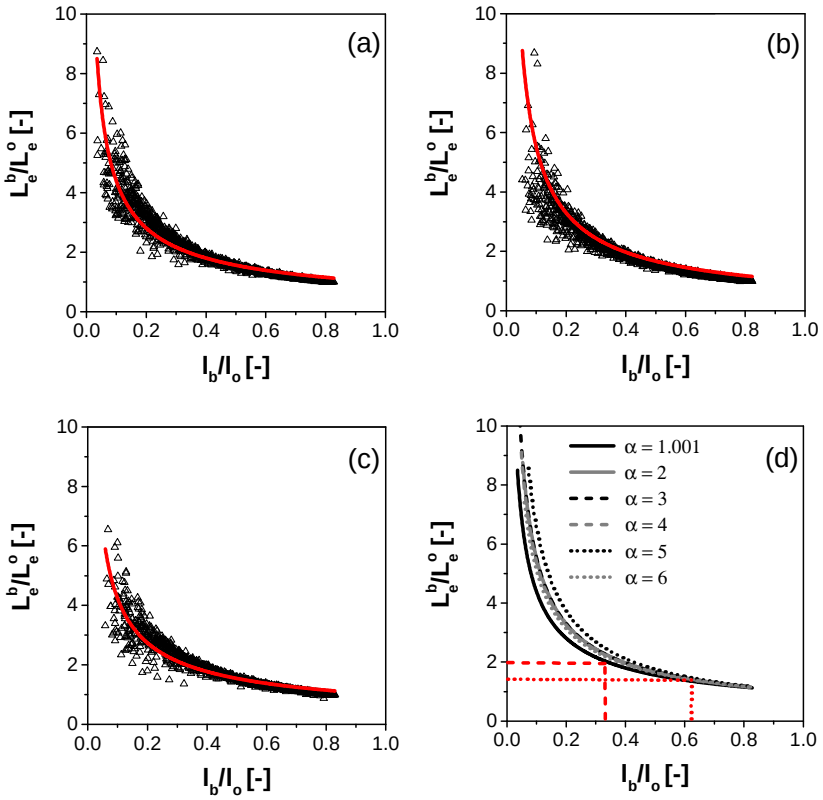


***Figure 3.5*** *Equivalent matrix length of the dominant sub-network ($L_e^b$) normalized by the equivalent matrix length of the original fracture network ($L_e^o$), plotted against the length of the backbone of the truncated fracture network ($l_b$) normalized by the total length of the original fracture network ($l_o$): power-law aperture distributions with (a) α = 1.001, (b) α = 2, (c) α = 6. Results of 100 realizations are shown for each value of α. The red curve is the average trend curve. (d) average curves from (a-c), including additional values of α. Also shown are values of $l_b/l_o$ for the sub-network retaining 90% of the equivalent network permeability and resulting values of $L_e^b/L_e^o$ for α = 1.001 (red dashed line) and α = 6 (red dotted line), respectively.*

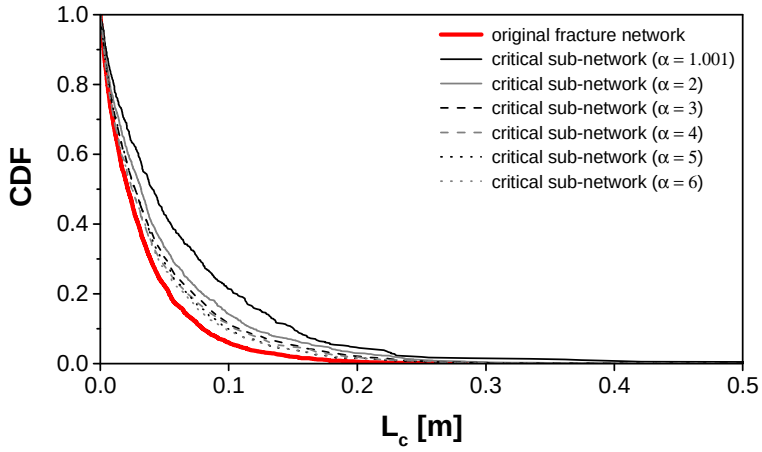


***Figure 3.6*** *Cumulative distribution function (CDF) for the characteristic radius of matrix blocks $L_c$ formed by the original fracture network (the bottom curve) and the dominant sub-network: power-law aperture distributions with α = 1.001 - 6. The results of one realization are shown for each value of α.*

### 3.5.2 Results for Cases with Log-Normal Aperture Distribution

Similar to the results for the cases with power-law aperture distributions, as more fractures are eliminated according to the flow-simulation results, the equivalent matrix-block radius and equivalent matrix-block length become larger for the cases with log-normal aperture distributions (Fig. 3.7 and Fig. 3.10), and the overall trends are almost not affected by the breadth of the aperture distribution (Fig. 3.7d and Fig. 3.10d).

However, the dominant sub-network, defined in our previous study as the sub-network retaining 90% of the original equivalent network permeability after eliminating a portion of fractures, is strongly affected by the aperture distribution : for the broadest aperture distribution cases ($\sigma$ = 0.6), the flow-path length is roughly 20% of the total length of the original fracture network ($l_b/l_o$ = 0.2), while for the narrowest aperture distribution ($\sigma$ = 0.1), the ratio $l_b/l_o$ is approximately 0.6 (Fig. 3.8). Correspondingly, as presented in Fig. 3.7, the ratio between the equivalent radius of the dominant sub-network and that of the entire fracture network ($r_e^b/r_e^o$) is around 3.5 when $\sigma$ = 0.6 (the red dashed line in Fig.3.7d), which is the broadest aperture distribution examined here. The ratio $r_e^b/r_e^o$ decreases as the aperture distribution becomes narrower, and reaches roughly 1.5 for the cases with the narrowest aperture distribution with $\sigma$ = 0.1 (the red dotted line in Fig.3.7d). The equivalent matrix length ($L_e^b$) presents similar behavior as the equivalent matrix radius (Fig. 3.10).

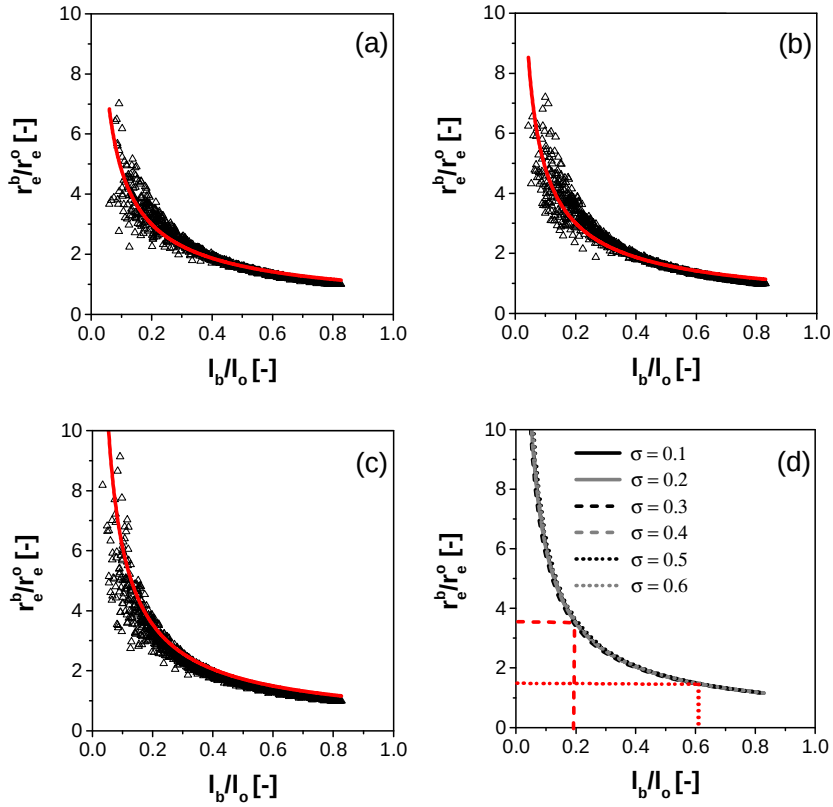


***Figure 3.7*** *Equivalent matrix radius of the dominant sub-network ($r_e^b$) normalized by the equivalent matrix radius of the original fracture network ($r_e^o$), plotted against the length of the backbone of the truncated fracture network ($l_b$) normalized by the total length of the original fracture network ($l_o$): log-normal aperture distributions with (a) σ = 0.1, (b) σ = 0.2, (c) σ = 0.6. Results of 100 realizations are shown for each value of σ. The red curve is the average trend curve. (d) Average curves from (a-c), including additional values of σ. Also shown are values of $l_b/l_o$ for the sub-network retaining 90% of the equivalent network permeability and resulting values of $r_e^b/r_e^o$ for σ = 0.1 (red dotted line) and σ = 0.6 (red dashed line), respectively.*

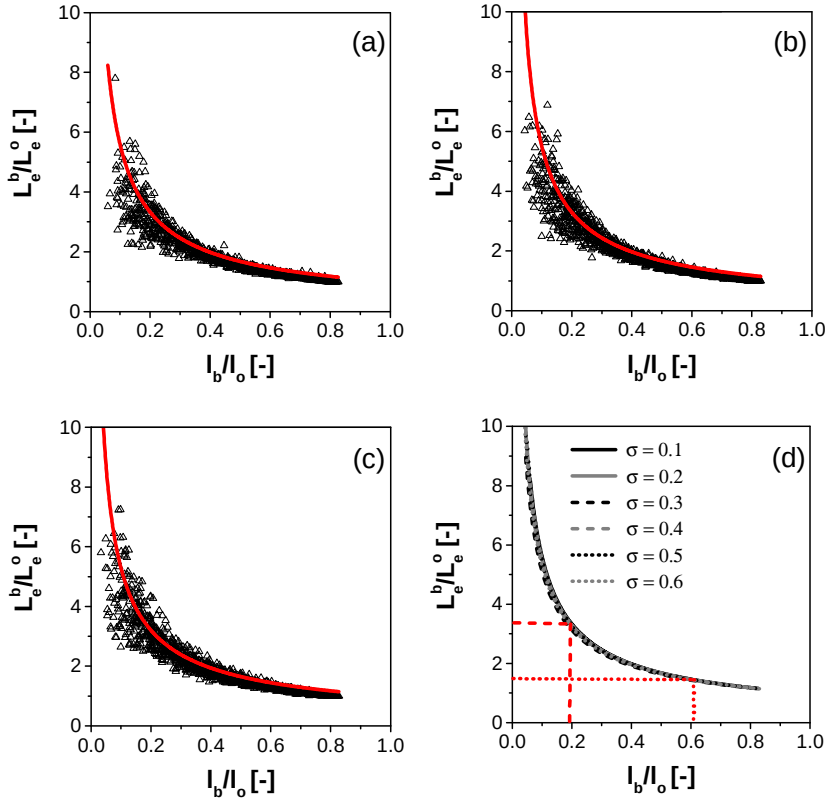


***Figure 3.8*** *Equivalent permeability of the dominant sub-network ($K_b$) normalized by the equivalent permeability of the original fracture network ($K_o$), plotted against the length of the backbone of the truncated fracture network ($l_b$) normalized by the total length of the original fracture network ($l_o$): log-normal aperture distributions with (a) σ = 0.1, (b) σ = 0.2, (c) σ = 0.6. Results of 100 realizations shown for each value of σ. Red curve is the average trend curve, (d) average curves from (a-c), including additional values of σ, also shown are values of $l_b/l_o$ retaining 90% of the equivalent network permeability for σ = 0.1 and σ = 0.6, respectively.*

Similar to our approach with the cases of power-law aperture distributions, we select one realization for each value of *σ*, and examine the characteristic-radius and characteristic-length distributions of the original fracture network and the dominant sub-network. As presented in Figs. 3.9 and 3.11, the characteristic radius and the characteristic length of matrix blocks formed by the dominant sub-network are larger than those of the matrix blocks formed by the entire fracture network.

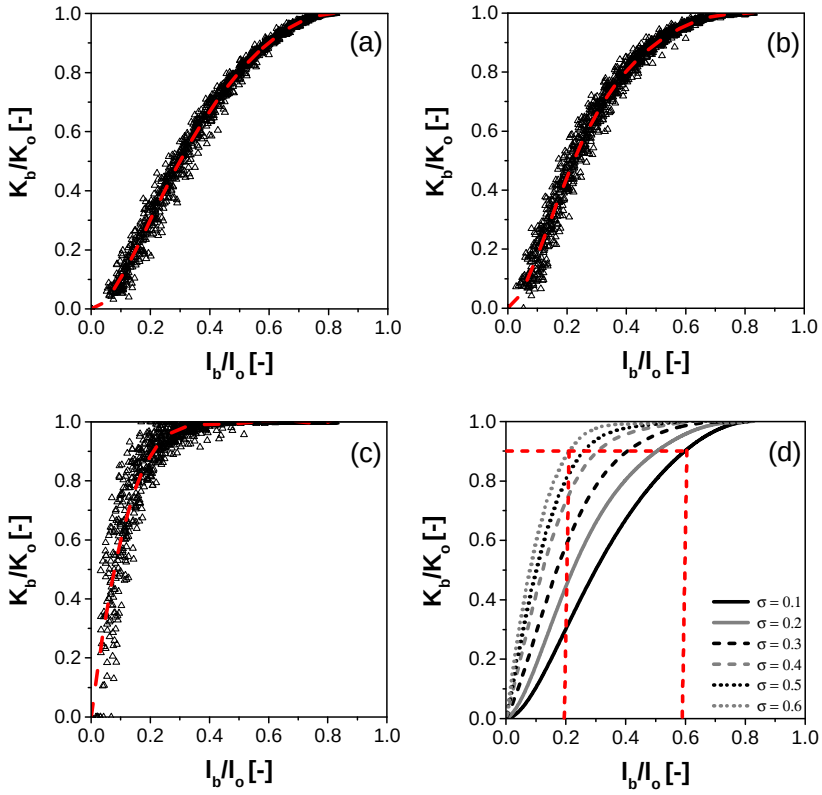


***Figure 3.9*** *Cumulative distribution function (*CDF*) for the characteristic radius of matrix blocks* $r_c$ *formed by the original fracture network (the bottom curve) and the dominant sub-network: log-normal aperture distributions with* σ *= 0.1 – 0.6. The results of one realization are shown for each value of* σ*.*

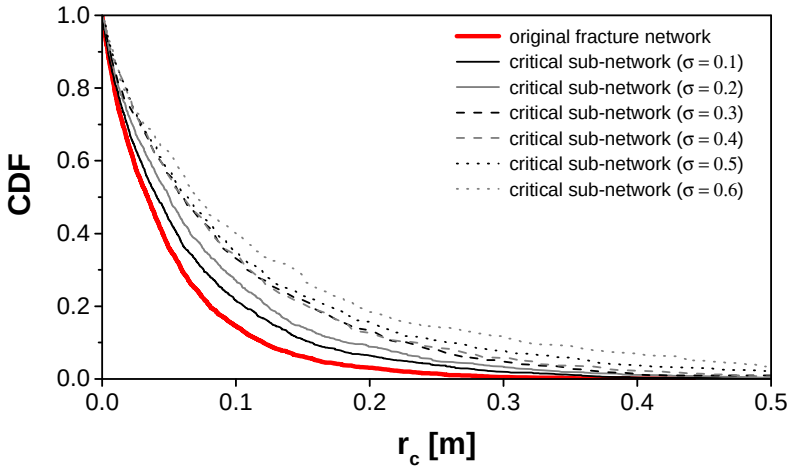


***Figure 3.10*** *Equivalent matrix length of the dominant sub-network (*$L_e^b$*) normalized by the equivalent matrix length of the original fracture network (*$L_e^o$*), plotted against the length of the backbone of the truncated fracture network (*$l_b$*) normalized by the total length of the original fracture network (*$l_o$*): log-normal aperture distributions with (a)* σ *= 0.1, (b)* σ *= 0.2, (c)* σ *= 0.6, results of 100 realizations are shown for each value of* σ*. The red curve is the average trend curve. (d) average curves from (a-c), including additional values of* σ*, also shown are values of* $l_b/l_o$ *retaining 90% of the equivalent network permeability and resulting values of* $L_e^b/L_e^o$ *for* σ *= 0.1 (red dotted line) and* σ *= 0.6 (red dashed line), respectively.*

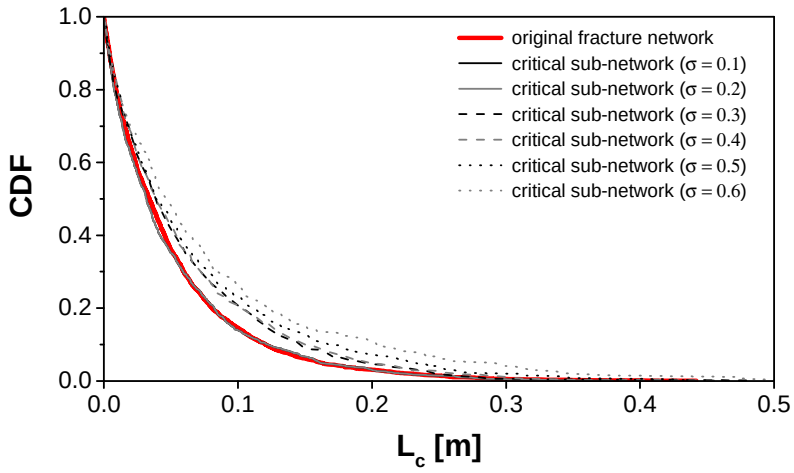


***Figure 3.11*** *Cumulative distribution function (*CDF*) for the characteristic length of matrix blocks* $L_c$ *formed by the original fracture network (the bottom curve) and the dominant sub-network: log-normal aperture distributions with* σ *= 0.1 – 0.6. The results of one realization are shown for each value of* σ*.*

## 3.6 Discussion

Naturally fractured oil reservoirs, like all reservoirs, are exploited in two stages: primary recovery and secondary recovery. The recovery mechanisms are different in these two processes. During primary production, the reservoir is produced by fluid expansion. The pressure drops rapidly in the fractures because of the high permeability, while, in contrast, the matrix remains at higher pressure. This creates a pressure difference between the fracture and the adjacent matrix block, and in turn, leads to flow of oil from the matrix to the fracture. In this scenario, as long as all the fractures are much more conductive than the matrix, one might expect that all connected fractures are conductive enough to bring oil that resides in matrix to the wells.

In secondary recovery, since the fractures have much higher permeability than the matrix, water from an injection well invades the fractures much faster than the matrix. The water rapidly flows through the fracture network and surrounds a matrix block. If the matrix block has water-wet characteristics, water imbibes into the matrix block because of capillary pressure. In many cases, this is a counter-current imbibition process: water and oil flow in opposite directions, although co-current imbibition is faster and can be more efficient than counter-current imbibition (Ramirez et al. 2009).

In this case, the cumulative oil recovery from matrix blocks surrounded by water in fractures can be scaled by an exponential equation (Aronofsky et al. 1958):

$$R = R_\infty(1 - e^{-\lambda t}) \tag{3.11}$$

where $R$ is the recovery, $R_\infty$ is the ultimate cumulative recovery, $\lambda$ is a constant and $t$ is time. Mattax and Kyte (1962) redefined the scale equation for imbibition recovery through experimental investigations:

$$R = R_\infty(1 - e^{-\lambda_D t_D}) \tag{3.12}$$

where

$$t_D = \left[\sqrt{\frac{k}{\phi}}\left(\frac{\sigma}{\mu_w {L_m}^2}\right)\right] t \tag{3.13}$$

and $t_D$ is a dimensionless time, $k$ is the permeability of the matrix block, $\varphi$ is the porosity of the matrix block, $\sigma$ is the interfacial tension, $\mu_w$ is the water viscosity, $L_m$ is the matrix block size, and $t$ is imbibition time.

Kazemi *et al*. (1992) further modified the Mattax and Kyte's scaling equation by introducing the shape factor ($F_S$), which considered the effect of matrix block shapes and boundary conditions. Eq.3.13 becomes

$$t_D = \left[\sqrt{\frac{k}{\phi}}\left(\frac{\sigma F_S}{\mu_w}\right)\right] t \tag{3.14}$$

$$t_D = \left[\sqrt{\frac{k}{\phi}}\left(\frac{\sigma}{\mu_w {L_C}^2}\right)\right] t \tag{3.15}$$

The definitions of the shape factor ($F_S$) and the characteristic length ($L_c$) are described in Eqs. 3.8 and 3.9. Thus, when the shape factor of a matrix block becomes smaller, or the characteristic length becomes greater, it takes a longer time to recover a certain portion of oil; the imbibition recovery process is slower. As presented in Figs. 3.6 and 3.11, in general, for all the cases the characteristic length ($L_c$) of the matrix blocks formed by the dominant sub-networks are larger than that of the matrix blocks formed by the entire fracture networks. This implies that the rate of oil recovery from the matrix blocks is overestimated if the entire fracture network is considered to take part in the waterflooding process.

Eq. 3.15 is for one matrix block; here we apply this formula to the average value of a series of matrix blocks in order to approximately estimate the effect of matrix block sizes on the speed of oil recovery during the waterflooding process. For the cases with broadest aperture distributions ($\alpha$ = 1.001 for a power-law aperture distribution and $\sigma$ = 0.6 for a log-normal aperture distribution), the characteristic length ($L_c$) of the matrix block formed by the dominant sub-networks are on average about twice and three times larger than that formed by the entire fracture networks, respectively (Fig. 3.5 and Fig. 3.10). This suggests that, for the cases with the broadest power-law aperture distribution, if the entire fracture network is considered to take part in the water-flooding process, the imbibition recovery rate from matrix blocks can be on average four times faster than if only the dominant sub-network is taken into account. For the cases with the broadest log-normal aperture distribution, it can be on average nine times faster. Even for the cases with the narrowest aperture distributions ($\alpha$ = 6 for a power-law aperture distribution and $\sigma$ = 0.1 for a log-normal aperture distribution), the imbibition recovery process can be more than twice as fast.

As discussed above, most water does not flow through the entire fracture network, but mainly through the dominant sub-network, and the rest portion of the fractures can be ignored without strongly affecting the overall flow. Considering the recovery mechanism of waterflooding, if the entire fracture network is taken into account, it means we assume the water flows through all the fractures. Then the sizes of matrix blocks formed by fractures and typical fracture spacing are smaller than in the dominant sub-network, which makes the estimated imbibition recovery process faster than it really is. Since dual-porosity/dual-permeability models do not represent fractures explicitly, but assign average properties to grid cells, taking the entire fracture network into account may lead to an inaccurate shape factor, and in turn, give rise to inaccuracy for dual-porosity/dual-permeability simulation of the secondary recovery. The same argument would apply to EOR processes, which depend on penetration of the injected fluid through the fracture network, as waterflooding depends on water.

This suggests that the shape factor for dual-porosity/dual-permeability simulation should depend on the process involved. Specially, it should be different for primary and for secondary or tertiary recovery. For primary recovery, all fractures should be included, while for waterflooding or EOR, only taking into account the dominant sub-network which carries almost all water might give a better estimation.

## 3.7 Conclusions

Even in a well-connected fracture network, injected water does not flow through the entire fracture network; it mainly flows through a dominant sub-network which is strongly affected by the aperture distribution. The remaining fractures can be ignored without strongly affecting the overall flow through the fracture network.

The typical fracture spacing and sizes of matrix blocks defined by the entire fracture network are generally larger than those formed by the dominant sub-work which carries most of the flow. If the typical fracture spacing used to calculate the shape factor for a waterflooding process accounts for the entire fracture network, it means the water is assumed to flow through all fractures and all fractures participate in the imbibition process, which is not the case. The shape factor calculated by taking all fractures into account may lead to inaccurate dual-porosity/dual-permeability simulation of the water-flood process. A similar argument applies to EOR; the injected EOR agent does not flow equally through all the fractures.

This suggests that the shape factor for dual-porosity/dual-permeability simulation should be different for primary and for secondary recovery and EOR. Specifically, for primary recovery, all fractures should be included, while for the processes in which delivery of injected fluids plays a limiting role, such as secondary recovery and EOR, the characteristic matrix-block size utilised in simulation should be larger.

# 4

# CHARACTERISTIC FRACTURE SPACING IN PRIMARY AND SECONDARY RECOVERY FOR NATURALLY FRACTURED RESERVOIRS

The content described in this chapter is submitted to Fuel for publishing.

## 4.1 Introduction

A significant amount of hydrocarbon reserves across the world resides in naturally fractured reservoirs (Saidi 1987). Accurate simulation of oil recovery is required for the efficient exploitation of these naturally fractured reservoirs. However, because of the complexity and limited information on the sub-surface fracture networks, field-scale reservoir simulation requires the reservoir description to be simplified.

If the fracture network is well connected, this is often done with a dual-porosity or dual-permeability (DP/DK) description. In the DP/DK concept, the fracture and matrix systems are treated as separate domains; interconnected fractures serve as fluid-flow paths between injection and production wells, while the matrix provides fluid storage for nearby fractures. Limited fluid flow between matrix blocks is allowed in dual-permeability models (Gilman, Kazemi 1988; Hill, Thomas 1985). The interaction between the fracture network and matrix is represented by an exchange function which is characterized by a shape factor (Barenblatt et al. 1960; Warren, Root 1963; Kazemi et al. 1976). During the last decades, discrete fracture models (DFMs) have attracted increasing research interest. In these models, the fracture geometry and complex flow patterns in fracture networks are simulated more accurately (Kim, Deo 2000; Karimi-Fard, Firoozabadi 2003; Karimi-Fard et al. 2004; Geiger et al. 2004; Matthäi et al. 2007; Li, Lee 2008). However, DFMs are typically computationally more expensive. Thus, although DP/DK models are much-simplified characterizations of naturally fractured reservoirs, they are still the most widely used methods for field-scale fractured-reservoir simulations, as they address the dual-porosity nature of fractured reservoirs and are computationally cheaper. To generate a DP/DK model, it is necessary to define the average properties for each grid block, such as porosity, permeability and matrix-fracture interaction parameters (typical spacing or shape factor). (Dershowitz et al. 2000). Therefore, the discrete fracture network considered to generate the DP/DK model parameters is crucial. If homogenization is applied, matrix-fracture exchange can be treated more accurately than in DP/DK simulations (Salimi, Bruining 2010), but, again, one needs a characteristic matrix-block size. However, if the fracture network shows a non-uniform flow, then characterizing fracture spacing or shape factor can be ambiguous.

As we presented in a previous study (Gong, Rossen 2017), even in a well-connected fracture network, there is a dominant sub-network which carries almost all the flow, but it is much sparser than the original network. In this study we refer to fractures in the dominant sub-network as "primary" fractures, and the remaining fractures as "secondary". Primary fractures tend to be wider, but they are not necessarily the widest, longest or most highly connected fractures in the network (Gong, Rossen 2017). The flow-path length of the dominant sub-network can be as little as 30% of that of the corresponding original fracture network. This suggests that in secondary production or enhanced oil recovery (EOR), injected water or an EOR agent flows mainly along a small portion of the fracture network. In contrast, in primary production even relatively small fractures can be an efficient path for oil to flow to a production well.

In fractured reservoirs, oil is produced by different recovery mechanisms. During primary production, oil is mainly recovered by fluid expansion. In secondary production, spontaneous imbibition is the dominant recovery mechanism in water-wet reservoirs. In primary recovery, production depends only on a path to the well, whereas in secondary recovery or EOR, it depends on the injected agent reaching the matrix. This difference suggests that relevant fracture spacing should be different for primary recovery and for waterflood or EOR (Gong, Rossen 2016). We investigate this hypothesis in this study.

### 4.2 Problem Description

This study concerns the flow pattern within a fractured region (which can be seen as a grid block in a DP/DK model) in primary production or a waterflood process. Within a grid block, there is an

interconnected network of primary fractures. The grid defined by this network is inter-penetrated by secondary fractures (tertiary fractures are also included in some cases below). We examine a simplified representation of a unit cell within that region. Specifically, we represent a region bounded by primary fractures and penetrated by secondary fractures (also by tertiary fractures in some cases). In our simple model, the primary fractures are wider, though in reality the aperture is only one factor in determining which fractures carry most of the injected fluid (Gong, Rossen 2016).

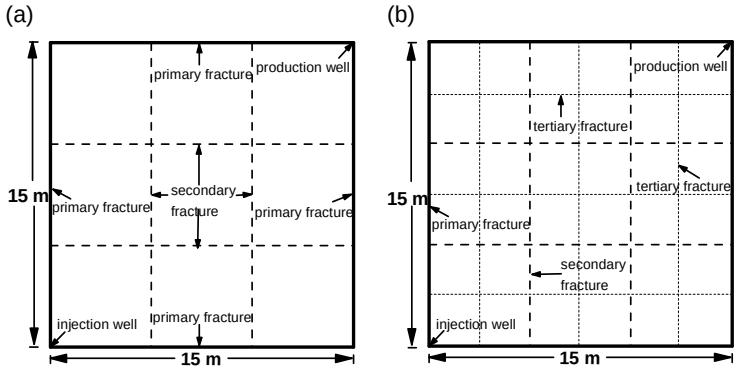


***Figure 4.1*** *Schematic of the region of study. The fractured region studied is 15 m × 15 m, with injection and production wells placed at the bottom-left and the top-right corners, respectively. The injection well and production well are directly connected to primary fractures without contacting the matrix block. (a) The region is bounded by primary fractures, and penetrated by secondary fractures. The number of secondary fractures varies in different cases. In the case shown,* $R_n$ *= 1/3. (b) Tertiary fractures are included in some cases. As in the cases examined below, there are as many tertiary fractures as primary and secondary fractures combined.*

The model employed here is illustrated in Fig. 4.1. It is a 2D, 15 m × 15 m region bounded by four primary fractures (with the same aperture) and penetrated by several secondary fractures. Tertiary fractures (narrower than secondary fractures) are also included in some cases. The injector and producer are connected to the primary fractures and placed at the bottom left and top right corner, respectively. The matrix permeability ($k_m$) in both directions is the same, i.e. 0.5 md. The directional permeability ($k_f$) of the fractures along the fracture direction is given by $d^2/12$, where $d$ is the fracture aperture, while permeability in the direction perpendicular to the fracture is the same as the matrix permeability. The other petrophysical properties are listed in Table 1. The fracture cells are assigned zero capillary pressure and straight-line relative permeabilities. The matrix blocks are water-wet (Fig.4.2). The relative-permeability and capillary-pressure functions for the matrix are (Pooladi-Darvish, Firoozabadi 2000; Brooks, Corey 1964; Corey 1954)

$$k_{ro} = k_{ro}^{o}(1-S)^{n_o}$$

$$k_{rw} = k_{rw}^{o}S^{n_w}$$

$$\mathrm{S} \equiv \frac{S_w - S_{wr}}{1 - S_{wr} - S_{or}} \tag{4.1}$$

$$P_c(S) = -B\ln(S) \tag{4.2}$$

where $S_w$, $S_{wr}$ and $S_{or}$ are water saturation, irreducible water saturation and residual oil saturation; $k_{ro}^{o}$ and $k_{rw}^{o}$ are the end-point oil and water-relative permeabilities, respectively, and $B$ is a constant. Their values are listed in Table 4.2.

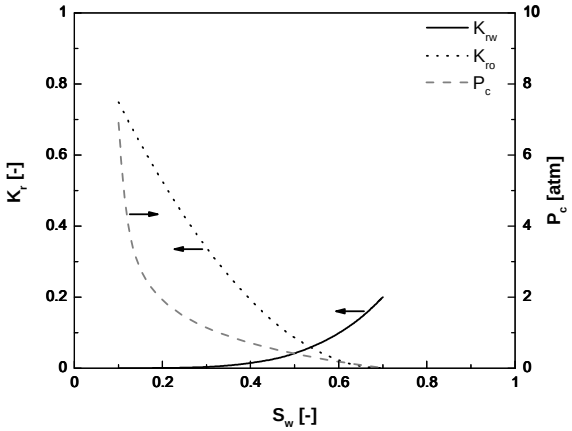


***Figure 4.2*** *The relative permeability and capillary-pressure functions for matrix blocks in all the cases in this study.*

**Table 4.1** Summary of petrophysical properties assumed in this study

| Parameter | *Units* | Value |
|---|---|---|
| Matrix porosity | fraction | 0.2 |
| Fracture porosity | fraction | 1 |
| Oil viscosity | *Pa·s* | 0.0015 |
| Water viscosity | *Pa·s* | 0.00105 |
| Oil density | $kg/m^3$ | 835 |
| Water density | $kg/m^3$ | 999 |

**Table 4.2** Values of parameters in eqs. 4.1 and 4.2 adopted in this study

| Parameter | *Units* | Value |
|---|---|---|
| $n_o$ | - | 2 |
| $n_w$ | - | 4 |
| $k_{ro}^o$ | - | 0.75 |
| $k_{rw}^o$ | - | 0.2 |
| $B$ | $Pa$ | $1.01\times10^5$ |

### 4.3 Methodology

In order to identify the roles played by primary and secondary or tertiary fractures, we examine the flow behavior in three cases: (1) all fractures present; (2) secondary or tertiary fractures excluded; and (3) all fractures present, but with the same average aperture (specifically, the arithmetic-average aperture of all the fractures in case (1)). In case (3), all fractures play a similar role, as is assumed in the traditional DP/DK concepts.

The results are analysed according to three dimensionless groups.

The Peclet number indicates the relative importance of advection and diffusion to the transport of a physical quantity in a given system. In this study, the intent is to represent the relative efficiency of matrix production and fracture flow: i.e., how conductive fractures are compared to matrix productivity. Details of our analysis can be found in the appendix. Considering the different oil-recovery mechanisms

in primary and secondary recovery (or EOR), we propose different Peclet numbers for the two oil-recovery processes. The Peclet numbers proposed in this study are based on primary fractures.

During primary production, oil is produced by fluid expansion. The pressure drops rapidly in the fractures because of the high permeability while, in contrast, the matrix remains at higher pressure. This creates a pressure difference between the fracture and the adjacent matrix block, and in turn, leads to the flow of oil from the matrix to the fracture.

We define the Peclet number for primary production as the ratio of the time taken for the matrix to deliver 1 $m^3$ fluid to the time for the adjacent fracture to transport 1 $m^3$ fluid:

$$Pe \equiv \left(\frac{L^2/\alpha_h}{L^2 h\phi S_{oi}\, C_t\, \Delta p}\right)/\left[\mu_o L/\left(k_f\, d\, h\, \Delta p\right)\right] \tag{4.3}$$

where

$$\alpha_h = \frac{k_m}{\phi \mu c_t} \tag{4.4}$$

is the hydraulic diffusivity, $h$ is the thickness of the model, $C_t$ is the total compressibility, $S_{oi}$ is the original oil saturation, $\Delta p$ is the pressure difference, $\mu_o$ is the oil viscosity, $k_f$ is the fracture permeability, $L$ is the matrix (fracture) length and $d$ is the fracture aperture. When $Pe$ is large, the surrounding fractures are highly conductive compared to the matrix, while a small $Pe$ indicates that the fractures are not efficient.

In a waterflood, we focus on counter-current imbibition. Injected water rapidly flows through the fracture network and surrounds a matrix block. If the matrix block is water-wet, the injected water imbibes into the matrix block because of capillary pressure.

The $Pe$ for counter-current imbibition is defined as follows:

$$Pe \equiv \left[\frac{L^2/\alpha_m}{L^2 h\phi(S_{oi} - S_{or})}\right]/\left(\frac{1}{Q f_{wI}}\right) \tag{4.5}$$

where the capillary diffusion coefficient $\alpha_m$ is defined as:

$$\alpha_m(S_w) \equiv -\frac{k_m}{\phi} f_w \lambda_o \frac{dP_C}{dS_w} \tag{4.6}$$

with the water fractional flow $f_w$ given by

$$f_w = \frac{k_{rw}/\mu_w}{k_{rw}/\mu_w + k_{ro}/\mu_o} \tag{4.7}$$

where $P_c$ is capillary pressure, $k_{rw}$ is water relative permeability and $k_{ro}$ is the oil relative permeability (all three are functions of $S_w$), and $\mu_w$ and $\mu_o$ are water and oil viscosity, respectively. $S_{oi}$ is the initial oil saturation, $Q$ is the volumetric flow rate through the fracture and $f_{wI}$ is the water fraction entering the fracture. Coefficient $\alpha_m$ is not a constant, but if one chooses an approximate average value for the recovery process, one can define a characteristic time. In this study, we apply a value of $\alpha_m \cong 1.9 \times 10^{-9}$ $m^2/s$, as discussed in the appendix.

In addition, we consider two additional dimensionless groups:

- The ratio of aperture $d$ of primary and secondary fractures ($R_d$). We specify an aperture of 1 mm for the primary fractures and vary the aperture of secondary fractures in the cases with $R_d \leq 12.6$. In order to avoid possible numerical problems with extremely narrow fractures, in the cases with $R_d \geq 12.6$, we specify an aperture of 1 mm for all fractures and make up the difference by adjusting fracture permeability $K_f$. In these cases the fracture aperture we use in the ratio $R_d$ is that corresponding to the same fracture transmissivity as in the simulation, i.e. (in m) $[12 \times 10^{-3}\ k_f]^{1/3}$. Since fracture permeability is defined as $d^2/12$, the ratio of permeabilities is

square of the corresponding ratio of aperture. For example, for $R_d$ = 10, the ratio of permeability is 100. If tertiary fractures are included, $R_{d3}$ is the ratio between the apertures of primary and tertiary fractures.

- The ratio of the numbers of primary fractures to the total of primary and secondary fractures ($R_n$) in a unit cell. $R_n$ = 1/3 approximately corresponds to our previous DFN study.

## 4.4 Results

### 4.4.1 Primary Production

Since the Peclet number reflects the relative capacity of the fractures and the matrix to transport oil, we first present the flow patterns in the region studied with different values of the Peclet number, including some extreme cases in which the fracture permeability is very limited. The cumulative oil production and the pressure-distribution map are the bases for comparison. The results are presented as functions of dimensionless time $t_D$, defined by Eq. A3 in the appendix. We compare the original fracture network, the network where all fractures have an average aperture of the fractures in the original network, and the network with secondary fractures excluded. Cumulative oil recovery is normalized by producible oil for the given process.

Fig. 4.3 shows the results for $R_d \cong 2.5$. This value of $R_d$ approximates the results of our DFN study (Gong, Rossen 2017), i.e. that just 1/3 of the fractures account for 90% of the permeability of the fracture network. The pressure drops equally near both primary and secondary fractures for *Pe* = 1,000; all the fractures are conductive enough to transport the oil delivered by the surrounded matrix block. All the fractures contribute equally (figs. 4.3a and b) and the matrix limits oil production. For *Pe* = 10, all the fractures contribute nearly equally, but the fracture network limits oil production. For *Pe* = 0.1, even the primary fractures are unable to accommodate matrix productivity, and secondary fractures hardly matter. Oil recovery slows as *Pe* decreases, because the fractures are less able to transport oil produced by the matrix block (Fig. 4.4). For *Pe* = 1,000, treating all the fractures equally is a better approximation than excluding the secondary fractures; for *Pe* = 10 or less, it is more accurate to exclude the secondary fractures, the error in excluding the secondary fractures is not large.

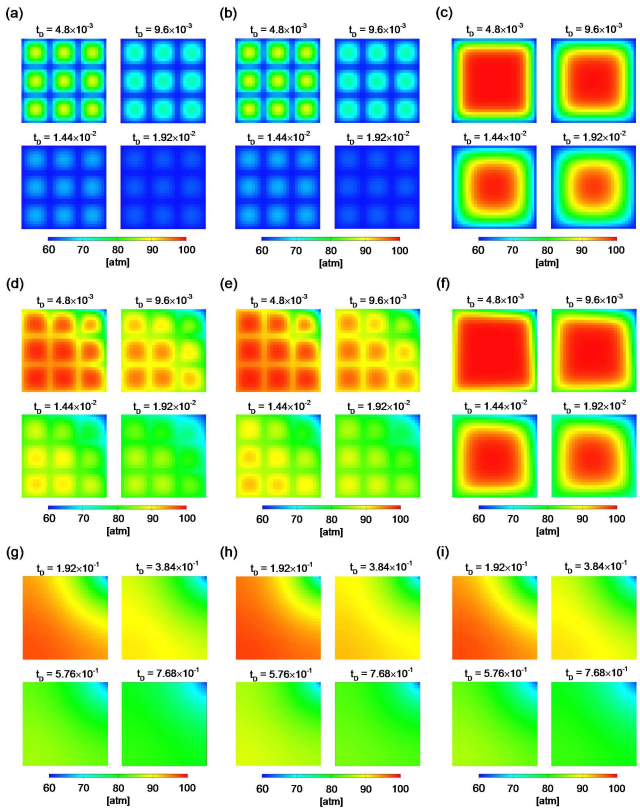


***Figure 4.3*** *Pressure distribution during primary production for different* Pe*, with* $R_d$ *= 2.5 and* $R_n$ *= 1/3. (a)* Pe *= 1,000, with all fractures; (b)* Pe *= 1,000, with all average fractures; (c)* Pe *= 1,000, without secondary fractures; (d)* Pe *= 10, with all fractures; (e)* Pe *= 10, with all average fractures; (f)* Pe *= 10, without secondary fractures; (g)* Pe *= 0.1, with all fractures; (h)* Pe *= 0.1, with all average fractures; (i)* Pe *= 0.1, without secondary fractures.*

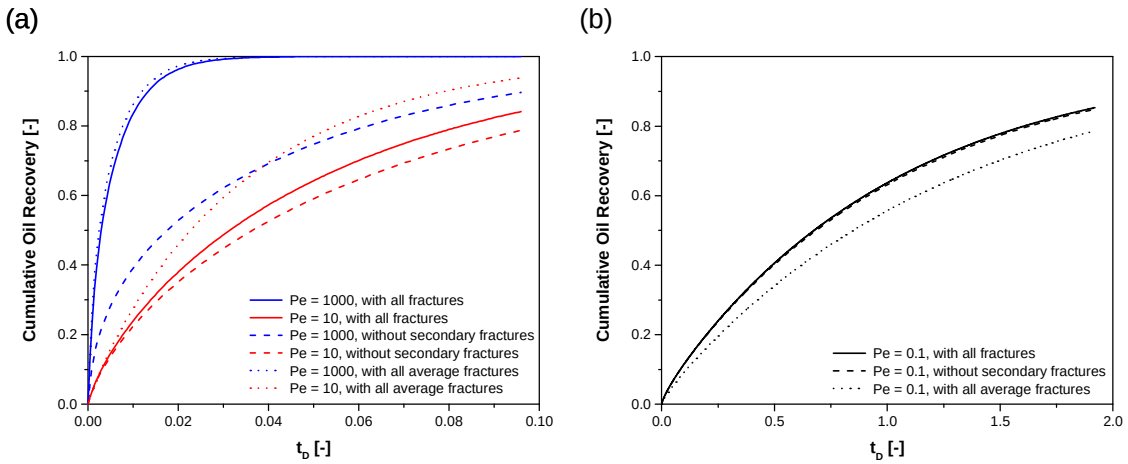


***Figure 4.4*** *Cumulative oil recovery during primary production for different* Pe*,* $R_d$ *= 2.5 and* $R_n$ *= 1/3. The cumulative oil recovery is normalized by the producible oil for the given pressure reduction.*

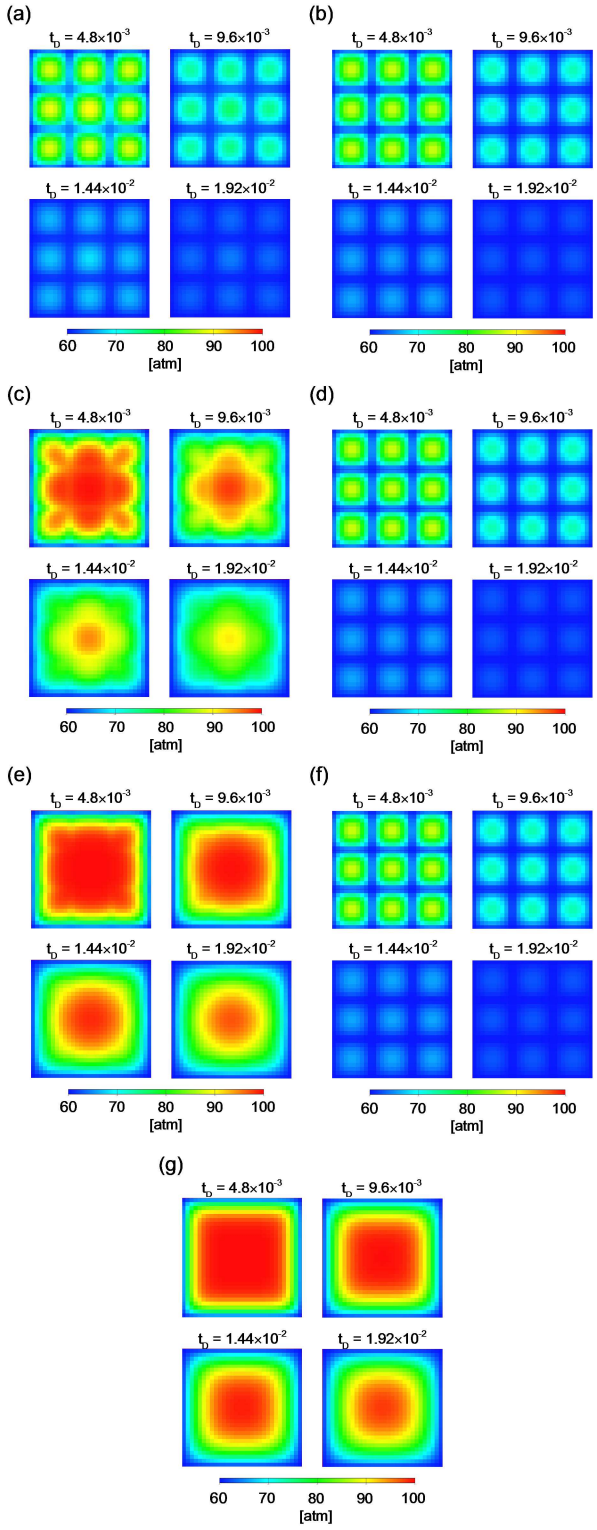


***Figure 4.5*** *Pressure distribution during primary production for different* $R_d$ *with* Pe *= 10,000 and* $R_n$ *= 1/3. (a)* $R_d$ *= 5.8, with all fractures; (b)* $R_d$ *= 5.8, with all average fractures; (c)* $R_d$ *= 43.1, with all fractures; (d)* $R_d$ *= 43.1, with all average fractures; (e)* $R_d$ *= 79.4, with all fractures; (f)* $R_d$ *= 79.4, with all average fractures; (g) without secondary fractures.*

Fig. 4.5 shows the effect of $R_d$ with *Pe* = 10,000. For $R_d \cong 5.8$ or less, the secondary fractures play a similar role to the primary fractures; they carry oil produced by the matrix blocks to the production well as efficiently as the primary fractures do. As $R_d$ increases to 43.1, the flow capacity of the secondary fractures is much less than the primary fractures (but still 2000 times more permeable than the matrix);

the secondary fractures still deliver oil, but play a less-important role than the primary fractures. For $R_d \cong 79.4$, the secondary fractures only slightly affect oil recovery, and the flow pattern is very close to the case without secondary fractures.

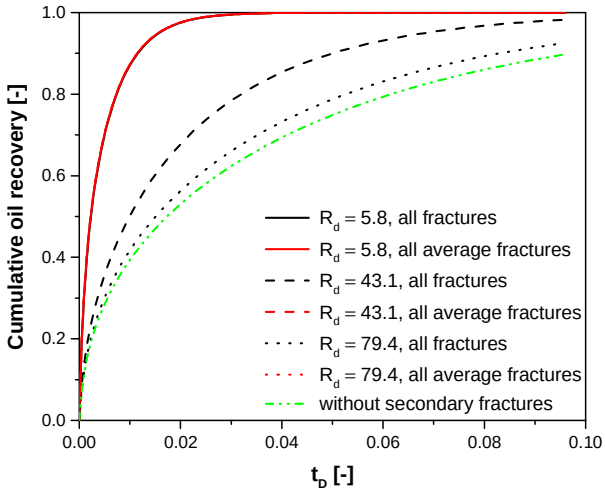


***Figure 4.6*** *Cumulative oil recovery during primary production for different* $R_d$ *with* Pe *= 10,000 and* $R_n$ *= 1/3. The curves for models with all average fractures for all three values of* $R_d$ *overlie each other. The cumulative oil recovery is normalized by the producible oil for the given pressure reduction.*

Fig. 4.6 compares the cumulative oil recovery of the original model, the model with all average fractures and the model without secondary fractures for the values of $R_d$ in Fig. 4.5. The curves for the models with all average fractures for all the $R_d$ values examined overlie each other. For $R_d \cong 5.8$, the model with all average fractures provides a good approximation to the original model. As $R_d$ increases (the secondary fractures become less permeable), the oil-production curve approaches that for the model without secondary fractures. For $R_d \cong 43.1$, production is approximately midway between that with all average fractures and that excluding the secondary fractures. In summary, if the secondary fractures are much narrower than the primary fractures, and *Pe* is large, the secondary fractures can be ignored without much loss of accuracy for simulation of primary production. Otherwise, treating the primary and secondary fractures equally approximates the original fractured region well during primary production.

Fig. 4.7 shows the effect of $R_n$ (i.e., changing the number of secondary fractures) with *Pe* = 10,000 and $R_d \cong 2.5$. The rate of oil recovery is heavily affected by $R_n$. But, again, the models that represent all the fractures as equally important provides a better approximation to the original models than those ignoring the secondary fractures.

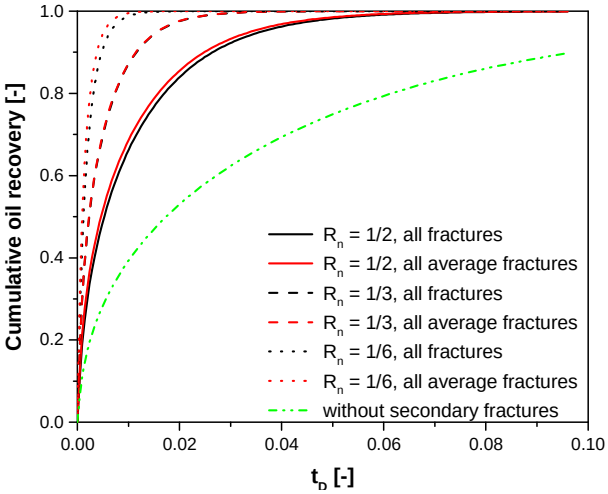


***Figure 4.7*** *Cumulative oil recovery during primary production for different* $R_n$ *with* Pe *= 10,000 and* $R_d$ *= 2.5.*

### 4.4.2 Secondary Production

The Peclet number for waterflood as defined in this study depends on the injection rate and water fraction in the injected fluid ($f_{wI}$). In most of the simulations below, $f_{wI}$ = 1. The relative amounts of water carried by the primary and secondary fractures are dominated by the ratios of fracture apertures ($R_d$) and number of fractures ($R_n$).

As noted above, the case with $R_d \cong 2.5$ and $R_n$ = 1/3 approximates the flow distribution in our previous DFN study (Gong, Rossen 2017). Fig. 4.8 shows the effect of *Pe* for this case. For *Pe* = 6,000, injected water flowing through both the primary and secondary fractures is able to supply all the water that the matrix can imbibe (Fig. 4.8a). The fluid exchange between the matrix and both primary and secondary fractures is counter-current imbibition. As the Peclet number decreases to 600, the injected water in the secondary fractures is unable to satisfy the adjacent matrix (Fig. 4.8d). The secondary fractures contribute to oil recovery by enabling co-current imbibition from the primary fractures, as confirmed by the examination of oil velocity at the face of the secondary fractures (not shown). Eventually, water reaches all the matrix blocks. For *Pe* = 60, the secondary fractures are less able to satisfy the adjacent matrix, but the matrix adjacent to the primary fractures expels oil by co-current imbibition. The role of co-current imbibition is evident in a comparison of Figs. 4.8g and i: at $t_D$ = 0.5 PV, oil is expelled more rapidly from the matrix adjacent to primary fractures, if secondary fractures are available to carry away the oil. The central matrix block, however, must wait for water from the secondary fractures. The secondary fractures provide a capillary barrier to co-current imbibition from the primary fractures.

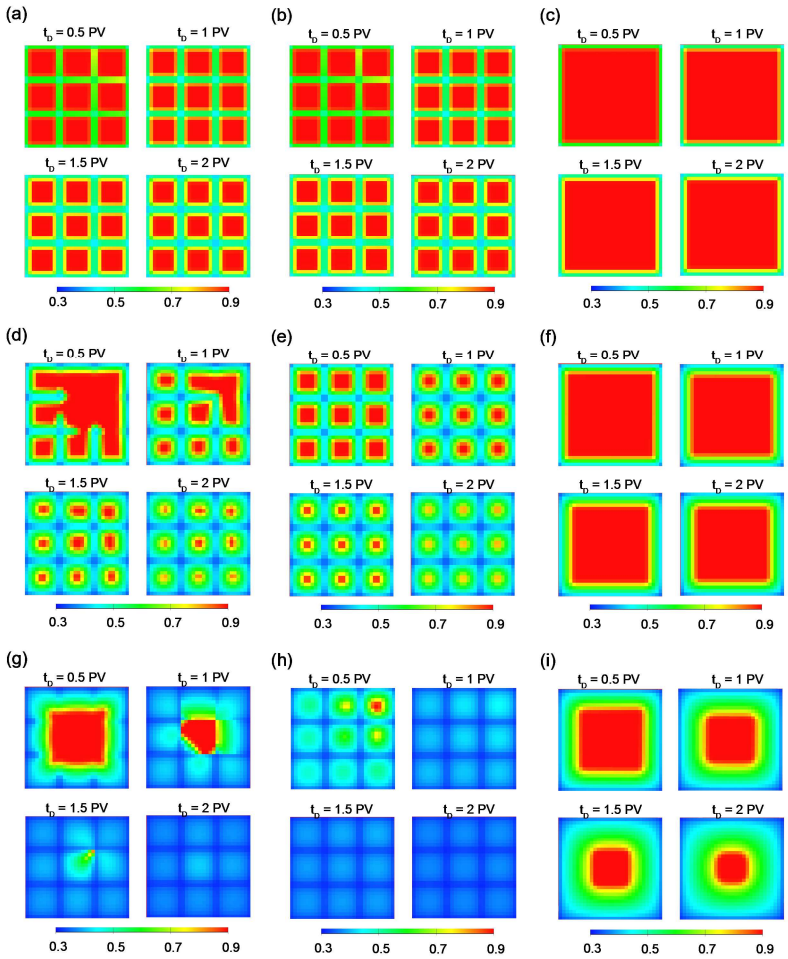


***Figure 4.8*** *Oil saturation during secondary production for different* Pe*, with* $R_d$ *= 2.5, and* $R_n$ *= 1/3. (a)* Pe *= 6,000, with all fractures, (b)* Pe *= 6,000, with all average fractures, (c)* Pe *= 6,000, without secondary fractures, (d)* Pe *= 600, with all fractures, (e)* Pe *= 600, with all average fractures, (f)* Pe *= 600, without secondary fractures, (g)* Pe *= 60, with all fractures, (h)* Pe *= 60, with all average fractures, (i)* Pe *= 60, without secondary fractures.*

Fig. 4.9 shows oil recovery for these cases. In all the cases, oil recovery is better approximated by treating all the fractures equally than by excluding secondary fractures. For *Pe* = 600 or less, however, treating all fractures equally overestimates oil recovery in the early stages. In none of the cases examined for the ratio of apertures based on our earlier DFN study (Gong, Rossen 2017) does simply excluding secondary fractures give a better approximation of oil recovery.

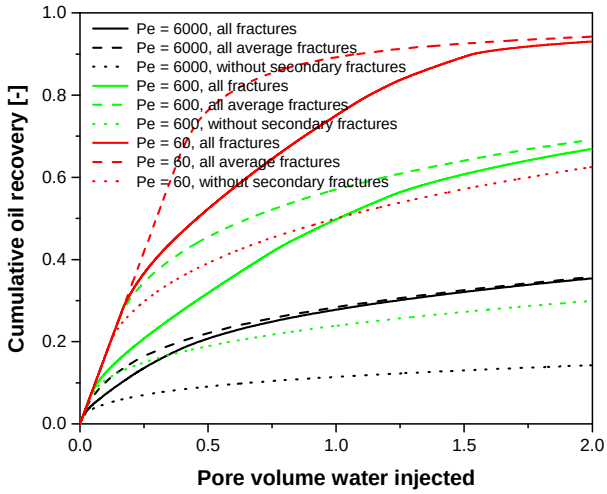


***Figure 4.9*** *Cumulative oil recovery during secondary production for different* Pe*, with* $R_d$ *= 2.5 and* $R_n$ *= 1/3. The cumulative oil recovery is normalized by the producible oil.*

We next hold the Peclet number at *Pe* = 6,000, and vary the aperture ratio $R_d$. Fig. 4.10 shows that for $R_d \cong 2.5$, the injected water flows rapidly through both the primary and secondary fractures. Fluid exchange between the matrix and both the primary fractures and secondary fractures is by counter-current imbibition. Primary fractures and secondary fractures play similar roles (Figs. 4.10a and b). Fig. 4.11 shows that the model with all average fractures gives a better approximation of the rate of oil recovery than the model without secondary fractures.

For $R_d \cong 6.3$, the injected water flows rapidly through the primary fractures, but slowly through the secondary fractures (Fig. 4.10c). For the matrix blocks bounded by both primary and secondary fractures, the injected water imbibes into the matrix block from the primary fractures, and some oil flows into the secondary fractures, allowing co-current imbibition. Therefore, although the secondary fractures do not carry much injected water, they still provide paths for oil to flow to the production well. Nevertheless, Fig. 4.11 shows that for $R_d \geq 6.3$ or more, the model assuming that all the fractures have an average aperture considerably overestimates oil recovery; the model excluding secondary fractures provides a better approximation.

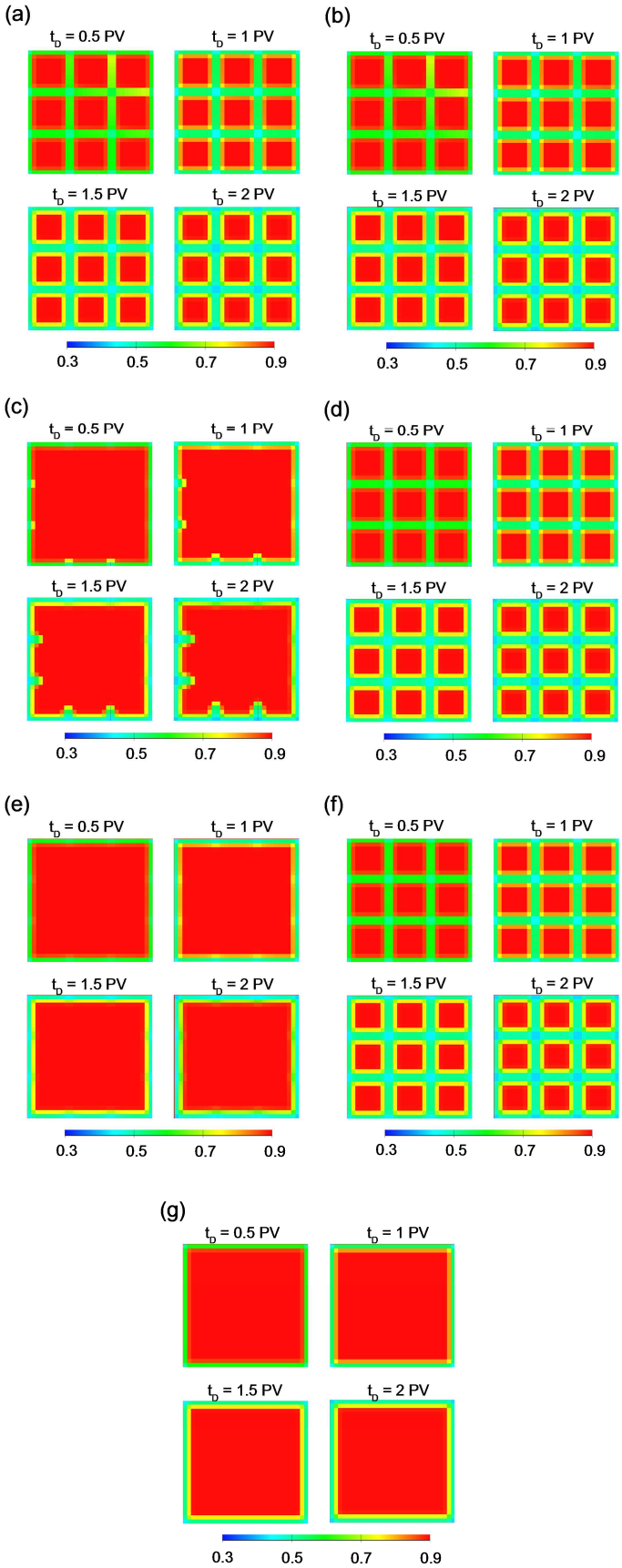


***Figure 4.10*** *Oil saturation during secondary production for different* $R_d$*, with* Pe *= 6,000,* $R_n$ *= 1/3. (a)* $R_d$ *= 2.5, with all fractures, (b)* $R_d$ *= 2.5, with all average fractures, (c)* $R_d$ *= 6.3, with all fractures, (d)* $R_d$ *= 6.3, with all average fractures, (e)* $R_d$ *= 12.6, with all fractures, (f)* $R_d$ *= 12.6, with all average fractures, (g) without secondary fractures.*

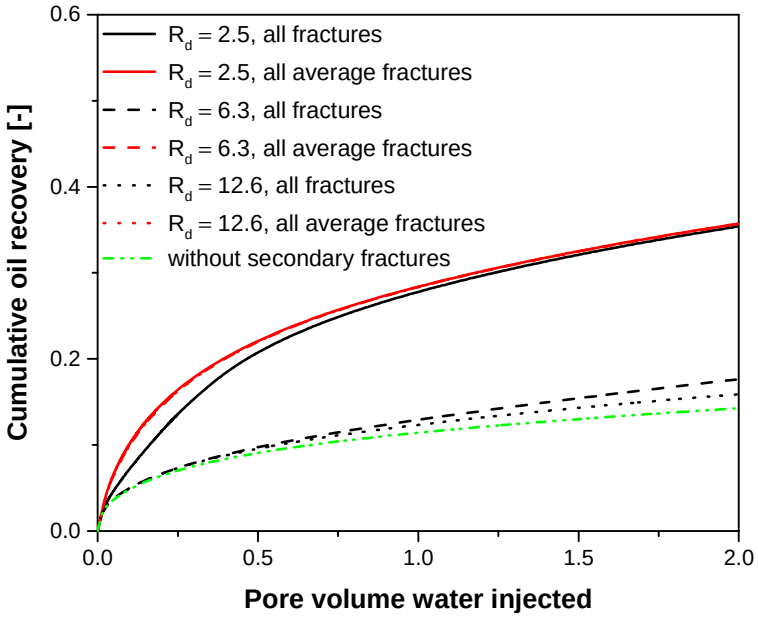


***Figure 4.11*** *Cumulative oil recovery during secondary production for different* $R_d$*, with* Pe *= 6,000,* $R_n$ *= 1/3, and different* $R_d$*. The cumulative oil recovery is normalized by the producible oil. All the cases with all average fractures overlie each other.*

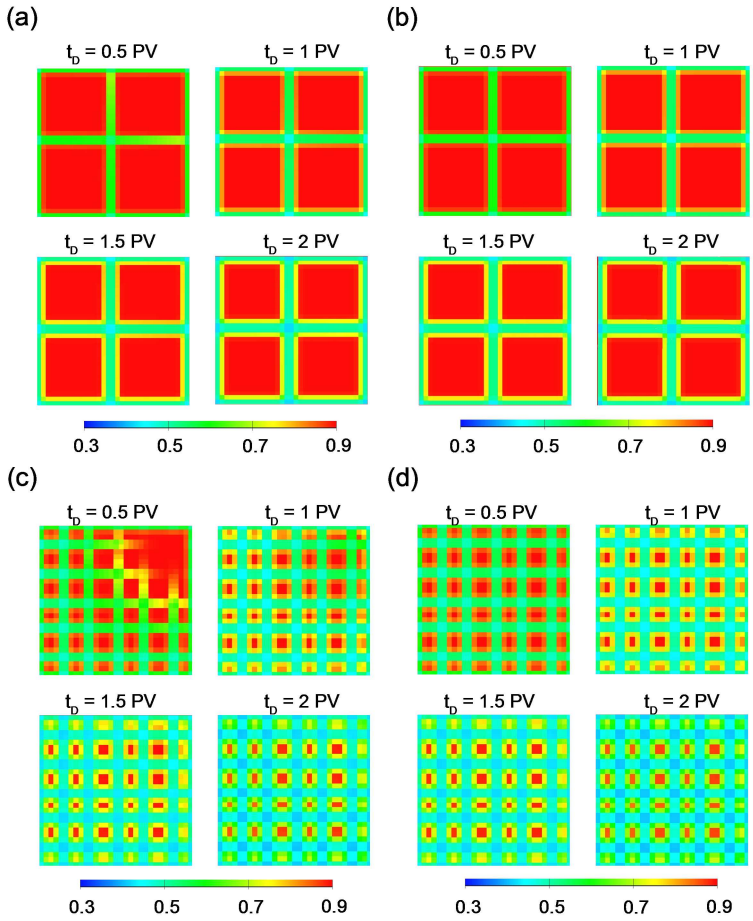


***Figure 4.12*** *Oil saturation during secondary production for different* $R_n$*, with* Pe *= 6,000 and* $R_d$ *= 2.5. (a)* $R_n$ *= 1/2, with all fractures; (b)* $R_n$ *= 1/2, all average fractures; (c)* $R_n$ *= 1/6, with all fractures; (d)* $R_n$ *= 1/6, all average fractures.*

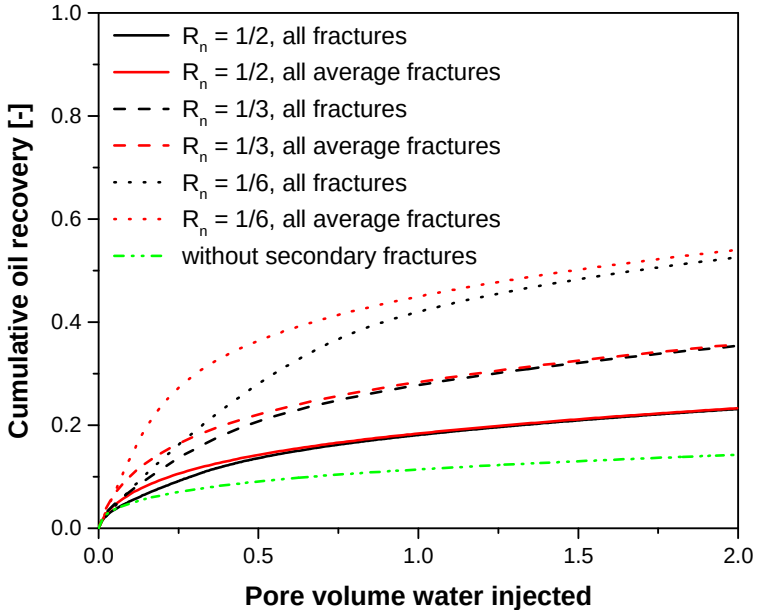


***Figure 4.13*** *Cumulative oil recovery during secondary production for different* $R_n$*, with* Pe *= 6,000 and* $R_d$ *= 2.5. The cumulative oil recovery is normalized by the producible oil.*

Figs. 4.12 and 4.13 show the effect of the ratio of numbers of primary and secondary fractures ($R_n$) for *Pe* = 6,000 and $R_d \cong 2.5$. It is more accurate to treat all the fractures equally than to exclude the secondary fractures.

The very definition of primary and secondary fractures, however, is affected by the truncation of the fracture distribution imposed by the length scale and the resolution of the fracture trace map. In reservoir simulation, considering the resolution of the fracture trace map of a field, as well as computational capacities, the set of fractures taken into account is truncated within a certain range. For a power-law distribution of apertures, very few of the narrowest fracture in the truncated distribution are among the primary fractures, and there would be many of these narrower fractures just below the aperture cutoff. For example, in our previous DFN study (Gong, Rossen 2017), the fractures are restricted to within a certain range of lengths (one order of magnitude) and aperture (three orders of magnitude). For broad aperture distributions, almost no primary fractures were near the lower limit of aperture. Thus if the distribution considered was extended to narrower fractures, there would be many narrower fractures in the distribution as a whole, with little change in the primary fracture network. We therefore examine next the role that excluded narrower fractures play during a waterflood process by including tertiary fractures in the model. In this case, $R_{d3}$ is the ratio of the apertures of the primary and tertiary fractures.

In Figs. 4.14 and 4.15, the aperture ratio between the primary and secondary fractures is 2.5, and the tertiary fractures are half as wide as the secondary fractures ($R_{d3}$ = 5). In all the cases, there are as many tertiary fractures as primary and secondary fractures combined. The tertiary fractures play a role in producing oil, although they are not as important as the primary and secondary fractures. The tertiary fractures become less important as the Peclet number becomes smaller. When *Pe* decreases to 60, the tertiary fractures are not very helpful. Considering all the fractures to be equally conductive overestimates the oil recovery for all *Pe* examined here. For *Pe* = 60, excluding the tertiary fractures leads to a more accurate prediction of oil recovery than treating them as equal to the other fractures.

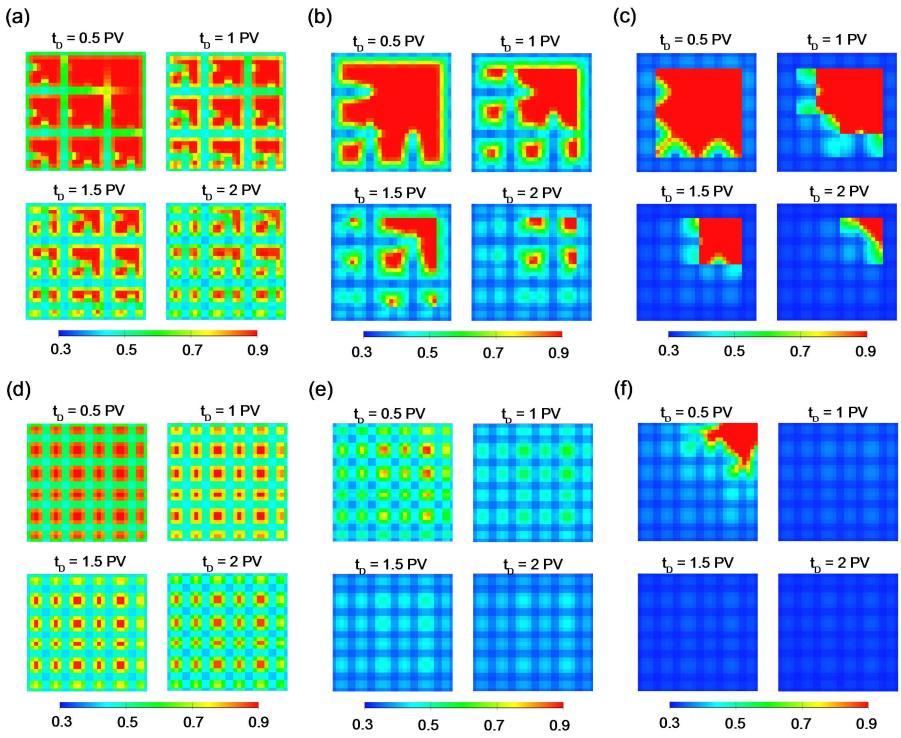


***Figure 4.14*** *Oil saturation during secondary production with tertiary fractures for different* Pe. *(a)* Pe *= 6,000,* $R_d$ *= 2.5,* $R_{d3}$ *= 5, (b)* Pe *= 600,* $R_d$ *= 2.5,* $R_{d3}$ *= 5, (c)* Pe *= 60,* $R_d$ *= 2.5,* $R_{d3}$ *= 5, (d)* Pe *= 6,000, with all average fractures, (e)* Pe *= 600, with all average fractures, (f)* Pe *= 60, with all average fractures.*

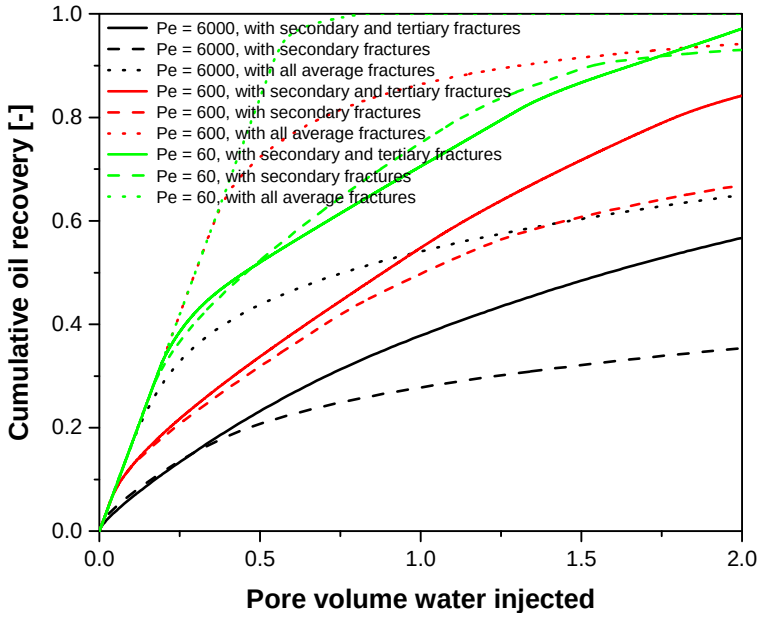


***Figure 4.15*** *Cumulative oil recovery during secondary production with tertiary fractures for different* Pe, $R_d$ *= 2.5,* $R_{d3}$ *= 5. The cumulative oil recovery is normalized by the producible oil.*

Figs. 4.16 and 4.17 show a more extreme case, with the aperture ratio between the primary and tertiary fractures ($R_{d3}$) set at 34.2. The injected water flows through the primary and secondary fractures and imbibes into the adjacent matrix, and then pushes oil into the tertiary fractures by co-current imbibition. The tertiary fractures help in producing oil in this case.

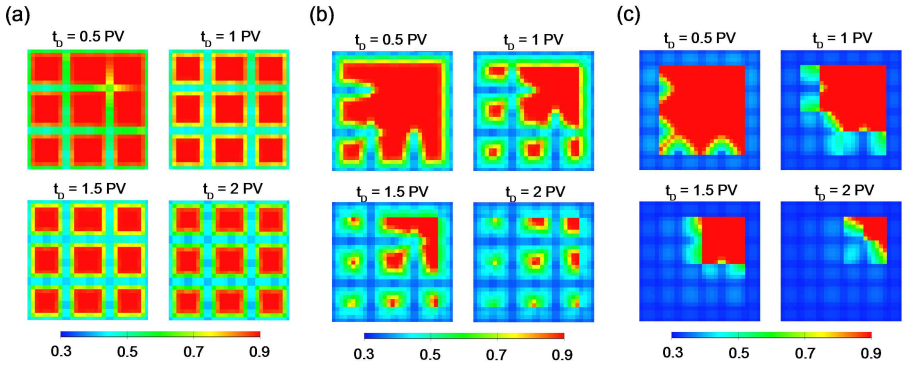


***Figure 4.16*** *Oil saturation during secondary production with tertiary fractures for different* Pe. *(a)* Pe *= 6,000,* $R_d$ *= 2.5,* $R_{d3}$ *= 34.2, (b)* Pe *= 600,* $R_d$ *= 2.5,* $R_{d3}$ *= 34.2, (c)* Pe *= 60,* $R_d$ *= 2.5,* $R_{d3}$ *= 34.2.*

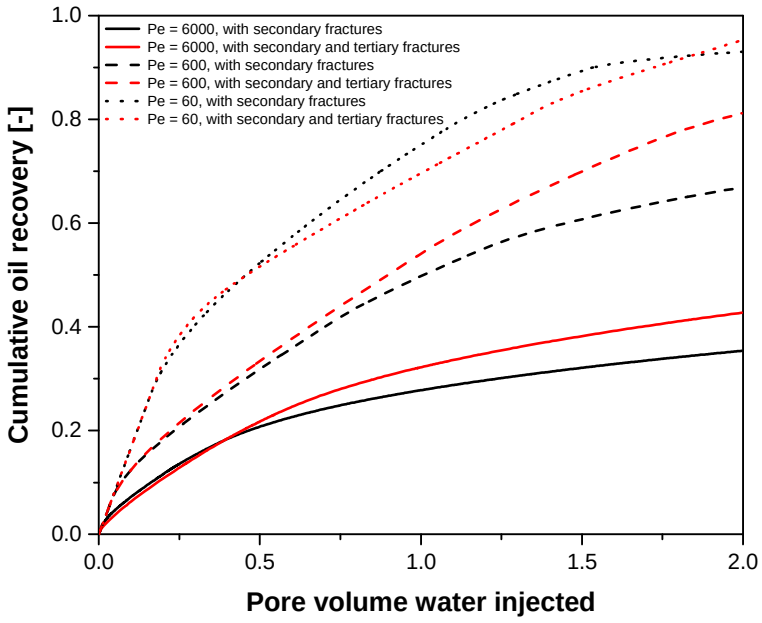


***Figure 4.17*** *Cumulative oil recovery during secondary production with tertiary fractures for different* Pe, $R_d$ *= 2.5,* $R_{d3}$ *= 34.2. The cumulative oil* recovery *is normalized by the producible oil.*

Figs. 4.18 and 4.19 show flow behavior of the fractured region with narrower secondary fractures ($R_d \cong 12.6$), and the tertiary fractures with the same aperture as in the previous case ($R_{d3} \cong 34.2$). For *Pe* = 6,000 and 600, the cases with and without tertiary fractures show similar oil recovery after 2 PV of water injected. When *Pe* decreases to 60, the oil residing in the matrix adjacent to the primary fractures is produced as in the case without tertiary fractures, but the rest of the matrix, bounded by tertiary fractures, hardly produces any oil. Evidently the tertiary fractures act as capillary barriers, not helping, but limiting, oil production. In translating a fracture map to a DP/DK model, there are two issues: whether all the fractures contribute to recovery, and whether some may act as barriers to recovery.

The effect of the unavoidable truncation of a measured fracture distribution requires further study. The wider the range of fractures included, the larger the number of secondary (and narrower) fractures included and the less accurate inclusion of all fractures on an equal basis in the definition of fracture spacing and shape factor. Those just before the truncation cut-off and excluded may have either no effect or a significant effect on the matrix-fracture exchange.

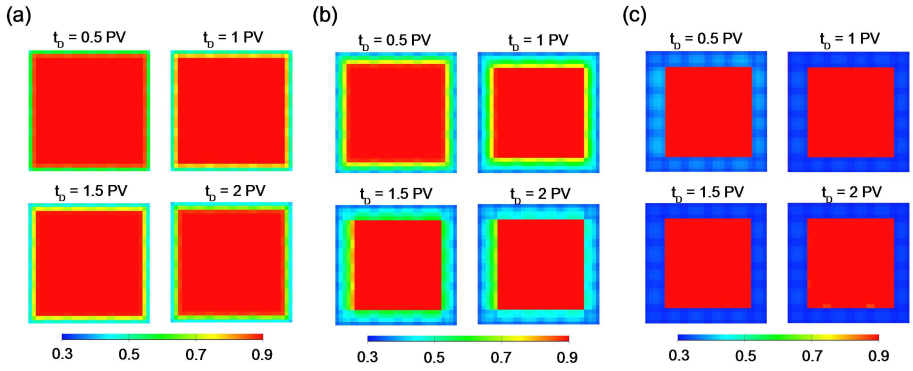


***Figure 4.18*** *Oil saturation during secondary production with tertiary fractures for different* Pe*. (a)* Pe *= 6,000,* $R_d$ *= 12.6,* $R_{d3}$ *= 34.2, (b)* Pe *= 600,* $R_d$ *= 12.6,* $R_{d3}$ *= 34.2, (c)* Pe *= 60,* $R_d$ *= 12.6,* $R_{d3}$ *= 34.2.*

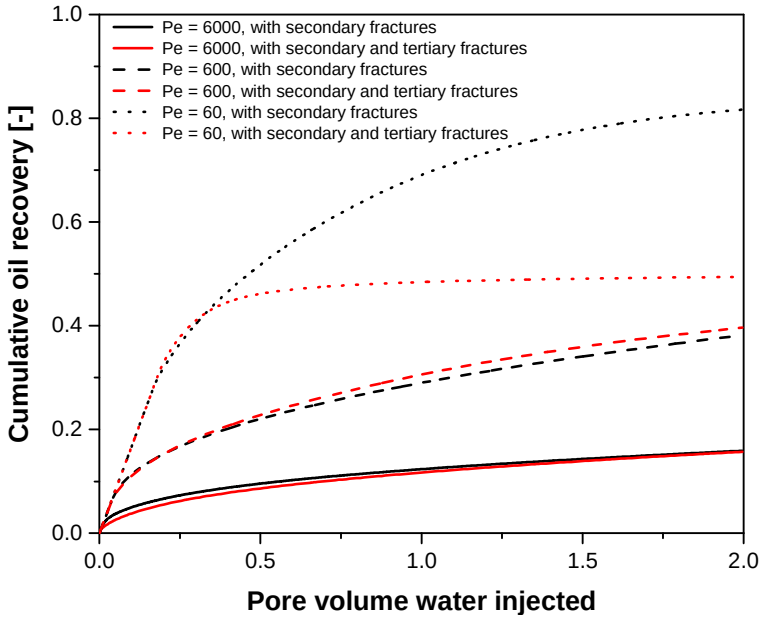


***Figure 4.19*** *Cumulative oil recovery during secondary production with tertiary fractures for different* Pe*,* $R_d$ *= 12.6,* $R_{d3}$ *= 34.2. The cumulative oil recovery is normalized by the producible oil.*

### 4.4.3 Conclusions and Discussion

In this chapter we consider the effect of heterogeneity on flow through a fracture network on the best characterization of the network for reservoir simulation. The results depend on the relative flow rates through primary and secondary fractures, represented here by the ratio of their apertures, the ratio of the number of primary and secondary fractures, and a Peclet number defined in the appendix. As shown in the appendix, this definition of a Peclet number works better than a previous published definition for the purpose of this study. This Peclet number depends on the matrix and fracture properties and, for waterflood, on the flow rate and water fraction in the fracture network. We focus in particular on the case with $R_d \cong 2.5$ and $R_n = 1/3$, which approximates the flow distribution in our previous study (Gong, Rossen 2017).

Our focus in this study is limited to well-connected fracture networks; all the secondary (and tertiary) fractures are connected to the primary fractures. In nature, a fracture network may not be so well-connected, which would change the flow behavior of the fractured region in some aspects. In addition, in this study, we have disregarded gravity-driven flow between the matrix and fractures, which could change the scaling of matrix-fracture exchange in secondary and tertiary recoveries.

#### *4.4.3.1 Primary Production*

For $R_d \cong 2.5$, $R_n = 1/3$, the role that secondary fractures play during primary production can be divided into three categories according to the Peclet number. 1) For a very small Peclet number (*Pe* = 0.1), the secondary fractures play a minor role: even the primary fractures are unable to accommodate the matrix productivity. Excluding the secondary fractures gives a good approximation of the oil production, somewhat better than including them as equally conductive to primary fractures. The best shape factor (characteristic fracture spacing) in DP/DK simulation should then only account for the primary fractures. 2) For somewhat larger *Pe* (10), the secondary fractures help in producing oil, but play a less important role than the primary fractures. Neither considering all the fractures equally nor excluding the secondary fractures provides a perfect approximation of the flow behavior of the fractured region. 3) For a larger Peclet number (*Pe* = 1,000), the secondary fractures are as important as the primary fractures. In other words, considering all the fractures to be equally conductive, as is assumed in a traditional DP/DK concept, provides a good approximation of the flow behavior of the fractured region. The effective fracturing or shape factor for a DP/DK simulation of a primary production process in this situation should consider both the primary and secondary fractures.

For an even larger Peclet number (*Pe* = 10,000), the secondary fractures play a less important role as $R_d$ increases. For $R_d \cong 5.8$, the secondary fractures play a similar role to the primary fractures. As $R_d$ increases to 79.4, the secondary fractures can be excluded without affecting oil recovery.

For *Pe* = 10,000, $R_d \cong 2.5$, considering all the fractures as equally conductive provides a good approximation for all the value of $R_n$ examined. The smaller the value of $R_n$ is, the worse the approximation given by excluding the secondary fractures.

#### *4.4.3.2 Waterflood*

For $R_d \cong 2.5$ and $R_n = 1/3$, considering all the fractures as equally conductive approximates oil recovery better than excluding the secondary fractures, for all the values of *Pe* examined. But the secondary fractures are not as important as the primary fractures. For *Pe* = 600 and 60, the secondary fractures are important because they allow co-current imbibition from the primary fractures and the adjacent matrix blocks. Recovery with a heterogeneous fracture network is intermediate between that without secondary fractures and with all fractures equally conductive.

For large Peclet number (*Pe* = 6,000) and $R_d \cong 2.5$, recovery with the heterogeneous fracture network is nearly the same as with all fractures equally conductive. For $R_d \cong 6.3$ or larger, secondary fractures carry little injected water, and matter little to oil recovery. In that case, excluding secondary fractures provides a better approximation than considering all fractures as equally conductive. The effective fracture spacing or shape factor for a DP/DK simulation of a waterflood process in this situation should consider only the primary fractures.

For *Pe* = 6,000 and $R_d \cong 2.5$, in which the injected water can flow through all the factures efficiently, all the fractures are nearly equally important for all the values of $R_n$ examined.

#### *4.4.3.3 Effect of Truncation of the Fracture Distribution*

The fractures with an aperture below the cut-off of a truncated aperture distribution, referred to here as tertiary fractures, can be helpful in producing oil, although they are less important than the primary and secondary fractures (Figs. 4.14a and b, Figs. 4.16a and b, Figs. 4.18a and b). Tertiary fractures can also behave as capillary barriers and limit oil recovery (Fig. 4.18c).

In considering the effect of truncating a fracture aperture distribution, one must consider that excluded fractures could either help or hinder oil recovery. The effect of truncation of the fracture distribution on our conclusions deserves further study.

# 5

# CONCLUSIONS AND DISCUSSION

## 5.1 Conclusions

In this dissertation, we explore the implications of non-uniform flow in fracture networks for the dual-porosity/dual-permeability simulation of fractured reservoirs, and the roles that different levels of fractures play in primary and secondary production. Here we present the major conclusions.

### 5.1.1 Effect of Fracture Aperture Distribution on Dominant Sub-Network for Flow (Chapter 2)

This chapter examines the effect of fracture aperture distribution on the dominant sub-network that by itself retains 90% of the effective permeability of the original fracture network. We focus on non-uniform flow in well-connected fracture networks. A number of aperture distributions are tested: log-normal and power-law distributions (from narrow to broad), and one where the aperture is proportional to the fracture length.

- If the aperture distribution is broad enough (exponent $\alpha \leq 2$ for a power-law aperture distribution and log-standard deviation $\sigma \geq 0.4$ for a log-normal aperture distribution), most of the fractures can be eliminated without significantly reducing the effective permeability. As the exponent $\alpha$ increases or the value of $\sigma$ decreases, fewer and fewer fractures can be removed without significantly reducing the network equivalent permeability.
- The importance of each fracture to the overall flow cannot be simply related to the fracture aperture or length. For the cases of both the log-normal and power-law aperture distributions, and that where the aperture is proportional to the fracture length, there are some fractures with a relatively narrow aperture that play a greater role in the overall flow than some others with a larger aperture. It is also true that some fractures with a relatively large aperture carry much less flow than most of the fractures.
- Flow simulations are more effective at identifying the dominant sub-network that by itself retains 90% of the original permeability than eliminating fractures based on length, aperture, or number of intersections. Among those properties, eliminating fractures based on aperture is the most efficient criterion considered here, but it is not as efficient as using flow calculations.

### 5.1.2 Effect of Non-Uniform Flow in Fracture Network on Shape Factor for Dual-Porosity/Dual-Permeability Fractured-Reservoir Simulation (Chapter 3)

In this chapter, we study the influence of the aperture distribution (exponent $\alpha$ in a power-law distribution and log-standard deviation $\sigma$ in a log-normal distribution) on the characteristic sizes of matrix blocks formed by the dominant sub-network. We analyze the sizes of the matrix blocks formed by the entire fracture network and the corresponding dominant sub-network. The implications of this distinction for the dual-porosity/dual-permeability fractured reservoir simulation are as follows:

- The typical fracture spacing and the sizes of matrix blocks defined by the entire fracture network are generally larger than those defined by the dominant sub-network which carries most of the flow.
- If the typical fracture spacing used to calculate the shape factor for a waterflooding process accounts for the entire fracture network, it means that the water is assumed to flow though all fractures, which is not the case. The shape factor calculated by taking all fractures into account may lead to an inaccurate dual-porosity/dual-permeability simulation of the waterflood process. A similar argument applies to the EOR process.
- These results suggest that the shape factor for a dual-porosity/dual-permeability simulation should be different for primary recovery and secondary recovery and EOR. In particular, for the process in which the delivery of injected fluids plays a limiting role, such as secondary recovery and EOR, the characteristic matrix-block size or the shape factor utilized in simulation should be larger than that used to simulate primary production.

### 5.1.3 Characteristic Fracture Spacing in Primary and Secondary Recovery for Naturally Fractured Reservoirs (Chapter 4)

In this part of the work, we investigate in greater detail the effect of heterogeneity in the flow through a fracture network on the best characterization for a fractured-reservoir simulation of primary and secondary production. A simple representation of a fractured region, such as a grid block in a dual-porosity/dual-permeability model, is employed. The results show that the roles of fractures depend on a dimensionless ratio of characteristic times for the matrix and fracture flow (Peclet number), and the ratio of flow carried by different fractures, represented in this model by the ratio of their apertures ($R_d$) and the ratio of the number of the primary and the secondary fractures ($R_n$). The cases with $R_d$ = 2.5 and $R_n$ = 1/3 approximate the results of our DFN study in Chapter 2, i.e. that just 1/3 of the fractures account for 90% of the permeability of the fracture network. Our focus in this study is limited to well-connected fracture networks; all the secondary (and tertiary) fractures are connected to the primary fractures.

- For $R_d$ = 2.5, $R_n$ = 1/3, the secondary fractures play different roles during primary production depending on the Peclet number. The best shape factor for the simulation of primary production should not always take all the fractures into account. For a very small Peclet number (*Pe* = 0.1), the secondary fractures play a minor role; excluding the secondary fractures approximates oil production well. The best shape factor in this case should account only for the primary fractures. For a somewhat larger *Pe* (10), the secondary fractures help in producing oil, but play a less-important role than the primary fractures. Neither considering all fractures equally nor excluding the secondary fractures provides a perfect approximation of the flow behavior of the fractured region. For a larger Peclet number (1,000), the secondary fractures are as important as the primary fractures. In this case, considering all the fractures as equally conductive, as is assumed in a traditional dual-porosity/dual-permeability simulation, gives a good description of the flow behavior of the fractured region well.
- In primary production, for an even larger Peclet number (10,000), the secondary fractures play a less important role as $R_d$ increases, i.e., as the secondary fractures carry less flow. For $R_d$ = 5.8, the secondary fractures play a similar role to the primary fractures. As $R_d$ increases to 79.4, the secondary fractures can be excluded without affecting oil recovery.
- For *Pe* = 10,000, $R_d$ = 2.5, considering all the fractures as equally conductive provides a good approximation for all the values of $R_n$ examined. The smaller the value of $R_n$ is, the worse is the approximation given by excluding the secondary fractures.
- In a waterflood, for most cases examined in this study, considering all the fractures as equally conductive approximates oil recovery better than excluding the secondary fractures.
- However, for the cases with $R_d$ = 2.5, $R_n$ = 1/3, *Pe* = 600 and 60, the secondary fractures are important because they allow co-current imbibition from the primary fractures and the adjacent matrix blocks. Recovery with the heterogeneous fracture network is intermediate between that without the secondary fractures and with all fractures equally conductive.
- For *Pe* = 6,000, $R_n$ = 1/3, $R_d$ = 6.3 or larger, the secondary fractures carry little injected water, and they matter little to oil recovery. In these cases, excluding the secondary fractures provides a better approximation than considering all the fractures as equally conductive. The fracture spacing or the shape factor for a dual-porosity/dual-permeability simulation of a waterflood process should consider only the primary fractures.
- Fractures with an aperture below the cut-off of a truncated aperture distribution, referred to here as tertiary fractures, can be helpful in producing oil, although they are less important than the primary and secondary fractures. They can also behave as capillary barriers and limit oil recovery.
- A new definition of Peclet number for matrix-fracture flow is presented in this thesis. This Peclet number depends on the matrix and fracture properties for primary production and, for waterflood, on the flow rate and water fraction in the fracture network. The results show that this definition of Peclet number works better than a previously published definition (Salimi,

Bruining 2010) for the purpose of characterizing the relative time scales of the fracture flow and the matrix-fracture fluid exchange.

- We propose that the value of *Pe* characterizing a grid block in a simulation which includes $N_b$ x $N_b$ unit cells corresponds roughly to that we propose for a unit cell, divided by the number of unit cells ($N_b$ x $N_b$) defined by primary fractures across a simulation grid block.

## 5.2 Discussion

Our focus in this study is limited to well-connected fracture networks. In nature, a fracture network may not be so well connected, which would change the flow behavior of the fractured region in important aspects.

In addition, in this study, we have disregarded gravity-driven flow between the matrix and the fractures, which could change the scaling of the matrix-fracture fluid exchange in secondary and tertiary recovery.

We take no explicit account of the effect of geo-mechanical stresses on the fracture length and aperture distributions. Horizontal fractures and layers are not considered in this study. In particular, we assume the fracture aperture is uncorrelated with the fracture direction. It would be important to include this effect in future studies. A strong correlation between the fracture aperture and the fracture direction might alter the conclusions of Chapter 2.

Our study shows that sufficiently small fractures (smaller than the secondary fractures here) play an insignificant role in oil recovery except if they serve as capillary barriers. Any characterization of a fracture network includes a lower cut-off for the fracture aperture, explicitly or implicitly (based on the observability). Our results suggest that one should account for this cut-off in deciding which fractures to include in the characterization of matrix-block sizes in the dual-porosity/dual-permeability simulation of fractured reservoirs.

# BIBLIOGRAPHY

Aharony A, Stauffer D. Introduction to percolation theory. London: Taylor & Francis; 2003.

Akker HEA, Mudde RF. Transport Phenomena: The Art of Balancing. Delft Academic Press; 2014.

Aronofsky JS, Masse L, Natanson SG. A Model for the Mechanism of Oil Recovery from the Porous Matrix Due to Water Invasion in Fractured Reservoirs. Society of Petroleum Engineers; 1958.

Balberg I, Anderson C, Alexander S, Wagner N. Excluded volume and its relation to the onset of percolation. Phys Rev B: Condens Matter. 1984;30(7):3933.

Balberg I, Berkowitz B, Drachsler G. Application of a percolation model to flow in fractured hard rocks. J Geophys Res Solid Earth. 1991;96(B6):10015-21.

Barenblatt GI, Zheltov IP, Kochina IN. Basic concepts in the theory of seepage of homogeneous liquids in fissured rocks [strata]. J Appl Math Mech. 1960;24(5):1286-303.

Barker JA. Block-geometry functions characterizing transport in densely fissured media. J Hydrol. 1985;77(1):263-79.

Barton CA, Zoback MD. Self‐similar distribution and properties of macroscopic fractures at depth in crystalline rock in the Cajon Pass Scientific Drill Hole. J Geophys Res Solid Earth. 1992;97(B4):5181-200.

Barton CC, Hsieh PA, Angelier J, Bergerat F, Bouroz C, Dettinger M et al. Physical and Hydrologic-Flow Properties of Fractures Las Vegas, Nevada—Zion Canyon, Utah—Grand Canyon, Arizona—Yucca Mountain, Nevada July 20–24, 1989. Washington, D.C.: American Geophysical Union; 1989.

Belayneh M, Masihi M, Matthäi S, King P. Prediction of vein connectivity using the percolation approach: model test with field data. J Geophys Eng. 2006;3(3):219.

Belfield W, Sovich J, editors. Fracture statistics from horizontal wellbores. SPE/CIM/CANMET International Conference on Recent Advances in Horizontal Well Applications; 1994 March 20 - 23: Petroleum Society of Canada.

Berkowitz B. Analysis of fracture network connectivity using percolation theory. Math Geol. 1995;27(4):467-83.

Berkowitz B. Characterizing flow and transport in fractured geological media: A review. Adv Water Res. 2002;25(8):861-84.

Berkowitz B, Balberg I. Percolation theory and its application to groundwater hydrology. Water Resour Res. 1993;29(4):775-94.

Berkowitz B, Scher H. Anomalous transport in random fracture networks. Phys Rev Lett. 1997;79(20):4038.

Berkowitz B, Scher H. Theory of anomalous chemical transport in random fracture networks. Phys Rev E: Stat Nonlinear Soft Matter Phys. 1998;57(5):5858.

Bird RB, Stewart WE, Lightfoot EN. Transport Phenomena. Wiley; 2007.

Bisdom K. Burial-related fracturing in sub-horizontal and folded reservoirs: Delft University of Technology; 2016.

Bour O, Davy P. Connectivity of random fault networks following a power law fault length distribution. Water Resour Res. 1997;33(7):1567-83.

Brooks RH, Corey AT. Hydraulic properties of porous media and their relation to drainage design. Transactions of the ASAE. 1964;7(1):26-0028.

Cacas M, Ledoux E, de Marsily G, Barbreau A, Calmels P, Gaillard B et al. Modeling Fracture Flow With a Stochastic Discrete Fracture Network: Calibration and Validation 2. The Transport Model. Water Resour Res. 1990a;26:491-500.

Cacas M, Ledoux E, Marsily Gd, Tillie B, Barbreau A, Durand E et al. Modeling fracture flow with a stochastic discrete fracture network: Calibration and validation: 1. The flow model. Water Resour Res. 1990b;26(3):479-89.

Charlaix E, Guyon E, Roux S. Permeability of a random array of fractures of widely varying apertures. Transp Porous Media. 1987;2(1):31-43.

Cinco-Ley H, Samaniego V F, Kucuk F. The Pressure Transient Behavior for Naturally Fractured Reservoirs With Multiple Block Size. SPE Annual Technical Conference and Exhibition; 1985/1/1/; Las Vegas, Nevada. SPE: Society of Petroleum Engineers; 1985.

Corey AT. The interrelation between gas and oil relative permeabilities. Producers monthly. 1954;19(1):38-41.

de Dreuzy J-R, Davy P, Bour O. Hydraulic properties of two-dimensional random fracture networks following a power law length distribution: 1. Effective connectivity. Water Resour Res. 2001a;37(8):2065-78.

de Dreuzy J-R, Davy P, Bour O. Hydraulic properties of two-dimensional random fracture networks following a power law length distribution: 2. Permeability of networks based on lognormal distribution of apertures. Water Resour Res. 2001b;37:2079-95.

de Dreuzy J-R, Davy P, Bour O. Hydraulic properties of two‐dimensional random fracture networks following power law distributions of length and aperture. Water Resour Res. 2002;38(12):12-1--9.

Delaney PT, Pollard DD. Deformation of host rocks and flow of magma during growth of minette dikes and breccia-bearing intrusions near Ship Rock, New Mexico. Report1981. Report No.: 1202.

Dershowitz B, LaPointe P, Eiben T, Wei L. Integration of Discrete Feature Network Methods With Conventional Simulator Approaches. SPE-83633-PA. 2000;3(2):165-70.

Dershowitz B, LaPointe P, Eiben T, Wei L. User Documentation for FracMan. Seattle, Washington: Golder Associates Inc.; 2011.

Dershowitz WS, Einstein HH. Characterizing rock joint geometry with joint system models. Rock Mech Rock Eng. 1988;21(1):21-51.

Dverstorp B, Andersson J. Application of the discrete fracture network concept with field data: Possibilities of model calibration and validation. Water Resour Res. 1989;25(3):540-50.

Feng S, Halperin B, Sen P. Transport properties of continuum systems near the percolation threshold. Phys Rev B: Condens Matter. 1987;35(1):197.

Geiger S, Roberts S, Matthäi SK, Zoppou C, Burri A. Combining finite element and finite volume methods for efficient multiphase flow simulations in highly heterogeneous and structurally complex geologic media. Geofluids. 2004;4(4):284-99.

Gilman JR, Kazemi H. Improved Calculations for Viscous and Gravity Displacement in Matrix Blocks in Dual-Porosity Simulators (includes associated papers 17851, 17921, 18017, 18018, 18939, 19038, 19361 and 20174 ). SPE-16010-PA. 1988;40(01):60-70.

Gong J, Rossen WR. Shape Factor for Dual-Permeability Reservoir Simulation: Effect of Non-Uniform Flow in Fracture Network. ECMOR XIV - 14th European Conference on the Mathematics of Oil Recovery 8 - 11 September 2014 Catania, Italy: EAGE; 2014.

Gong J, Rossen WR. Modeling Flow in Naturally Fractured Reservoirs: Effect of Fracture Aperture Distribution on Dominant Sub-Network for Flow. TU Delft. Dataset.; 2015.

Gong J, Rossen WR. Shape factor for dual-permeability fractured reservoir simulation: Effect of non-uniform flow in 2D fracture network. Fuel. 2016;184:81-8.

Gong J, Rossen WR. Modeling flow in naturally fractured reservoirs: effect of fracture aperture distribution on dominant sub-network for flow. Pet Sci. 2017;14(1):138-54.

Hatton C, Main I, Meredith P. Non-universal scaling of fracture length and opening displacement. Nature. 1994;367(6459):160-2.

Heinemann Z, Mittermeir G. Derivation of the Kazemi–Gilman–Elsharkawy Generalized Dual Porosity Shape Factor. Transp Porous Media. 2012;91(1):123-32.

Hestir K, Long J. Analytical expressions for the permeability of random two‐dimensional Poisson fracture networks based on regular lattice percolation and equivalent media theories. J Geophys Res Solid Earth. 1990;95(B13):21565-81.

Hill AC, Thomas GW. A New Approach for Simulating Complex Fractured Reservoirs. Middle East Oil Technical Conference and Exhibition; 11-14 March, 1985; Bahrain. SPE: Society of Petroleum Engineers; 1985.

Johnston J, McCaffrey K. Fractal geometries of vein systems and the variation of scalingrelationships with mechanism. J Struct Geol. 1996;18(2):349-58.

Karimi-Fard M, Durlofsky LJ, Aziz K. An Efficient Discrete-Fracture Model Applicable for General-Purpose Reservoir Simulators. SPE-5719-PA. 2004;9(02):227-36.

Karimi-Fard M, Firoozabadi A. Numerical Simulation of Water Injection in Fractured Media Using the Discrete-Fracture Model and the Galerkin Method. SPE-83633-PA. 2003;6(02):117-26.

Katz A, Thompson A. Prediction of rock electrical conductivity from mercury injection measurements. J Geophys Res Solid Earth. 1987;92(B1):599-607.

Kazemi H, Gilman J, Eisharkawy A. Analytical and numerical solution of oil recovery from fractured reservoirs with empirical transfer functions. SPE Reservoir Engineering. 1992;7(2):219-27.

Kazemi H, Merrill LS, Jr., Porterfield KL, Zeman PR. Numerical Simulation of Water-Oil Flow in Naturally Fractured Reservoirs. SPE-5719-PA. 1976;16(06):317-26.

Kim J-G, Deo MD. Finite element, discrete-fracture model for multiphase flow in porous media. AlChE J. 2000;46(6):1120-30.

Landereau P, Noetinger B, Quintard M. Quasi-steady two-equation models for diffusive transport in fractured porous media: large-scale properties for densely fractured systems. Adv Water Res. 2001;24(8):863-76.

Lee SH, Lough MF, Jensen CL. Hierarchical modeling of flow in naturally fractured formations with multiple length scales. Water Resour Res. 2001;37(3):443-55.

Lemonnier P, Bourbiaux B. Simulation of Naturally Fractured Reservoirs. State of the Art-Part 2–Matrix-Fracture Transfers and Typical Features of Numerical Studies. Oil & Gas Science and Technology–Revue de l'Institut Français du Pétrole. 2010;65(2):263-86.

Li L, Lee SH. Efficient Field-Scale Simulation of Black Oil in a Naturally Fractured Reservoir Through Discrete Fracture Networks and Homogenized Media. SPE-83633-PA. 2008;11(04):750-8.

Li L, Lee SH, Jensen C. Method, system and apparatus for simulating fluid flow in a fractured reservoir utilizing a combination of discrete fracture networks and homogenization of small fractures. Google Patents; 2009.

Lim KT, Aziz K. Matrix-fracture transfer shape factors for dual-porosity simulators. Journal of Petroleum Science and Engineering. 1995;13(3–4):169-78.

Long J, Billaux DM. From field data to fracture network modeling: An example incorporating spatial structure. Water Resour Res. 1987;23(7):1201-16.

Margolin G, Berkowitz B, Scher H. Structure, flow, and generalized conductivity scaling in fracture networks. Water Resour Res. 1998;34(9):2103-21.

Marrett R. Aggregate properties of fracture populations. J Struct Geol. 1996;18(2):169-78.

Masihi M, King PR, Nurafza PR, editors. Fast estimation of performance parameters in fractured reservoirs using percolation theory. 67th EAGE Conference & Exhibition 2005 June 13-16; Madrid, Spain: Society of Petroleum Engineers.

Masihi M, King PR, Nurafza PR. Connectivity prediction in fractured reservoirs with variable fracture size: Analysis and validation. SPE J. 2008;13(01):88-98.

Mattax CC, Kyte JR. Imbibition Oil Recovery from Fractured, Water-Drive Reservoir. SPE-5719-PA. 1962;2(02):177-84.

Matthäi S, Geiger S, Roberts S, Paluszny A, Belayneh M, Burri A et al. Numerical simulation of multi-phase fluid flow in structurally complex reservoirs. Geological Society, London, Special Publications. 2007;292(1):405-29.

Matthai SK, Belayneh M. Fluid flow partitioning between fractures and a permeable rock matrix. Geophys Res Lett. 2004;31(7):L07602.

Matthai SK, Nick HM. Upscaling two-phase flow in naturally fractured reservoirs. AAPG Bull. 2009;93(11):1621-32.

Mirzaei-Paiaman A, Masihi M. Scaling Equations for Oil/Gas Recovery from Fractured Porous Media by Counter-Current Spontaneous Imbibition: From Development to Application. Energy & Fuels. 2013;27(8):4662-76.

Moinfar A, Narr W, Hui M-H, Mallison BT, Lee SH. Comparison of Discrete-Fracture and Dual-Permeability Models for Multiphase Flow in Naturally Fractured Reservoirs. SPE Reservoir Simulation Symposium; 21-23 February, 2011; The Woodlands, Texas, USA. SPE: Society of Petroleum Engineers; 2011.

Neretnieks I. Solute transport in fractured rock: applications to radionuclide waste repositories. Flow and contaminant transport in fractured rock. London: Academic Press Limited; 1993. p. 39-127.

Neretnieks I, Eriksen T, Tähtinen P. Tracer movement in a single fissure in granitic rock: Some experimental results and their interpretation. Water Resour Res. 1982;18(4):849-58.

Nick HM, Paluszny A, Blunt MJ, Matthai SK. Role of geomechanically grown fractures on dispersive transport in heterogeneous geological formations. Physical Review E. 2011;84(5):056301.

Nicol A, Walsh J, Watterson J, Gillespie P. Fault size distributions—are they really power-law? J Struct Geol. 1996;18(2):191-7.

Noetinger B, Roubinet D, Russian A, Le Borgne T, Delay F, Dentz M et al. Random Walk Methods for Modeling Hydrodynamic Transport in Porous and Fractured Media from Pore to Reservoir Scale. Transp Porous Media. 2016;115(2):345-85.

Nordqvist AW, Tsang YW, Tsang C-F, Dverstorp B, Andersson J. Effects of high variance of fracture transmissivity on transport and sorption at different scales in a discrete model for fractured rocks. J Contam Hydrol. 1996;22(1):39-66.

Odling NE. Scaling and connectivity of joint systems in sandstones from western Norway. J Struct Geol. 1997;19(10):1257-71.

Ortega O, Marrett R. Prediction of macrofracture properties using microfracture information, Mesaverde Group sandstones, San Juan basin, New Mexico. J Struct Geol. 2000;22(5):571-88.

Pooladi-Darvish M, Firoozabadi A. Cocurrent and Countercurrent Imbibition in a Water-Wet Matrix Block. SPE J. 2000;5(01):3-11.

Quintard M, Whitaker S. One- and Two-Equation Models for Transient Diffusion Processes in Two-Phase Systems. In: Hartnett JP, Irvine TF, editors. Advances in Heat Transfer. Elsevier; 1993. p. 369-464.

Quintard M, Whitaker S. Transport in chemically and mechanically heterogeneous porous media. I: Theoretical development of region-averaged equations for slightly compressible single-phase flow. Adv Water Res. 1996;19(1):29-47.

Ramirez B, Kazemi H, Al-kobaisi M, Ozkan E, Atan S. A Critical Review for Proper Use of Water/Oil/Gas Transfer Functions in Dual-Porosity Naturally Fractured Reservoirs: Part I. SPE-83633-PA. 2009;12(02):200-10.

Rangel-German ER, Kovscek AR. Experimental and analytical study of multidimensional imbibition in fractured porous media. Journal of Petroleum Science and Engineering. 2002;36(1–2):45-60.

Ranjbar E, Hassanzadeh H, Chen Z. One-Dimensional Matrix-Fracture Transfer in Dual Porosity Systems with Variable Block Size Distribution. Transp Porous Media. 2012;95(1):185-212.

Renshaw CE, Park JC. Effect of mechanical interactions on the scaling of fracture length and aperture. Nature. 1997;386(6624):482-4.

Robinson P. Connectivity of fracture systems-a percolation theory approach. J Phys A: Math Gen. 1983;16(3):605.

Robinson P. Numerical calculations of critical densities for lines and planes. J Phys A: Math Gen. 1984;17(14):2823.

Rodriguez-N R, Cinco-L H, Samaniego-V F. A Variable Block Size Model for the Characterization of Naturally Fractured Reservoirs. SPE Annual Technical Conference and Exhibition; 30 September-3 October,2001; New Orleans, Louisiana. SPE: Society of Petroleum Engineers; 2001.

Rouleau A, Gale J. Statistical characterization of the fracture system in the Stripa granite, Sweden. Int J Rock Mech Min Sci. 1985;22(6):353-67.

Sahimi M. Flow and transport in porous media and fractured rock: from classical methods to modern approaches. John Wiley & Sons; 2011.

Saidi AM. Reservoir engineering of fractured reservoirs (fundamental and practical aspects). Paris: Total Edition Press; 1987.

Salimi H. Physical Aspects in Upscaling of Fractured Reservoirs and Improved Oil Recovery Prediction. TU Delft, Delft University of Technology; 2010.

Salimi H, Bruining J. Improved Prediction of Oil Recovery From Waterflooded Fractured Reservoirs Using Homogenization. SPE-83633-PA.2010;13(01):44-55.

Segall P, Pollard DD. Joint formation in granitic rock of the Sierra Nevada. Geol Soc Am Bull. 1983;94(5):563-75.

Shouxiang M, Morrow NR, Zhang X. Generalized scaling of spontaneous imbibition data for strongly water-wet systems. Journal of Petroleum Science and Engineering. 1997;18(3–4):165-78.

Snow DT. The frequency and apertures of fractures in rock. Int J Rock Mech Min Sci. 1970;7(1):23-40.

Stone D. Sub-surface fracture maps predicted from borehole data: An example from the Eye-Dashwa pluton, Atikokan, Canada. Int J Rock Mech Min Sci. 1984;21(4):183-94.

Tsang C, Neretnieks I. Flow channeling in heterogeneous fractured rocks. Rev Geophys. 1998;36(2):275-98.

Tsang Y, Tsang C. Channel model of flow through fractured media. Water Resour Res. 1987;23(3):467-79.

Tsang Y, Tsang C, Hale F, Dverstorp B. Tracer transport in a stochastic continuum model of fractured media. Water Resour Res. 1996;32(10):3077-92.

Tsang Y, Tsang C, Neretnieks I, Moreno L. Flow and tracer transport in fractured media: A variable aperture channel model and its properties. Water Resour Res. 1988;24(12):2049-60.

van Golf-Racht TD. Fundamentals of fractured reservoir engineering. Amsterdam: Elsevier 1982.

Vermilye JM, Scholz CH. Relation between vein length and aperture. J Struct Geol. 1995;17(3):423-34.

Warren J, Root PJ. The behavior of naturally fractured reservoirs. SPE-5719-PA. 1963;3(03):245-55.

White FM. Heat and Mass Transfer. Addison-Wesley; 1988.

Wong TF, Fredrich JT, Gwanmesia GD. Crack aperture statistics and pore space fractal geometry of Westerly granite and Rutland quartzite: Implications for an elastic contact model of rock compressibility. J Geophys Res Solid Earth. 1989;94(B8):10267-78.

Zhang X, Morrow NR, Ma S. Experimental Verification of a Modified Scaling Group for Spontaneous Imbibition. SPE Reservoir Engineering. 1996;11(04):280-5.

Zimmerman RW, Bodvarsson GS. Effective block size for imbibition or absorption in dual-porosity media. Geophys Res Lett. 1995;22(11):1461-4.

Zimmerman RW, Chen G, Hadgu T, Bodvarsson GS. A numerical dual‐porosity model with semianalytical treatment of fracture/matrix flow. Water Resour Res. 1993;29(7):2127-37.

# APPENDIX

## *Definition of Peclet Number*

A Peclet number indicates the relative importance of advection and diffusion to the transport of a physical quantity in a given system. In this study, it represents the relative capacity for oil transport of matrix production and fracture flow: i.e., how conductive fractures are compared to matrix productivity. We propose separate versions of the Peclet number for the two oil-recovery processes, primary and secondary recovery. The Peclet number proposed here is based on the spacing of primary fractures, without secondary fractures. We consider a square matrix block, of size *L* x *L*, bounded by primary fractures, as illustrated in Fig. A.1a. Within a reservoir, this region represents a unit cell surrounded by other unit cells. Each fracture must accommodate flow from matrix blocks on both sides; therefore the fracture permeability we assign, which accommodates flow from the given matrix block, is only half the total fracture permeability. Then, because there are two (half-)fractures on opposite sides of the matrix in the two directions, the total flow capacity of the fractures surrounding the matrix block is equal to that of one fracture.

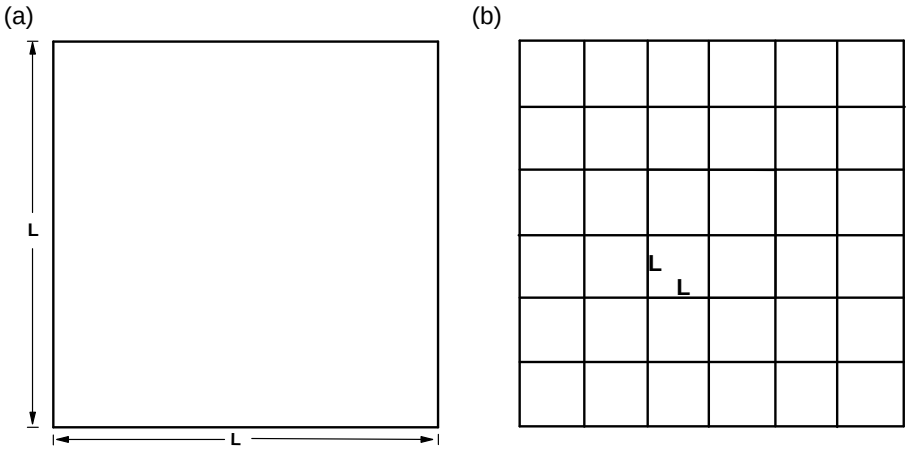


***Figure A.1*** *(a) Region of interest for defining Peclet number for matrix-fracture flow: a square matrix block bounded by primary fractures. (b) Schematic of a hypothetical simulation grid block containing 6 × 6 unit cells defined by the primary fractures.*

## *Definition of Pe for Primary Recovery*

During primary production, oil is produced by fluid expansion from an initial pressure $p$ to a reduced pressure ($p$-$\Delta p$). Pressure drops rapidly in the fractures, while the matrix initially remains at higher pressure. The pressure difference between fracture and adjacent matrix block drives oil from the matrix to the fracture. In comparing the flow capacities of matrix and fractures individually, we assume that each is unconstrained by the other. We assume a slightly compressible oil and incompressible water, which is at irreducible water saturation $S_{wr}$, and matrix.

A one-dimensional (1D) primary-production process in matrix bounded by parallel fractures at uniform and constant pressure on opposite sides, is governed by (White 1988; Bird et al. 2007; Akker, Mudde 2014)

$$\frac{\partial p}{\partial t} = \alpha_h \frac{\partial^2 p}{\partial x} \tag{A.1}$$

where

$$\alpha_h = \frac{k_m}{\phi \mu_o c_t} \tag{A.2}$$

where $p$ is pressure, $\alpha_h$ hydraulic diffusivity, $k_m$ is matrix permeability, $\varphi$ is matrix porosity, $\mu_o$ is oil viscosity, and $c_t$ is total fluid compressibility. We assume the oil is slightly compressible, so oil density is linearly related to pressure. Eq. A.1 is in the form of the well-known equation governing unsteady heat conduction in a solid (Bird et al. 2007; White 1988; Akker, Mudde 2014). Recovery in a square matrix block is governed by the square of dimensionless average pressure derived from Eq. A.1 (White 1988). Dimensionless time for this process is

$$t_D = \frac{\alpha_h t}{L^2} \quad . \tag{A.3}$$

We take the characteristic time $t_c$ for the process as that at a dimensionless time of 1; thus

$$t_c = \frac{L^2}{\alpha_h} \quad . \tag{A.4}$$

Production is very uneven during this period, with production much faster at the start than at the end. Moreover, this characteristic time extends well beyond the period when almost all oil is recovered; we discuss this further below. Virtually all the oil is recovered by this time; the volume of oil recovered is $(L^2 h \phi S_{oi} C_t \Delta p)$, where $S_{oi}$ is the initial oil saturation, $\varphi$ matrix porosity, and $h$ is the height of the system perpendicular to the cross-section shown in Fig. A.1. Averaged over the characteristic time, the time to produce one unit volume of oil is $\left(\frac{L^2/\alpha_h}{L^2 h \phi S_{oi}\, C_t\, \Delta p}\right)$.

For the fracture, we assume the same pressure difference $\Delta p$ across the length of the fracture; this gives a flow rate of $\left(\frac{k_f\, d\, h\, \Delta p}{\mu_o\, L}\right)$, where $k_f$ is the fracture permeability and $d$ is the fracture aperture. The product ($k_f d$) is fracture transmissivity; for smooth slits, it equals ($d^3$/12). The time for the fracture to transport one unit volume of oil is thus $\left(\frac{\mu_o L}{k_f\, d\, h\, \Delta p}\right)$. The Peclet number is the ratio of these two characteristic times:

$$Pe \equiv \left(\frac{L^2/\alpha_h}{L^2 h \phi S_{oi}\, C_t\, \Delta p}\right) \Big/ \left[\mu L / \left(k_f\, d\, h\, \Delta p\right)\right] \quad . \tag{A.5}$$

If $Pe$ is large, the surrounding fractures are relatively conductive compare to the matrix's ability to produce, while a small $Pe$ indicates that the fractures are limiting on overall oil production.

### *Definition of Pe for Secondary Recovery by Counter-Current Imbibition*

In waterflood, we assume counter-current imbibition is the dominant oil-recovery mechanism. This process governed by Eq. A.1, with the coefficient $\alpha_m$ defined as

$$\alpha_m(S_w) \equiv -\frac{k_m}{\phi} f_w \frac{k_{ro}}{\mu_o} \frac{dP_c}{dS_w} \tag{A.6}$$

with water fractional flow $f_w$ given by

$$f_w = \frac{k_{rw}/\mu_w}{k_{rw}/\mu_w + k_{ro}/\mu_o} \tag{A.7}$$

where $P_c$ is the capillary pressure, $k_{rw}$ is the water relative permeability and $k_{ro}$ is the oil relative permeability (all three are functions of $S_w$), and $\mu_w$ and $\mu_o$ are the water and oil viscosities, respectively. Coefficient $\alpha_m$ is not a constant, but if one chooses an approximate average value for the recovery process (Rangel-German, Kovscek 2002), one can define a characteristic time using Eq. A.1. Again, virtually all oil is recovered during this time; the volume recovered is $[L^2 h\phi(S_{oi} - S_{or})]$, where $S_{or}$ is residual oil saturation.

The fracture limits the process according to its ability to transport water to imbibe into the matrix and replace oil. The fracture supplies water at a rate ($Q\, f_{wI}$), where $Q$ is the volumetric flow rate through the fracture and $f_{wI}$ is the water fraction entering the fracture. As shown in Fig. A.2, the cumulative oil recovery is roughly the same for a constant volume of water injected into the fracture, for total flow rates varying by a factor of 20. The time for the fracture to provide one unit volume of water (which could displace one unit volume of oil from the matrix) is [1/($Q\, f_{wI}$)]. This leads to a Peclet number for counter current imbibition defined by

$$Pe \equiv \left[\frac{L^2/\alpha_m}{L^2 h\phi(S_{oi}-S_{or})}\right] \Big/ \left(\frac{1}{Q\, f_{wI}}\right) \quad . \tag{A.8}$$

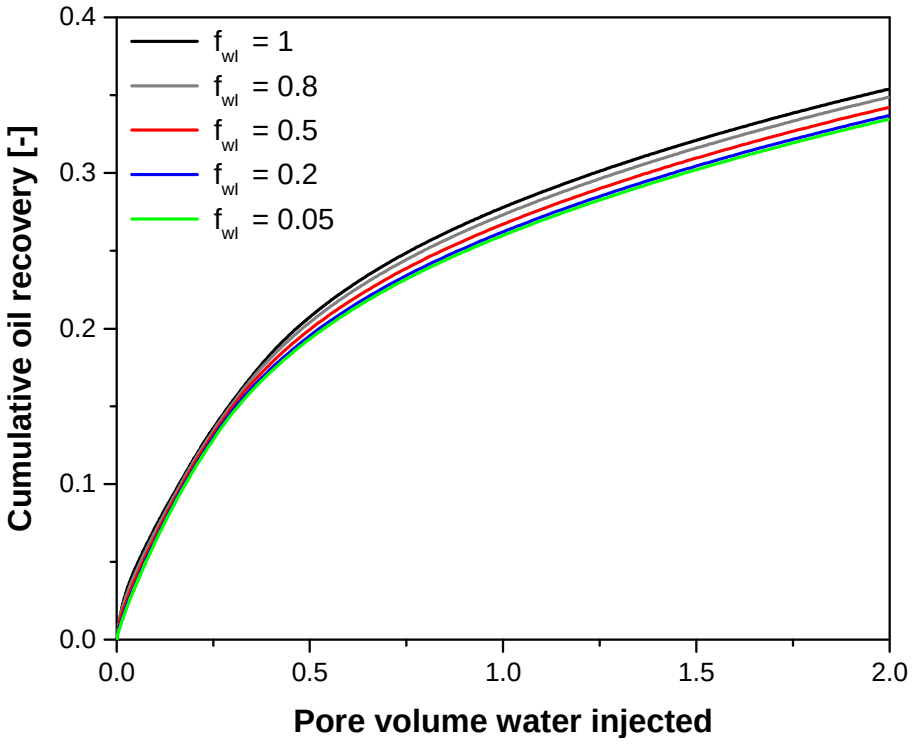


***Figure A.2*** *Cumulative oil recovery for different injected water fractions $f_{wI}$ with a constant water injection rate $Qf_{wI}$,* Pe = *6,000,* $R_d$ = *2.5,* $R_n$ = *1/3.*

We assume a constant coefficient $\alpha_m$ for counter-current imbibition only to define a Peclet number, not in our simulations of oil recovery. Nonetheless, a useful average value would apply approximately over the period of recovery of most of the oil. Fig. A.3 compares solutions for fraction of recoverable oil still in place (ROIP) in a 2D recovery process with various constant values of $\alpha_m$ to the numerical solution of the same process using the capillary-pressure and relative-permeability functions used in this chapter (solid line). In the numerical solution, fractures were flushed with large volumes of water so that fracture flow is not limiting on the rate of matrix recovery. A value of $\alpha_m$ = 1.9 × $10^{-9}$ $m^2/s$ gives a reasonable fit over the period in which 80% of the oil is recovered (Fig. A.3a). The fit is not so good at short times (Fig. A.3b). Nevertheless, this value suffices to roughly characterize the time scales of the recovery process.

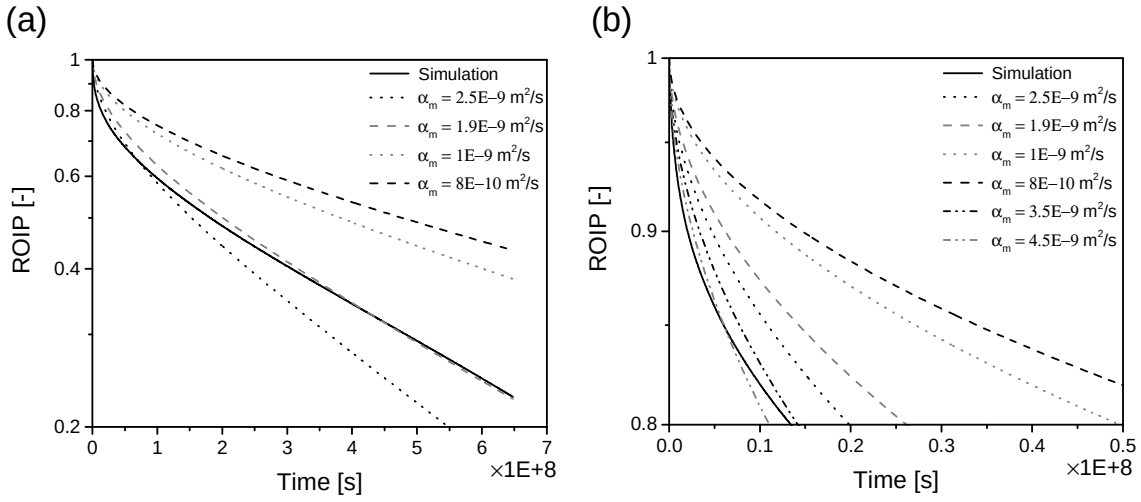


***Figure A.3*** *Fraction of remaining oil in place (ROIP) for a 2D recovery process calculated numerically (solid line) and with constant coefficient $\alpha_m$ for different values of $\alpha_m$. (a) long time scale, during which most oil is recovered. (b) Short times.*

Salimi and Bruining (2010) proposed a definition of Peclet number for waterflood based on characteristic times without the volumes of oil residing in the matrix or fracture considered. The characteristic time for the fracture is then the time to replace the fluids in the fracture, whatever the fracture volume. This gives

$$Pe \equiv [L^2/\alpha_m]/\left(\frac{2\,L\,d\,h}{Q\,f_{wI}}\right) \quad . \tag{A.9}$$

Fig. A.4 compares the Peclet number of Salimi and Bruining (2010) to that defined by Eq. A.8. In the reference case, *Pe* = 6,000, $R_d$ = 2.5 and $R_n$ = 1/3. In this case, the injected fluid flows rapidly through both the primary and secondary fractures. Primary and secondary fractures play similar roles. In the second case, fracture length ($L$), thickness ($h$), porosity ($\varphi$) and permeability ($k_m$) of matrix blocks change to keep the value of *Pe* in Eq. A.8 unchanged, while that of Salimi and Bruining doubles. In the third case, the value of *Pe* in Eq. A.8 decreases four fold, the value of Salimi and Bruining is unchanged. The capillary coefficient $\alpha_m$ remains the same. For the second case, the cumulative oil recovery is close to the oil recovery of the reference case. In the third case, the cumulative oil recovery at a given time decreases by approximately a factor of 4, approximating the change in Eq. A.8. Thus, the Peclet number defined in this study better fits the purpose of this study.

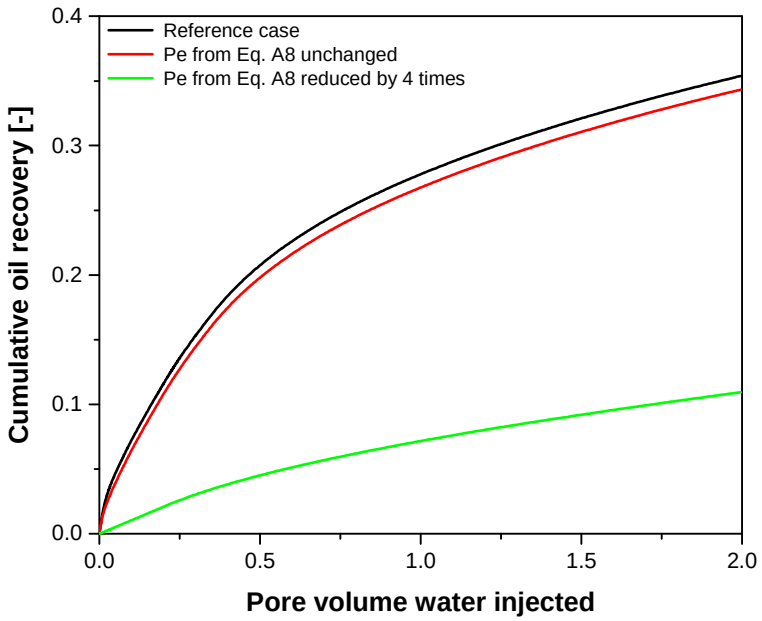


***Figure A.4*** *Comparison of oil recovery as a function of time for different definitions of Peclet number.*

## *Interpreting the Magnitude of Pe*

As noted, even for a constant value of $\alpha_h$ or $\alpha_m$, oil recovery is not constant in time for either primary or secondary recovery; the rate of oil recovery is much faster at the start than at the end. It is instructive to consider the time at which the flow capacities of matrix and fractures are comparable, as a function of *Pe*.

We expect the fractures to be limiting only relatively early in the oil-recovery process, when production from matrix is greatest. For constant $\alpha_m$, for short dimensionless times $t_D$ (less than 0.05), oil production in 1D scales with $\sqrt{t_D}$ (Akker, Mudde 2014). The fraction of recoverable oil remaining in the square matrix region is approximately $\left(1 - C_1\sqrt{\alpha_m t/L^2}\right)^2$, with $C_1$ approximately 2.24 (obtained by a curve fit for the 1D recovery process in previous studies (Bird et al. 2007; Akker, Mudde 2014)) Therefore the rate of oil recovery from matrix, if unlimited by fracture flow capacity, is given by

$$Q_m = -\frac{d}{dt}\left[(L^2 h\phi S_{oi}\, C_t\, \Delta p)\left(1 - C_1\sqrt{\alpha_m\, t/L^2}\right)^2\right]$$

$$= (L^2 h\phi S_{oi}\, C_t\, \Delta p)2\left(1 - C_1\sqrt{\alpha_m\, t/L^2}\right)C_1\frac{1}{2}\sqrt{\alpha_m/tL^2} \qquad \text{(A.10)}$$

for primary production. The time at which this capacity equals the flow capacity of the matrix is likely to be short, for which the second term in brackets is approximately 1. Therefore

$$Q_m \approx (L^2 h\phi S_{oi}\, C_t\, \Delta p)C_1\sqrt{\alpha_m/tL^2} \quad . \qquad \text{(A.11)}$$

The time at which matrix flow capacity equals fracture flow capacity is therefore given by

$$\left(\frac{k_f\, d\, h\, \Delta p}{\mu L}\right) \approx (L^2 h\phi S_{oi}\, C_t\, \Delta p)C_1\sqrt{\alpha_m/tL^2} \quad . \qquad \text{(A.12)}$$

Rearranging,

$$\sqrt{\alpha_m\, t/L^2} \approx (L^2 h\phi S_{oi}\, C_t\, \Delta p)C_1(\alpha_m/L^2)\left(\frac{\mu L}{k_f\, d\, h\, \Delta p}\right) = C_1\left(\frac{1}{Pe}\right) \qquad \text{(A.13)}$$

$$t_D \approx 5\, Pe^{-2} \tag{A.14}$$

where dimensionless time $t_D$ is defined in Eq. A.3. For instance, for *Pe* = 10, the fractures would be limiting on oil recovery for $t_D \leq 0.05$. The times in Figs. 4.3d-f are shorter than this, and matrix-fracture exchange has progressed further in matrix closer to the production well. For *Pe* = 1,000, primary fractures are limiting for $t_D \leq 5 \times 10^{-6}$, and in Figs. 4.3a-c matrix-fracture exchange is nearly uniform along the primary fractures. For secondary recovery, a similar derivation leads to the same result, albeit assuming a constant value of $\alpha_m$.

## *Interpretation of* Pe *for Secondary Fractures*

We define *Pe* based on the network of primary fractures, and account for secondary fractures using the dimensionless ratio of fracture apertures $R_d$ and number of secondary fractures $R_n$. It is instructive to compare the values of *Pe* that would obtain from consideration of matrix bounded by secondary fractures. The size of the region is now ($L\ R_n$) × ($L\ R_n$). For both primary production and waterflood, the flow rate in the definition of Eqs. A.5 and A.9 is reduced by a factor of roughly $R_d^3$. The value of *Pe* changes by a factor $\{(R_n^{-1})/[(R_d^{-3})]^{-1}\}$. For the case $R_n$ = 1/3 and $R_d$ = 2.5, the value of *Pe* for a matrix block surrounded by secondary fractures is a factor $(3/2.5^3) \cong (1/5)$ of that based on primary fractures. The fractures are somewhat less able to accommodate the flow capacity of the matrix. For larger values of $R_d$, the factor is smaller, e.g. 0.0015 for $R_d$ = 12.6.

## *Interpretation of* Pe *for Grid Blocks in Simulation*

In a dual-porosity or dual-permeability simulation, a grid block represents a region containing many unit cells as defined above. Suppose there are $N_b$ x $N_b$ unit cells in the simulation grid block and consider fracture flow in one of the coordinate directions (*cf*. Fig. A.1b, where $N_b$ = 6). There are $N_b$ fractures to carry away oil or provide water, but $N_b^2$ matrix blocks to produce oil. The time to produce a unit volume of oil from the matrix grid block decreases by $N_b^2$ while the time for fractures to provide a unit volume of water or carry away oil decreases by $N_b$; *Pe* decreases by a factor $N_b$. The pressure in the grid block and water fraction in the fractures is assumed uniform within a grid block in the dual-porosity approach, but both vary from grid block to grid block and with time for any grid block. At each time state a new boundary condition is applied to matrix blocks by the changing conditions in the fractures. The state of the matrix is the superposition of the effects of all these changes. We propose that the value of *Pe* characterizing a grid block in a simulation corresponds roughly to that we propose for a unit cell, divided by the number of unit cells defined by primary fractures across a simulation grid block.

# SUMMARY

A large number of oil and gas reservoirs across the world are naturally fractured, from which a significant amount of hydrocarbons are produced. Naturally fractured reservoirs, like all reservoirs, are exploited in two stages: primary recovery and secondary recovery (sometimes followed by tertiary recovery, i.e. enhanced oil recovery (EOR)), with different recovery mechanisms. During primary production, the reservoir is produced by fluid expansion. In secondary production and EOR, since the fractures are much more permeable than the matrix, the injected water or EOR agent flows rapidly through the fracture network and surrounds the matrix blocks. Oil recovery then depends on efficient delivery of water or EOR agent to the matrix through the fracture network.

Efficient exploitation of naturally fractured reservoirs requires accurate simulation. If the fracture network is well-connected, the simulation of naturally fractured reservoirs is often done with a dual-porosity/dual-permeability description. In the dual-porosity/dual-permeability approaches, the fracture and matrix systems are treated as separated domains; the interconnected fractures serve as fluid flow paths between injection and production wells, while the matrix acts only as fluid storage, and these two domains are connected with an exchange term. Limited fluid flow between matrix blocks is allowed in dual-permeability models. In order to simulate the fracture geometry more realistically, and account explicitly for the effect of individual fracture on fluid flow, discrete fracture models have attracted increasing research interests in the last decades. However, dual-porosity/dual-permeability models are still the most widely used methods for field-scale fractured-reservoir simulation, as they address the dual-porosity nature of fractured reservoirs and are computationally cheaper, although they are much-simplified characterizations of naturally fractured reservoirs.

To generate a dual-porosity/dual-permeability model, it is necessary to define average properties for each grid cell, such as porosity, permeability, matrix-fracture-interaction parameters (typical fracture spacing, matrix-block size or shape factor), etc.. Therefore, the fracture network used to generate the dual-porosity model parameters is crucial. Homogenization and other modelling approaches likewise require one to designate a typical fracture spacing. The hierarchical fracture model also requires that one define effective properties of the matrix blocks and fractures which are too small to be represented explicitly.

In the first part of this research (chapter 2), we systematically study the influence of the fracture aperture distribution on the dominant sub-network for flow. The “dominant sub-network ” is defined as the sub-network obtained by eliminating a portion of fractures while retaining 90% of the original network equivalent permeability. We model a two-dimensional fractured reservoir in which the matrix is impermeable and the fractures are well-connected. The fractures obey a power-law length distribution, as observed in natural fracture networks. For the aperture distribution, we test a number of cases: log-normal distributions, power-law distributions, and one case where the aperture is proportional to the fracture length. We find that even a well-connected fracture network can behave like a much sparser network when the aperture distribution is broad enough (power-law exponent $\alpha \leq 2$ for power-law aperture distributions and log standard deviation $\sigma \geq 0.4$ for log-normal aperture distributions). Specifically, most fractures can be eliminated leaving the remaining dominant sub-network with 90% of the permeability of the original fracture network. We determine how broad the aperture distribution must be to approach this behavior and the dependence of the dominant sub-network on the parameters of the aperture distribution. We also explore whether one can identify the dominant sub-network without doing flow calculations.

In chapter 3, we focus on the influence of eliminating unimportant fractures which carry little flow on the inferred characteristic matrix-block size. As a follow-up study of chapter 2, we model a two-dimensional fractured reservoir in which the fractures are well-connected, as in chapter 2. The fractures obey a power-law length distribution, as observed in natural fracture networks. For the aperture distribution, because information from the subsurface is limited, we test a number of cases: log-normal distributions (from narrow to broad), and power-law distributions (from narrow to broad). The matrix blocks in fractured reservoirs are of varying sizes and shapes; we adopt the characteristic radius and the characteristic length to represent the characteristic matrix-block size. We show how the characteristic

matrix-block sizes increase from the original fracture network to the dominant sub-network. During a waterflood or enhanced-oil-recovery (EOR) process, the production of oil depends on the supply of injected water or EOR agent. This suggests that the matrix-block size, or shape factor, used in dual-porosity or dual-permeability waterflood or enhanced oil recovery (EOR) simulations or in homogenization should be based not on the entire fracture population but on the sub-network that carries almost all of the injected fluid (water or EOR agent).

In chapter 4 we test the hypothesis, that the characteristic fracture spacing for the dual-porosity/dual-permeability simulation of waterflood or EOR in a naturally fractured reservoir should account not for all fractures but only the relatively small number of fractures carrying almost all the injected water or EOR agent. In this chapter, we define the “primary” fractures as those in the dominant sub-network which carries most of the injected agent in previous chapters, and the secondary and, in some cases, tertiary fractures as the remaining fractures. In primary production even a relatively small fracture represents an effective path for oil to flow to a production well. This distinction suggests that the "shape factor" in dual-permeability reservoir simulators and the repeating unit in homogenization should depend on the process involved: specifically, it should be different for primary and secondary or tertiary recovery. In chapter 4, we test this hypothesis in a simple representation of a fractured region with a non-uniform distribution of fracture flow conductivities. We compare oil production, flow patterns in the matrix, and the pattern of oil recovery with and without the "secondary" fractures that carry only a small portion of injected fluid.

The role of secondary fractures depends on a dimensionless ratio of characteristic times for matrix and fracture flow (Peclet number), and the ratio of flow carried by the different fractures. In primary production, for a large Peclet number, treating all fractures equally is a better approximation than excluding secondary fractures; the shape factor should reflect both primary and secondary fractures. For a sufficiently small Peclet number, it is more accurate to exclude the secondary fractures. For waterflood or EOR, in most cases examined, the appropriate shape factor or repeating-unit size should reflect both primary and secondary fractures. If secondary fractures are much narrower than primary fractures, then it is more accurate to exclude them. Yet-narrower "tertiary fractures" are not always helpful for oil production, even if they are more permeable than matrix. They can behave as capillary barriers to imbibition, reducing oil recovery.

We present a new definition of Peclet number for primary and secondary production in fractured reservoirs that provides a more accurate predictor of dominant recovery mechanism in fractured reservoirs than the previously published definition.

# SAMENVATTING

Een groot aantal olie- en gasreservoirs over de hele wereld zijn van nature gescheurd. Hieruit wordt een significante hoeveelheid koolwaterstoffen geproduceerd. Zoals alle reservoirs worden van nature gescheurde reservoirs in twee stappen geëxploiteerd: primaire and secundaire winning (soms opgevolgd door tertiaire winning, d.w.z. verbeterde oliewinning (Engels: enhanced oil recovery EOR)) die verschillende methodes van olie- en gaswinning gebruiken. Tijdens de primaire productie worden de koolwaterstoffen gewonnen door expansie van de fluïda. Tijdens de secundaire productie en EOR fase kan, vanwege de hogere permeabiliteit van de scheuren vergeleken met de matrix, geïnjecteerd water of EOR fluïdum snel door het scheurnetwerk stromen en wordt de matrix omzeild. De mate van oliewinning hangt dan af van de efficiëntie waarmee het water of EOR substantie binnen de matrix wordt gebracht vanuit het scheurnetwerk.

Er is nauwkeurige simulatie nodig voor efficiënte exploitatie van natuurlijk gescheurd gesteente. Voor een goed verbonden scheurnetwerk wordt de simulatie van natuurlijk gescheurd gesteente vaak gedaan met duale-porositeit/duale-permeabiliteit beschrijving. Binnen de duale-porositeit/duale-permeabiliteitsaanpak worden de scheur- en matrixsystemen als een apart domein behandeld. De verbonden scheuren dienen als stromingspaden tussen injectie- en productieputten en de matrix dient slechts als opslag van het fluïdum. De twee domeinen zijn met elkaar verbonden via een uitwisselingsterm. Beperkte stroming tussen de matrixblokken is toegestaan in duale-permeabiliteitsmodellen. Om de scheurgeometrie realistischer te kunnen simuleren is de laatste decennia de interesse naar onderzoek van discrete scheurmodellen toegenomen. Hierin wordt het effect van individuele scheuren op de stroming expliciet wordt meegenomen. Toch zijn de duale-porositeit/duale-permeabiliteitsmodellen nog steeds het meest in gebruik voor simulaties van gescheurde reservoirs op de veldschaal, omdat ze de duale porositeit van de gescheurde reservoirs in acht nemen en computationeel goedkoper zijn, hoewel ze een vereenvoudigde beschrijving van natuurlijk gescheurde reservoirs zijn.

Om een duaal-porositeit/duaal-permeabiliteitsmodel te maken is het nodig om gemiddelde eigenschappen te definiëren voor elke gridcel, zoals porositeit, permeabiliteit, matrix-scheur-interactie parameters (typische ruimte tussen de scheuren, matrixblokgrootte of vormfactor), etc. Daarom is het scheurnetwerk dat wordt gebruikt om de duale-porositeitsmodelparameters te maken cruciaal. Voor homogenisatie en andere modelaanpakken is het eveneens nodig om een typische ruimte tussen de scheuren vast te leggen. Voor het hiërarchische scheurmodel is het verder nodig om de effectieve eigenschappen te definiëren van de matrixblokken en scheuren die te klein zijn om expliciet te modelleren.

In het eerste deel van dit onderzoek (Hoofdstuk 2) bestuderen we systematisch de invloed van de verdeling van de scheuropeningen op het dominante stroming sub-netwerk. Het “dominante sub-netwerk is gedefinieerd als het sub-netwerk dat wordt verkregen door een deel van de scheuren te verwijderen terwijl 90% van de equivalente permeabiliteit van het originele netwerk wordt behouden. We modelleren een tweedimensionaal gescheurd reservoir waarin de matrix impermeabel is en de scheuren onderling goed verbonden zijn. De scheuren voldoen hierbij aan een machtsfunctie-verdeling, zoals die ook in natuurlijke scheurnetwerken optreden. Voor de verdeling van de scheuropening testen we verschillende gevallen: log-normale verdelingen, machtfunctie-verdelingen en een geval waar de opening evenredig is met de scheurlengte. Hieruit concluderen we dat zelfs een goed verbonden network zich kan gedragen als een veel minder goed verbonden netwerk wanneer de verdeling van de scheuropeningen breed genoeg is (machtsfunctie-exponent $\alpha \leq 2$ voor machtsfunctie verdelingen van scheuropeningen en log standaard deviatie $\sigma \geq 0.4$ voor lognormale verdelingen van scheuropeningen). De meeste scheuren kunnen hierbij worden verwijderd waardoor het dominante sub-netwerk overblijft met 90% van de permeabiliteit van het originele scheurnetwerk. We bepalen hoe breed the verdeling van scheuropeningen moet zijn om dit gedrag te benaderen en de afhankelijkheid van het dominante sub-netwerk op de parameters van de verdeling van scheuropeningen. Verder onderzoeken we of het mogelijk is om het dominante scheurnetwerk te identificeren zonder stromingsberekeningen te doen.

In Hoofdstuk 3 richten we ons op de invloed van het verwijderen van onbelangrijke scheuren, die slechts een klein deel van de stroming bevatten, op de karakteristieke matrix-blokgrootte. Net als in Hoofdstuk 2 modelleren we een tweedimensionaal gescheurd reservoir waarin de scheuren goed onderling verbonden zijn. De scheuren voldoen aan een machtsfunctie lengte verdeling, zoals die ook te vinden is in natuurlijke scheurnetwerken. Voor de verdeling van de scheuropeningen testen we een aantal gevallen, omdat informatie uit de ondergrond beperkt is. We testen log-normale verdelingen (van smal tot breed) en machtsfunctie verdelingen (van smal tot breed). De matrixblokken in gescheurde reservoirs hebben verschillende groottes en vormen. We kiezen een karakteristieke radius en lengte om de karakteristieke matrixblokgrootte te vertegenwoordigen. We tonen aan dat deze karakteristieke grootte toeneemt van het originele scheurnetwerk naar het dominante sub-netwerk. Tijdens een doorstroming met water of een EOR-proces hangt de olieproductie af van de toevoer van het geïnjecteerde water of EOR substantie. Dit suggereert dat de matrixblokgrootte, of de vormfactor, die wordt gebruikt in duale porositeits- of duale permeabiliteitssimulaties of in homogenisatie van water doorstromingen of EOR processen, niet moet worden gebaseerd op alle scheuren, maar op het sub-netwerk dat het meeste van het geïnjecteerde fluïdum (water of EOR substantie) transporteert.

In Hoofdstuk 4 testen we de hypothese dat de karakteristieke ruimte tussen de scheuren, voor een duale-porositeits/duale-permeabiliteitssimulatie van een doorstroming met water of EOR proces in een van nature gescheurd reservoir, niet afhangt van alle scheuren, maar alleen van het relatief kleine aantal scheuren die het meeste geïnjecteerde water of EOR substantie transporteren. In dit hoofdstuk worden de “primaire” scheuren gedefinieerd als diegene in het dominante sub-netwerk die het meeste van het geïnjecteerde fluïdum transporteren. De secundaire en, in sommige gevallen, tertiaire scheuren zijn de overgebleven scheuren. Binnen de primaire productie kan zelfs een relatief kleine scheur een effectief pad vormen voor olie om naar de productieput te stromen. Dit zorgt ervoor dat de vormfactor in duale-permeabiliteitssimulatoren en de zich herhalende eenheid in de homogenisatie moeten afhangen van het proces dat gaande is. Er moet daarbij verschil zijn tussen de primaire, secundaire of tertiaire winning. In Hoofdstuk 4 testen we deze hypothese voor een eenvoudig model van een gescheurde zone met een niet-uniforme verdeling van stromingen in de scheuren. We vergelijken olieproductie, stromingspatronen in de matrix en het patroon van de oliewinning met en zonder de “secundaire” scheuren die slechts een klein deel van het geïnjecteerde fluïdum transporteren.

De rol van de secundaire scheuren hangt af van de dimensieloze verhouding tussen de karakteristieke tijden voor stroming in de matrix en de scheuren (Peclet getal) en de verhouding van de stroming binnen de verschillende scheuren. Binnen de primaire productie en voor een groot Peclet getal is het een betere benadering om alle scheuren op dezelfde manier te behandelen dan om de secundaire scheuren uit te sluiten. De vormfactor moet rekening houden met zowel de primaire als de secundaire scheuren. Voor een klein genoeg Peclet getal is het echter nauwkeuriger om de secundaire scheuren uit te sluiten. Voor waterdoorstroming of EOR moet, voor de meeste hier onderzochte gevallen, de correcte vormfactor of de zich herhalende eenheidsgrootte rekening houden met zowel primaire als secundaire scheuren. Als de secundaire scheuren veel smaller zijn dan de primaire scheuren is het nauwkeuriger om ze uit te sluiten. Nog smallere “tertaire scheuren” zijn niet altijd nuttig voor de olieproductie zelfs als ze een hogere permeabiliteit hebben dan de matrix. Ze kunnen zich gedragen als capillaire barrières voor imbibitie waarmee de oliewinning wordt verlaagd.

# ACKNOWLEDGEMENTS

After many years of my life in Delft, my PhD journey is coming to an end. Words cannot describe my feeling at this moment. This thesis would have been impossible to be finished without the contribution from numerous people. I want to take this opportunity to express my gratitude to them.

I greatly appreciate the China Scholarship Council (CSC) and Saudi Amarco for supporting this research.

My very special gratitude goes to Prof. Bill Rossen for giving me the opportunity to pursue a PhD under his guidance. I cannot expect to be more fortunate to have the ideal supervision of Prof. Bill Rossen during my PhD. I heartily appreciate his guidance, with his impressive knowledge and expertise, which enabled me to develop a progressive understanding of the subject. Thank you for all our valuable and inspiring discussions, the endless hours of work and all opportunities that helped me improve my critical thinking and scientific output. Through the years you has been a fantastic mentor. I cannot imagine how my PhD would go without your constant support, positive outlook, encouragement and trust.

I would like to express my gratitude to Prof. Giovanni Beltotti and Dr. Kevin Bisdom for the valuable discussions and suggestions about the modelling of fracture networks, which benefits not only this study, but also my further research.

I would like to thank Prof. Peter King for discussing with me the pecolation theory and the effect of cut-off of fracture networks on the flow behavior.

To my doctoral committee, Prof. Peter King, Prof. Benoît Noetinger, Prof. David Bruhn, Prof. Giovanni Bertotti, Dr. Denis Voskov and Dr. Hadi Hajibeygi, and Prof. Jan Dirk Jansen, thank you for accepting to be part of the committee, spending time in reviewing and providing precious feedbacks on the thesis.

During my PhD, I also had the opportunity to assist in teaching “Rock fluid physics”. Thanks to Dr. Hadi Hajibeygi, the teacher from whom I have had the privilege to learn. Thank you for encouraging me take the challenge. I learned a great deal about the art and responsibilities of teaching.

I also want to thank Janice Rossen for her enthusiasm, kind words and encouragement to both Yan and me over the years. You and Bill set a good example for Yan and me of how to inspire and support each other.

I am thankful to Chris for translating the proposition and summary from English into Dutch. I appreciate Claire, Matei, Yang and Guanqun for proof reading my thesis.

During my PhD, I have been so fortunate to work alongside cool guys from all corners of the earth. I will never forget all the good times we spent together both inside and outside the office. I truly feel like I have made a lot of lifelong friends here. I will always remember the colourful life we had, Tuesday football, Sunday basketball, group dinners, football matches, and of course, the endless coffee break. To all my friends and colleagues at Petroleum engineering group, whose support and friendship I could always count on. Thank you! I will always fondly remember the company of everyone in the petro-family – Chris, Rahul, Dudu, Siavash, Mojtaba, Tianqi, Nik, Durgesh, Hua, Saskia, Daniel, Matteo, Ehsan, Elisa, Sian, Grigori, Negar, Roozbeh, Elham, Jakolien, Leon, Amin, Maryam, Anna, Amin Fatemi, Matei, Jinyu, Guanqun, Bander, Rodrigo, Ahmed, Mohammed, Rafael, Faisal, Rodrigo, Martijn, Mark, Yang, Mosen, Mousa, Longlong, Swej, and all my other colleagues and friends.

I am also grateful to the administrative support I have received. Thank you Marlijn, Margot, Lydia, Marja, Anke, Hannie and Ralf.

During the past years, I have been so lucky that firstly chaired the Association of Chinese Students and Scholars in the Netherlands – Delft Branch (ACSSNL-Delft) and then the Association of Chinese Students and Scholars in the Netherlands (ACSSNL). It was my great honour to work together with you guys: Fuyu, Lingtong, Yawen, Wei, Huatang, Guannan, Anran, Yasheng, Bao, Jiao, Dingding, Xinyuan, Xuliang, Chenjie, Xialu, Zhe, Wenjing, Hao, Lizuo, Xiaowei, Pengcheng, Zekun, Yujie, Haoran, Qi, Xiyu, Jichao, Qinxuan, Sizhe, Zhengchao, Fei, Muxiang, Yiyun, Jia, Xiaoyin, Yitong, Li Huang and all the colleagues. I learned a lot from you. After organizing so many fantastic events, we grew together and became friends that we can always trust and rely on. I also want to thank Anka Mulder, Peter Wieringa, and Maddy Lansbergen, your trust and support brought the 2016 ACSSNL Talent Forum & Chinese New Year Gala to a much higher level and a great success. I will never forget our numerous emails during that time. Special thanks go to Counselor Qingyu Meng, Counselor Qingchao Fang, Yiwei Wang, Lei Xia and Xiaoxiao Cheng for their guidance, understanding, support, and encouragement. I really enjoy to work together with you. What I learned from you will be helpful for all my future. After four years, you are not only my teachers, but also my respectable friends that I can share my personal life with. Thank you so much.

As the only hobby, I enjoyed playing football on Mondays and Fridays with lots of friends in the DCF team: Yusong, Hao, Yuan, Yue, Yuan, Yunhe, Meng, Xinan, Qiang, Xiaochen, Min, Chenxiang, Boya, Min, Zhan, Guoliang, Yaxun, Fan, Lu, Jiao, Kang, Junchao, Zonghan, Jinku, Lujia, Dengyang, Di, Xiaoqian, Yangtian, Xun, Leyang, Pengqi, Simo, Yandong, Shuaiqiang, Andi and Kaixuan. Thank you for the pleasure time we shared together on the pitch and the champion we won. I will never forget the name of our team “wo da ye” for Monday football competition. I would extend my thanks to Boris, Carlos, Slawek, Michele, Michiel, Ricardo, Reinaldo, Dave, Fawad, Manuel, Mohammed, Bakjinnyam, Naveen, Soumya, Roel and all the members of the Tuesday Comedy Football Group. I cannot image this tradition can last for five years, with people join and go all the time. Thank you for the pleasure time we share after work.

Tianqi, Xuexue, you are my first roommates when I arrived in the Netherlands. I will never forget the days, the feeling we shared and the support you gave me. Feifei and Xinyuan, Ying and Xuliang, Lizuo and Yanbo, Jiao and Fei, Hongbo and Wenshi, Ping and Qingbao, Momo, Kang, Yajun, Jiao, Haoyu, Dichao, you are always there to support me for the highs and lows. Jinyu, Yang, Guanqun and Longlong, I learned a lot from you, especially the oil industry in China. You make me remember the feeling back to MSc and BSc period. Thank you. You are my true friends to whom I can always go for all the happy and sad times.

After nearly five-years simulation work, I got a chance to see what is happening in lab. I would like to thank Kal-Heinz, Michiel, Ellen, Jolanda, Mark, Jens, and all laboratorial stuff to help me become familiar with the experiments so quickly.

Words cannot express my gratitude to my lovely wife Xiaoyan. It is hard for me to say what should not be thankful from her. You taught me by action instead of words, how to sincerely love, how to think of others first. You were always unconditionally supportive in my hardest moments during my PhD and for every decision I made no matter it is good or bad. I will always remember all the happy and sad moments we had, and of course what we will share in the rest of our lives.

Last but not least important, my deepest gratitude goes to my family. Words are inadequate in offering my thanks to my parents for their love, support, encouragement, understanding and sacrifices. I could not have achieved any of this without your unconditional love in raising me and your lifelong support. You deserve far more credit that I can ever give.

# LIST OF PUBLICATIONS

## Journal Papers

- J. Gong, W. R. Rossen, Shape Factor for Dual-Permeability Fractured Reservoir Simulation: Effect of Non-Uniform Flow in 2D Fracture Network. Fuel, 2016, 184: 81-88. DOI: 10.1016/j.fuel.2016.06.113.
- J. Gong, W. R. Rossen, Modeling Flow in Naturally Fractured Reservoirs: Effect of Fracture Aperture Distribution on Dominant Sub-Network for Flow. Petroleum Science, 2017, 14: 138-154. DOI:10.1007/s12182-016-0132-3.
- J. Gong, W. R. Rossen, Characteristic Fracture Spacing in Primary and Secondary Recovery for Naturally Fractured Reservoirs. (Submitted to Fuel)

## Conference Proceedings

- J. Gong, W. R. Rossen, Characteristic Fracture Spacing for the Simulation of Primary and Secondary Recovery from Naturally Fractured Reservoirs, in 8th International Conference on Porous Media & Annual Meeting, Cincinnati, Ohio, USA, 2016.
- J. Gong, W. R. Rossen, Characteristic Fracture Spacing in Primary and Secondary Recovery from Naturally Fractured Reservoirs, AGU Fall Meeting, San Francisco, California, USA, 2015.
- J. Gong, W. R. Rossen, Modeling Flow in Naturally Fractured Reservoirs: Effect of Fracture Aperture Distribution on Critical Sub-Network for Flow, DFNE 2014 - 1st International Conference on Discrete Fracture Network Engineering, Vancouver, BC, Canada, 2014.
- J. Gong, W. R. Rossen, Shape Factor for Dual-Permeability Reservoir Simulation: Effect of Non-Uniform Flow in Fracture Network, ECMOR XIV - 14th European Conference on the Mathematics of Oil Recovery, EAGE, Catania, Italy, 2014.

# ABOUT THE AUTHOR

Jiakun Gong was born on January 21, 1986 in Zhangjiakou, Hebei, China. He obtained his bachelor's degree in Geological Engineering from Hebei University of Engineering, China and master's degree in Geotechnical Engineering from Hohai University, China. In 2012, he headed to the Netherlands to pursue his PhD study in the Delft University of Technology under the supervision of Prof.dr. William R. Rossen. During his PhD study, he served as the president of the Association of Students and Scholars in the Netherlands (ACSSNL), and the university ambassador of the Delft University of Technology. Since September 2016, he has been working in the Delft University of Technology as a researcher, mainly focusing on foam EOR. This is a different research direction from his PhD study. He will continue his work as a researcher in the same university after November 2017.